**FEATURE SELECTION ON HYPERSPECTRAL DATA FOR DISMOUNT SKIN ANALYSIS**

THESIS

Lindsay R. Cain, Second Lieutenant, USAF

AFIT-ENG-14-M-15

**DEPARTMENT OF THE AIR FORCE**
**AIR UNIVERSITY**

***AIR FORCE INSTITUTE OF TECHNOLOGY***

**Wright-Patterson Air Force Base, Ohio**

Distrubution Statement A: Approved for Public Release; Distribution Unlimited

The views expressed in this thesis are those of the author and do not reflect the official policy or position of the United States Air Force, the Department of Defense, or the United States Government.

This material is declared a work of the U.S. Government and is not subject to copyright protection in the United States.

AFIT-ENG-14-M-15

# FEATURE SELECTION ON HYPERSPECTRAL DATA FOR DISMOUNT SKIN ANALYSIS

THESIS

Presented to the Faculty

Department of Electrical and Computer Engineering

Graduate School of Engineering and Management

Air Force Institute of Technology

Air University

Air Education and Training Command

in Partial Fulfillment of the Requirements for the

Degree of Master of Science in Electrical Engineering

Lindsay R. Cain, B.S.E.E.

Second Lieutenant, USAF

March 2014

Distrubution Statement A: Approved for Public Release; Distribution Unlimited

AFIT-ENG-14-M-15

FEATURE SELECTION ON HYPERSPECTRAL DATA FOR

DISMOUNT SKIN ANALYSIS

Lindsay R. Cain, B.S.E.E.
Second Lieutenant, USAF

Approved:

| | |
|---|---|
| //signed// | 18 Feb 2014 |
| Lt Col Jeffrey D. Clark, PhD (Chairman) | Date |
| //signed// | 18 Feb 2014 |
| Col Matthew D. Sambora, PhD (Member) | Date |
| //signed// | 18 Feb 2014 |
| Maj Brian G. Woolley, PhD (Member) | Date |

AFIT-ENG-14-M-15

## Abstract

Many security applications require the ability to accurately identify dismounts based on their distinctive identification properties. A dismount can be identified by many personal characteristics to include clothing, height, and gait. In particular, a dismount's skin can be used as an identifying feature because of the vast variability of skin pigmentation amongst individuals. Hyperspectral data, which is comprised of hundreds of spectral channels sampled from a nearly contiguous electromagnetic spectrum, is used to detect skin spectral variability amongst dismounts. However, hyperspectral data is often highly correlated and computationally expensive to process. Feature selection methods can be employed to reduce the data to a manageable size. This thesis presents the results of applying the fast correlation based filter (FCFB) [51] to a data set that contains hyperspectral data from the forearms of 62 subjects. The reduced data is used to train an artificial neural network (ANN) to discriminate a dismount of interest (DOI) amongst a group of 4 non-DOI's. The trained model is then tested to find the same DOI amongst a group of 62 new non-DOI's. The FCBF selected four features (1014, 1024, 1033, and 1348nm) to discriminate amongst the dismounts. Using these four features, the ANN on average misclassified 4 dismounts amongst four separate DOI validation tests. More specifically, the amount of possible DOI suspects was reduced from 62 to 4 dismounts. The FCBF outperformed three other feature selection methods with 4 times less misclassified instances.

*To my husband, for your selfless love, support, patience, listening ear, sacrifices, and the list goes on...*

## Acknowledgments

A great thanks to my advisor, Lt Col Jeffrey Clark, I cannot quanitfy the amount of gratitude I have for all your help and support. You have made the thesis process so enjoyable. It is also because of you that I will never forget what entropy is.

Lindsay R. Cain

# Table of Contents

Page

## List of Figures

Figure Page

Figure Page

## List of Tables

## List of Symbols

## List of Acronyms

| Acronym | Definition |
|---|---|
| ANN | artificial neural network |
| ASD | Analytical Spectral Devices |
| DOI | dismount of interest |
| ELM | empirical line method |
| EWA | equal-weighted accuracy |
| FCBF | fast based correlation filter |
| HSD | hyperspectral data |
| HSI | hyperspectral imaging |
| MED | minimum euclidean distance |
| MMD | minimum mahalanobis distance |
| nm | nanometers |
| NIR | near-infrared |
| NIMI | near-infrared melanin index |
| PCA | principal component analysis |
| SAC | spectral angle classifier |
| SU | symmetrical uncertainty |
| SWIR | short-wave infrared |
| UV | ultraviolet |
| VIS | visible |

FEATURE SELECTION ON HYPERSPECTRAL DATA FOR DISMOUNT SKIN ANALYSIS

# I. Introduction

The human ability to recognize an individual person is based on a previously learned image of that person. While, minor features of an individual may change (e.g. wearing sunglasses, a new hairstyle, or different clothing), the cognitive process of the human brain has the remarkable ability to identify the basic characteristics that differentiate individuals. Technology has also enhanced the ability of humans to distinctly identify individuals. For example, a fingerprinting system collects the impressions left by the friction ridges of a finger, analyzes that information, and selects a match [11]. Fingerprinting systems are effective for identification because individual fingerprints are unique and time-invariant.

Typical fingerprint systems rely on physical contact to positively identify an individual. However, identifying a *dismount* (i.e. a person traveling by foot [16]) requires a passive system. This thesis investigates the capability of using the characteristics of skin as a discriminating feature in dismount identification. Identifying a dismount based on the properties of their skin will greatly enhance a multitude of applications, ranging from security and surveillance to target identification and tracking.

Section 1.1 introduces background information for this research. The problem statement and implications are presented in Section 1.2 and 1.3. The assumptions and scope are discussed in Section 1.4 and 1.5 to provide a bounding to the problem. Finally, the approach and tools necessary for the successful completion of this research are discussed in Sections 1.6 and 1.7.

## 1.1 Background

Recent techniques have been created to determine the presence of human skin in a scene [36]. Additionally, efforts to classify clothing based on textual properties have also been investigated [4]. Such efforts contribute to a dismount identification system. Each of these techniques are based on hyperspectral imaging (HSI) data, which collects the spatial and spectral information of a scene. Unlike conventional color imagery which collects in the visible spectrum, HSI acquires spectral information of a scene across a wide set of nearly contiguous wavelengths, revealing reflectance, absorbance, and emittance characteristics that cannot be seen by the human eye [8, 37]. This high resolution data of the combined spectral and spatial information yields the capability for lower false alarm rates when compared to traditional grayscale and color imagery detection systems [37]. The goal is to use hyperspectral information to not only detect dismounts, but actually characterize them using their spectral *fingerprint*.

In general, dismount detection is possible because skin has certain physical properties that can be identified in a hyperspectral signature. Typically, skin color is most affected by three types of light-absorbing chemical compounds, including melanin, hemoglobin, and carotene [18]. Small differences in the distribution of these pigments results in spectral variability of individuals [39]. HSI systems are able to detect these small changes by collecting data over hundreds to thousands of spectral channels creating fine resolution data. However, such large data sets are cumbersome and must be reduced to preclude processing delays from impeding the mission. Thus, it is often necessary to reduce the data for a deployable spectral imaging system where processing time and portability are important design considerations. One way to reduce the data set, which is employed here, is to determine the key discriminate wavelengths by using a feature selection method. Once the important features have been identified, a deployable system can be created that collects the desired wavelengths.

Feature selection also improves classification accuracy by removing redundant and highly correlated features within the hyperspectral data [17]. Once feature selection is complete, classification methods are applied to identify the source of the spectral data.

### 1.2 Problem Statement

Based on the background information the culminating problem that this research will address is stated as follows:

*Can a set of global features be determined that provide classification of dismounts based on the spectral properties of their skin?*

This thesis provides the necessary background and methodology to address this objective with a high degree of accuracy.

### 1.3 Justification

The implications of addressing dismount identification are wide-reaching for a variety of applications. Such a capability could enhance security and surveillance. Detection systems of this nature are passive, implying that it would not be necessary to have a compliant dismount to make an identification. This is not the case with other human identification systems, such as fingerprint, voice, hand and iris [42], which require compliant interaction in order to establish their identification. Previously, traditional facial recognition systems have been enhanced by HSI by matching the hyperspectral signatures of skin [8, 39]. The aim of this research is to expand on these techniques to include the application to dismount identification.

### 1.4 Assumptions

Some important assumptions will be made in this research. The first assumption is that skin is present in the scene. Since this research relies on the hyperspectral signature of skin, the assumption is that skin is exposed. The location of the exposed skin is also an

important consideration. As shown in Pan *et al.* the accuracy of identification is dependent on the location and amount of skin used for classification [39].

This research also assumes that the experiments will incorporate a calibrated illumination source. Typically, HSI systems are passive and therefore rely on an illumination source, usually the sun, to collect data. For this reason it will be assumed that the data will be collected under controlled illumination conditions.

The last assumption of the research is that a major change has not occurred to the skin between collections. For example, if the dismount has acquired a tan between collections the system may classify the dismount incorrectly due to the changes of the hyperspectral signature. Ideally, a dismount identification system should be able to withstand changes of this nature; however, that issue will not be addressed in this thesis.

## 1.5 Scope

This research will focus on feasibility rather than full application of the concept. Therefore, the scope of this thesis will be contained to determining a global feature set that produces a positive identification of a dismount.

The data collected for this research will be gathered using a spectroradiometer rather then an actual HSI system. This an important distinction because data collected using a HSI will generally have atmospheric effects that can be neglected when using a contact spectroradiometer. Eventually, the feature selection and classification techniques will need to be adapted for HSI. Thus, this research will focus on creating a technique that uses data from a laboratory spectroradiometer.

## 1.6 Approach

The process of selecting a global feature set for dismount identification begins with collecting skin reflectance measurements. To collect the data for this thesis, a spectroradiometer collected reflectance measurements from 350-2500 nanometers (nm)

with 1nm resolution which results in 2150 features for each instance. These measurements are processed through a feature selection method that statistically determines the irrelevant and redundant features that can be eliminated in order to improve classification performance. The feature selection method selected for this thesis is called the fast based correlation filter (FCBF) [51]. This method determines the relevant features by ranking each feature using the symmetrical uncertainty value which is a measure based on information theory. The redundant features are determined by searching through the selected relevant features using a search guided by three heuristics.

The reduced data set that contains only the selected features is classified using an artificial neural network (ANN), created using the back propagation algorithm. The classifier is trained to find a dismount of interest (DOI), which refers to the dismount that needs to be identified amongst a group of other dismounts. The classifier is tested by determining its accuracy for identifying specific DOI amongst a larger, previously untrained for, group of dismounts.

### 1.7 Material and Equipment

To successfully complete this thesis a variety of laboratory and software tools are required. The first is the laboratory spectroradiometer, specifically the ASD FieldSpec® 3 with a contact probe to collect the hyperspectral measurements [1]. In order to analyze the classification and feature selection techniques, MATLAB® [32] and WEKA® [13] will be used. WEKA® [13] provides a collection of machine learning algorithm written in Java®. This tool will allow for accurate and efficient testing of a wide variety of techniques to ensure the correct method is chosen.

### 1.8 Organization

The following chapters will discuss the necessary background, methods, and results of the thesis. Chapter II will provide an introduction to the physical properties of skin which

is reflected in the spectral signature. It will also explain important feature selection and classification methods. Finally, it will discuss the related works that provide a strong foundation for the research. Chapter III will discuss the methodological process that was followed in order to obtain sound results. Finally, Chapter IV and V provide the results, impacts, and possible future studies on this thesis.

# II. Background

As globalization becomes a reality with trade, technology, and the movement of people becoming more dynamic, the security implications also become global in scope [7]. The task of identifying a person of interest has proven to be a challenge. For decades, technology has been evolving to expand the capabilities of human identification systems. The most popular biometric technologies include fingerprint, voice, hand, iris, and face analysis [42]. A new approach to human identification could use hyperspectral imaging (HSI) to recognize a person based on the skin's specific properties. This approach exploits the rich data associated with HSI to stay abreast with the challenges of a dynamic world.

This chapter will provide a foundation for the current technologies, theory, and related works that have been explored in this area. Section 2.1 gives an overview of the terminology and advantages of HSI. Section 2.2 will discuss the optical properties of the skin that can be used to characterize a person. Section 2.3 discusses common data analysis approaches for hyperspectral data. Finally, Section 2.4 provides a literature review of previous work related to this area.

## 2.1 Hyperspectral Imaging

HSI refers to the process of collecting images across the electromagnetic spectrum typically spanning the visible (VIS) to the short-wave infrared (SWIR) part of the spectrum (0.4 to 2.4 micrometers ($\mu m$)) with high resolution (10nm wide). This collection of images is called a data cube, which is a three dimensional array with spatial information along the $x$ and $y$ axes and spectral along the $z$ axis [31]. Collecting a hyperspectral image results in a continuous radiance spectrum for each pixel in an image. The collection of hundreds of contiguous spectral channels results in high dimensional data.

HSI is employed in a wide variety of applications from detecting contamination in poultry to the presence of melanoma on human skin [34, 41]. In particular remote sensing is one area where HSI is widely used. It exploits the fact that everything absorbs, reflects, or transmits electromagnetic radiation differently depending on its molecular composition [31]. Therefore, HSI can detect certain objects based upon their specific spectral signature or "spectral fingerprint" [35, 47].

## 2.2 Optical Properties of Human Skin

Skin is not only the largest organ of the human body it is also pivotal for human health and responsible for providing a barrier for the internal organs against potentially harmful environmental factors [44]. It consists of multiple layers, each with varying thickness and optical properties. The three main layers are the epidermis, the dermis, and the subcutaneous fat. The epidermis contains many of the protective structures of skin. The dermis consists of connective tissue to give skin its flexibility and strength. Finally, the subcutis provides a foundation, comprised of fat that supplies nutrients to the other layers. The heterogeneous nature of skin allows for different distribution of blood, chromophores, and pigments all contributing to certain optical properties. [2] The main contributers of the skin's optical properties are melanosomes, hemoglobin, bilirubin, and $\beta$-carotene [49] chromophores. Small differences in the distribution of these pigments result in a spectral variability of individuals [39].

### *2.2.1 Melanosomes.*

Skin color is the most noticeable and varying characteristic of human skin. The color exists in a wide variety from white to black due to the presence of cells containing pigment in the epidermis; the pigment is called melanosomes [5]. The fairest skinned individuals will have melanin levels of 1.5% to 6% while the darkest will be as high as 43% [19]. Melanin plays an important role in protecting against the ultraviolet (UV) radiation of the sun, and can vary according to geographical location.

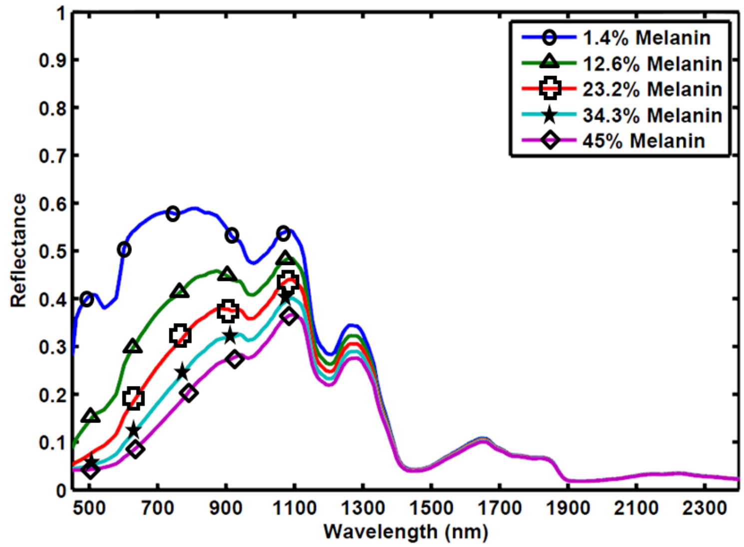


Figure 2.1: Spectral reflectance of human skin with varying melanin concentration [3].

In addition to being the most noticeable characteristic of skin, melanin dominates other chromophores in the VIS and the first part of the near-infrared (NIR) [50]. It has been shown that the spectral reflectance of skin varies according to melanin concentration [36]. As shown in Figure 2.1, there is a visible difference in melanin concentration from 350nm to 1300nm [3]. As the wavelength increases the absorption of melanosomes decreases resulting in nearly identical reflectance past 1300nm. This is a result of water absorption which dominates the reflectance spectrum beyond 1000nm [36].

Melanin levels and concentration can change based on many environmental factors to include pregnancy, aging, drug intake, and stress [5]. Since dismount characterization relies on repeatability, the knowledge that melanin concentration will change over time is an important consideration.

### *2.2.2 Hemoglobin.*

The second most distinct chromophore in skin is hemoglobin, which is a protein that is carried by red blood cells and exist within the dermis and subcutis [36]. There are two

types of hemoglobin, oxygenated and deoxygenated. The oxygenated hemoglobin has recently visited the lungs and is carrying essential oxygen to the rest of the body. The deoxygenated is returning back to the lungs to repeat the process. [36] Oxygenated hemoglobin in particular has a distinct absorption feature [8, 36]. Figure 2.2 shows that oxygenated hemoglobin in the VIS has a *w*-shaped feature around 570nm with a local minima at around 510nm [49]. Additionally, the deoxygenated hemoglobin has a local minimum and maximum at 480nm and 560nm respectively [49]. In Di *et al.* [8] the absorption bands related with hemoglobin were preferred over other chromophores because of their discriminative features. However, this feature is only predominantly valid for individuals with fair to moderate skin color [38]. In addition, the absorption of hemoglobin quickly decreases as wavelength increases making it a distinguishing chromophore for a limited wavelength range [36].

### *2.2.3 Bilirubin and $\beta$-carotene.*

Bilirubin and $\beta$-carotene are the last mentionable chromophores responsible for the distinctive color of skin [39]. Bilirubin is a byproduct of hemoglobin responsible for the yellow tint of the skin. An elevation of bilirubin levels can indicate disease such as jaundice which is typically caused by a disorder of the liver or gall bladder. $\beta$-carotene is a chrompohore that exists in the blood and skin yielding an orange tint. [27] These two pigments are mentioned for being important in giving skin its distinctive color; however, melanin and hemoglobin appear to be dominant in the study of the spectral properties of skin [38].

### *2.2.4 Bruising and Melanoma.*

In studying the pigments mentioned, HSI has been used to identify the presence of bruising and melanoma on skin [34, 45]. While it is obvious that not every dismount will have a bruise or cancerous skin cells, they provide possible distinguishing characteristics.

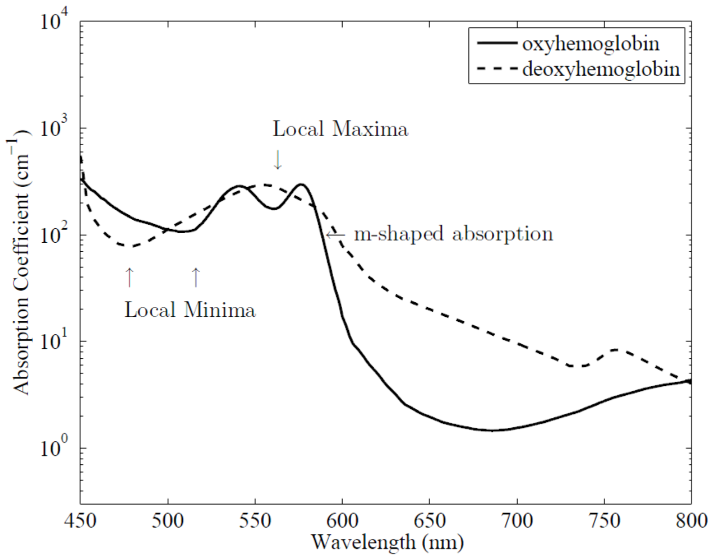


Figure 2.2: Oxygenated and deoxygenated hemoglobin absorption in the VIS with concentration of 150 g/L [36]. The labels indicate the location of the distinctive *w*-shaped (or *m*-shaped) hemoglobin spectral feature.

Randereberg *et al.* [45] used HSI to evaluate the development of bruises on the skin. The study quantified the hemoglobin oxygenation content, redness of the skin, and melanin index as a means to describe the chromophore distribution within a bruise. This study was able to discriminate between bruised and non-bruised skin areas. It is important to note that a bruise's spectral property is time variant, therefore lending a small window of opportunity to be used as a dismount discriminator.

Nagaoka *et al.* [34] was able to create a melanoma discrimination index in the VIS to distinguish cancerous skin cells from healthy skin cells. This recent 2012 study has only been tested on 9 cases of melanoma and 18 non-melanoma patients but was able to obtain results of 100% sensitivity and 94.4% specificity.

## 2.3 Hyperspectral Data Analysis

Having a fundamental understanding of the optical properties of the skin can provide *a priori* information as to what features will be important in HSI when characterizing an individual. This is important because hyperspectral data (HSD) is notorious for creating highly dimensional and highly correlated data which present a challenge for processing, also known as the curse of dimensionality [17]. High dimensional data creates a classic "needle in the haystack" problem which requires HSD to be reduced to a lower dimensional space while still containing the important features [9]. Once the data is contained in a lower dimensional space, classification techniques are employed in order to make a decision about the data, or in this case make a correct identification of the dismount.

### *2.3.1 Dimensionality Reduction.*

The high dimensional feature space created by HSI requires certain techniques to be employed in order to correctly process the data. There are two popular techniques that are used to reduce the dimensionality of data. The first is to transform the data to a lower dimensional space, which is called feature extraction [10]. The second is to reduce dimensionality is by identifying and discarding the redundant characteristics that do not contribute to the specific application, this is called feature selection. These redundant features can degrade accuracy and increase processing time due to the excess of irrelevant information [21].

#### *2.3.1.1 Feature Extraction.*

One popular method for dimension reduction is principal component analysis (PCA) [4, 20, 43]. This technique calculates orthogonal projections that maximize the amount of variance in the data and creates a dataset which is contained in an uncorrelated coordinate system [14, 20, 43]. This coordinate system is defined by the principal components or the eigenvectors that are calculated from the covariance

matrix [4]. The eigenvectors are chosen by their corresponding eigenvalues which are ordered in decreasing variance. Depending on the dimensionality of the data, only a small set of principal components is necessary to maintain separability between features [4, 14]. PCA is sufficient to reduce the data; however, it does not concentrate on individual spectra or signatures of interest [14, 20, 43]. For example, the first principal component contains the most variance but it is a linear combination of several spectral classes. The linear combination is due to the fact that HSD is highly correlated and the eigenvectors used to calculate the principal components are orthogonal. [14] This technique is used in many applications but depending on the dataset may not preserve the necessary information to obtain accurate classification [43].

#### *2.3.1.2 Feature Selection.*

PCA is a global transform and therefore does not account for the specific type of data that is being transformed [20, 43]. To correct this problem, Landgrebe [28] discusses the importance of finding the most appropriate subspace for a particular dataset by first selecting the features or classes that are important, also known as feature selection. There are two broad categories for feature selection algorithms, the filter method or wrapper method. The filter method focuses on the inherent characteristics of the training data set to select the important features. The wrapper method uses the performance of a predetermined classification method to select the feature subset. [51] The filter method is less computationally expensive because it does not rely on training a new classifier with each candidate feature subset [29]. The filter method is often chosen for data sets that have a large number of features or dimensions due to computational efficiency [51].

The filter feature selection method can be further separated into two main groups, feature weighting and subset search algorithm. Feature weighting algorithms will rank the features based on their individual relevance. A feature is deemed relevant if its goodness measure exceeds a predefined threshold. The goodness measure is chosen based on the

type of data and the goal of the feature selection method. [51] An example of a feature weighting method is ReliefF [23]. The concept of the ReliefF method is to estimate the ability of an individual feature to discriminate between classes. The ReliefF algorithm randomly samples instances from the training set and updates the relevance of the features by examining the difference between the selected instance and the user defined $k$ nearest instances within the same class and the other classes. The ReliefF method will remove irrelevant features however it does not remove redundant features. If a feature is selected as relevant it will be chosen regardless of the correlation with the other features. [51] A feature selection method that is ideal for high dimensional data should remove irrelevant and redundant features to improve the speed and accuracy of classification [12, 24].

The subset search algorithms select features by searching through feature subsets rather then evaluating each feature individually. Typical search strategies include exhaustive, heuristic, genetic, or random. The search is guided by an evaluation measure that determines the goodness of the subset. [51] Previously, consistency [6] or correlation [12] measure has been used to remove redundant and irrelevant features. Feature selection methods that employ search techniques are typically not scalable to high dimensional data due to the time complexity to locate an optimal subset [51].

#### *2.3.1.3 Correlation-Based Measures.*

The performance of a feature selection method relies on finding a suitable measure and an appropriate procedure to select the features using that measure. A feature is deemed *good* if it is *relevant* to the class but it is not *redundant* to any of the other relevant features. Focusing on using correlation as a goodness measure, a feature is good if it is highly correlated to the class but not correlated to any of the other features. To measure correlation there are two standard approaches. The first is based on the classical linear correlation approach while the other is derived from information theory. [51]

The classical approach will often use the linear correlation coefficient $r$ as a measure, with $X$ and $Y$ as a pair of two random variables as [51]:

$$r = \frac{\sum_i (x_i - \overline{x}_i)(y_i - \overline{y}_i)}{\sqrt{\sum_i (x_i - \overline{x}_i)^2} \sqrt{\sum_i (y_i - \overline{y}_i)^2}}, \tag{2.1}$$

where $\overline{[\cdot]}$ indicates the average. The value for $r$ is bounded between $-1$ and 1. If $X$ and $Y$ are highly correlated the value for $r$ will be close to $-1$ or 1. If the variables are independent, $r$ will be zero. The advantages of using linear correlation are to remove features with near zero correlation, and effectively determine the redundant features among the relevant features. However, this technique assumes that the correlation is linear which is not always a valid assumption. [51]

To account for the issues with the linear assumption, techniques based on information theory can be employed, specifically the measure of entropy [51]. Entropy ($H$) calculates the amount of uncertainty of a random variable, $X$, and is defined as [51]:

$$H(X) = -\sum_i P(x_i)\ log_2\left(P(x_i)\right), \tag{2.2}$$

where $P(\cdot)$ is the prior probability of the random variable. To calculate the entropy of $X$ from the observation of another random variable, $Y$, is [51]:

$$H(X|Y) = -\sum_j P(y_j) \sum_i P(x_i|y_i)\ log_2\left(P(x_i|y_i)\right) \tag{2.3}$$

where $P(x_i|y_i)$ is the posterior probability of $X$ given that values of $Y$. The amount of additional information about $X$ given the values of $Y$ is defined as information gain ($IG$) and given by [51]:

$$IG(X|Y) = H(X) - H(X|Y). \tag{2.4}$$

Using this measure, it can be determined if a feature $Y$ is more correlated to the feature $X$ then to feature $Z$, i.e. $IG(X|Y) > IG(Z|Y)$. The information gain measure is symmetric

which means that $IG(X|Y) = IG(Y|X)$. Symmetry is a desired property for correlation measures. Regardless of the symmetry property, this measure is biased for features that have more values and is not normalized. [51] Therefore, the symmetrical uncertainty ($SU$) measure can be used to obtain an unbiased and normalized measure as [51]:

$$SU(X,Y) = 2\left[\frac{IG(X|Y)}{H(X)+H(Y)}\right]. \tag{2.5}$$

The range of values for this measure is between 0 and 1, where a value of 1 indicates that the value of $X$ can be completely predicated by the value of $Y$ while a value of 0 indicates that the two values are independent [51].

### *2.3.2 Classification.*

After removing the irrelevant and redundant features, a classification technique can be used to match each instance of spectral data to the appropriate class. This thesis focuses on supervised learning techniques, therefore each training instance will be assigned a class label, or designated to a specific dismount. The goal of supervised learning is to build a model that learns the relationship between the inputs and the desired outputs using the labeled instances. This model is then used to predict the classification of testing instances where the class is unknown. [26] There are a wide variety of classification techniques, this thesis will focus on methods using distance measures and artificial neural networks (ANN's).

#### *2.3.2.1 Minimum Distance Classification Methods.*

Minimum distance classification techniques are one of the simplest forms of classification. This method calculates the distance between an instance and the class averages of each class. An instance will be assigned to the class that results in the shortest distance measure. [22] Typical minimum distance classification methods are minimum euclidean distance (MED), minimum mahalanobis distance (MMD), and spectral angle classifier (SAC).

The Euclidean distance ($D_{ED}$) between spectral measurements $a$ and $b$ is defined as [22]:

$$D_{ED}(a,b) = \sqrt{\sum_{k=1}^{B} \left(\overline{R}(\lambda_k, a) - \overline{R}(\lambda_k, b)\right)^2}, \tag{2.6}$$

$$= \left\|\overline{\boldsymbol{R}}(a) - \overline{\boldsymbol{R}}(b)\right\|, \tag{2.7}$$

where $\overline{\boldsymbol{R}}(\lambda_k, a)$ and $\overline{\boldsymbol{R}}(\lambda_k, b)$ are the normalized spectral reflectance vectors of $a$ and $b$ respectively, $\lambda_k$ denotes a particular wavelength, and $B$ is the number of spectral bands.

The square of the Mahalandobis distance ($D_{MD}$) between the spectral reflectance $a$ and $b$ is defined as [39]:

$$D_{MD}(a,b) = \left(\overline{\boldsymbol{R}}(a) - \overline{\boldsymbol{R}}(b)\right)^T \ \Sigma^{-1} \ \left(\overline{\boldsymbol{R}}(a) - \overline{\boldsymbol{R}}(b)\right), \tag{2.8}$$

where $\Sigma$ is the $B \times B$ covariance matrix for the distribution of the vector $\overline{\boldsymbol{R}}$ where $B$ is the number of spectral bands and $(\cdot)^T$ is the matrix transpose. The amount of data is often limited, therefore the covariance matrix is estimated as a diagonal matrix with each element corresponding to the average variance across all the subjects for each $\lambda_k$ [39].

The SAC measures the angle between two different spectra, as vectors in a space with the dimensionality equal to the number of bands. The values that results from SAC are between $\left[0, \frac{\pi}{2}\right]$ where the smaller angles represent a closer match to the reference spectrum [22]. The equation to calculate the spectral angle ($\theta$) between two spectra is [22]:

$$\theta(a,b) = arccos\left(\frac{\left\langle\overline{\boldsymbol{R}}(a), \overline{\boldsymbol{R}}(b)\right\rangle}{\left\|\overline{\boldsymbol{R}}(a)\right\| \ \left\|\overline{\boldsymbol{R}}(b)\right\|}\right), \tag{2.9}$$

the $\langle\cdot,\cdot\rangle$ is the dot product and $\|\cdot\|$ is the $\ell^2$-norm, similar to calculation used in Euclidean distance.

#### *2.3.2.2 Artificial Neural Network.*

An artificial neural network (ANN) represents a more complex classification method that is modeled after the processing techniques of the central nervous system. Unlike

conventional digital computers, the brain is considered a highly complex, nonlinear, and parallel computer that can organize neurons to preform computations such as pattern recognition. The general structure of a multilayer ANN consists of input, hidden, and output layers. All the layers are connected together and contain nodes called perceptrons that model the processing functions of a neuron. Each perceptron consists of synaptic weights, an adder, and an activation function. The synaptic weights represent the connection strength between the neurons. The weights are updated during the training of the ANN to create the network model. The adder sums the product of each inputs and the input weights which creates the induced local field. The activation function scales the induced local field into a proper range of values to make classifications. [15] A sigmoid function is a typical activation function that limits the output to values between −1 and 1 which is defined as [15]:

$$f(x) = (1 + e^{-x})^{-1}. \tag{2.10}$$

Back-propagation is one method used to train an ANN. This method consists of two phases, the forward pass processes the training data through the network to determine the output, the backward pass propagates the output error back through the network to update the weights. [15] To update the weight ($w$) based on the error associated with a particular neuron, $n$, in the $j$ layer to previous neurons in layer $i$, equation 2.11 is used [15]:

$$w_{ij}(n) = w_{ij}(n-1) + \eta\ \zeta_j(n)\ y_j(n), \tag{2.11}$$

where $\eta$ is the learn rate which is set by the user, $y(\cdot)$ is the output from the neuron in layer $j$, and $\zeta(\cdot)$ is the local gradient defined for neuron, $n$, in the output layer, $j$, as [15]:

$$\zeta_j(n) = \varphi_j^{'}(v_j(n))\ e_j(n), \tag{2.12}$$

where $\varphi^{'}(\cdot)$, is the derivative of the activation function, $v(\cdot)$ is the input to the derivative function which is the induced local field, and $e(\cdot)$ is the error at the output which is the

difference between the desired output and the calculated output. The equation for the local gradient, $\zeta_j(n)$, is different for a neuron in the hidden layers, defined as [15]:

$$\zeta_j(n) = \varphi_j^{'}(v_j(n)) \sum_k \zeta_k(n)\, w_{kj}(n), \tag{2.13}$$

where the $k$ is each neuron in layer $i$.

## 2.4 Related Work

It has been shown that dismount detection is possible by detecting the presence of skin using HSI [36, 37]. In order to accomplish skin identification it is important to study if a dismounts skin can actually be characterized based on their spectral properties. In previous studies on dismount detection, the melanosome level has often been calculated as a fundamental method to differentiate between people [38]. In addition, the area of facial recognition has benefited from the rich spectral data that HSI has offered [8, 39]. Unlike traditional facial recognition methods, which rely on face symmetry and position, HSI can bolster these techniques by detecting personal identification patterns in the skin [8]. Instead of using gray and color imagery for facial recognition, HSI can identify a person without suffering from the performance degradation associated with facial recognition, e.g. variation in face orientation and expression [8, 39].

### *2.4.1 Melanosome Estimation.*

Nunez *et al.* [36, 37] expanded the area of dismount detection by introducing a melanin estimation technique. Melanin is a key player in the spectral properties of skin, a method that detects the melanin level may be the first step in the ability to characterize an individual. To determine the melanosome level, the estimated reflectance was calculated using the empirical line method (ELM) [38].

The NIR is dominated by melanin absorption, an index denoted as near-infrared melanin index (NIMI),$N(\lambda, D)$, is used to describe melanin levels, as [38]:

$$N(\lambda, D) = \frac{P(\lambda, D)}{P(1270, D)}, \tag{2.14}$$

where $P(\lambda, D)$ is the output of the skin reflectance model at a specific wavelength $\lambda$ and $D$ is the estimated melanosome level in the epidermis. The value 1270nm was chosen as a value for $\lambda$ in the denominator of Eqn. 2.14 because the reflectance does not change as melanosome level increases. Therefore, this index is a ratio of the reflectance model at some $D$ and $\lambda$ and reflectance at $\lambda = 1270$nm with the same level of melanosome $D$. [38]

After using the NIMI to model the melanin index, regression coefficients were computed to characterize the behavior between 750nm and 1100nm. The final regression coefficients are represented as $S(\lambda)$ for the quadratic component, $M(\lambda)$ for linear, and $B(\lambda)$ for constant. [38] The equation used to estimate the melanosome level given the estimated reflectance $\hat{p}_i$ for the $i$th pixel is [38]:

$$D = S(\lambda)\left(\frac{\hat{p}_i(\lambda)}{\hat{p}_i(1270)}\right)^2 + M(\lambda)\left(\frac{\hat{p}_i(\lambda)}{\hat{p}_i(1270)}\right) + B(\lambda). \tag{2.15}$$

Using melanomsome levels in the NIR can be used in the characterization of a dismount. However, it is important to note that since melanin levels are dependent on environmental factors such as UV radiation, a characterization algorithm could not be dependent on melanin concentration alone.

### *2.4.2 Facial Recognition using HSI.*

The techniques used in facial recognition with HSI are valuable because as with dismount characterization, facial recognition is seeking to identify people based on their distinct features. Facial recognition using HSI has increased within the past few years due to its ability to capture "distinctive personal identification patterns" [8]. Traditional face recognition systems using color images suffer from performance issues related with facial

orientation, where even a 32 degree rotation will cause significant degradation in performance [8, 39, 46]. Pan *et al.* [39] were among the first to use HSI as a means for facial recognition. Di *et al.* [8] more recently studied the advantages of choosing selected feature bands over analyzing single or whole band data. These studies differ from dismount characterization because they were conducted in highly controlled environments. In dismount characterization environmental factors such as illumination variations, distance, and location of skin will present a different set of challenges [40].

Pan *et al.* [39] created a database with 200 subjects using a 31 band hyperspectral imager over the NIR (700nm to 1000nm). The NIR was chosen because skin has a larger penetration depth than in the VIS spectrum resulting in the imaging of subsurface characteristics that are not easily modified by an individual. Here the optical penetration is the depth at which 37 percent of the light intensity is reduced relative to the surface. [39] The optical penetration depth, $\delta_{PD}$, is defined by Eqn. 2.16, where $\mu_a$ and $\mu_s'$ are the absorption and reduced scattering coefficients of the tissue respectively and is calculated as [19]:

$$\delta_{PD} = \frac{1}{\sqrt{3\mu_a\mu_s'}}. \tag{2.16}$$

The typical absorption and scattering coefficients in the VIS (550nm) region are $0.77mm^{-1}$ and $1.89mm^{-1}$ yielding an optical penetration of 0.48mm, whereas in the NIR (550nm) the coefficients are $0.02mm^{-1}$ and $1.31mm^{-1}$ with an optical penetration of 3.57mm [19]. In addition to the increased optical penetration, the NIR is not dependent of skin temperature as in the thermal infrared region (8$\mu$m-12$\mu$m) [39].

Each subject was imaged over the 31 bands with 7 different orientations of the face. All 31 bands were used for the facial recognition algorithm, which calculated a spectral reflectance vector ($R$) from five manually selected regions of the face to include the forehead, left cheek, right cheek, hair, and lips. [39]

The spectral reflectance vector is estimated by averaging over the spectral bands for each tissue region as [39]:

$$R_t(\lambda_k) = \frac{1}{N}\sum_{x,y} R(x, y, \lambda_k) \qquad k=1,2,...,\mathrm{B}, \tag{2.17}$$

where $t$ is the tissue type, $\lambda_k$ denotes a particular wavelength, $N$ is the number of pixels in the chosen square, $x$ and $y$ are the spatial locations of the pixels within the square, and $B$ is the number of spectral bands which in this study was 31. This spectral vector is normalized using the $\ell^2$-norm, yielding $\overline{\boldsymbol{R}}_t$. [39] The square of the Mahalandobis distance is calculated between the spectral measurements $a$ and $b$ defined as [39]:

$$D_{MD}(a, b) = (\overline{\boldsymbol{R}}_t(a) - \overline{\boldsymbol{R}}_t(b))^T \Sigma_t^{-1} (\overline{\boldsymbol{R}}_t(a) - \overline{\boldsymbol{R}}_t(b)), \tag{2.18}$$

where $\Sigma$ is the $B \times B$ covariance matrix for the distribution of the vector $\overline{\boldsymbol{R}}$ for each subjects where $B$ is the number of spectral bands and $(\cdot)^T$ is the matrix transpose [39].

It was determined that combining the tissue types for recognition improved performance. From the data collected of the 200 subjects more then 90% of the probes were correctly identified when combining all of the tissue types. In addition, duplicate data was collected on 20 subjects up to 5 weeks after the first session. It was shown that while there is a reduction in performance relative to images taken on the first day, 92% of the correct probes where ranked in the top 10. The authors cited that the reason for the performance degradation occurred due to variations in blood,water concentration, blood oxygenation, and melanin. A comparison between the skin spectra for four different people and that of one person is shown in Figure 2.3. It is evident that there are significant differences between the amplitude and shape for different subjects while remaining relatively constant for the same subject. This study was able to show that HSI is a valid technology for facial recognition especially for variations in head orientation or facial expression. [39]

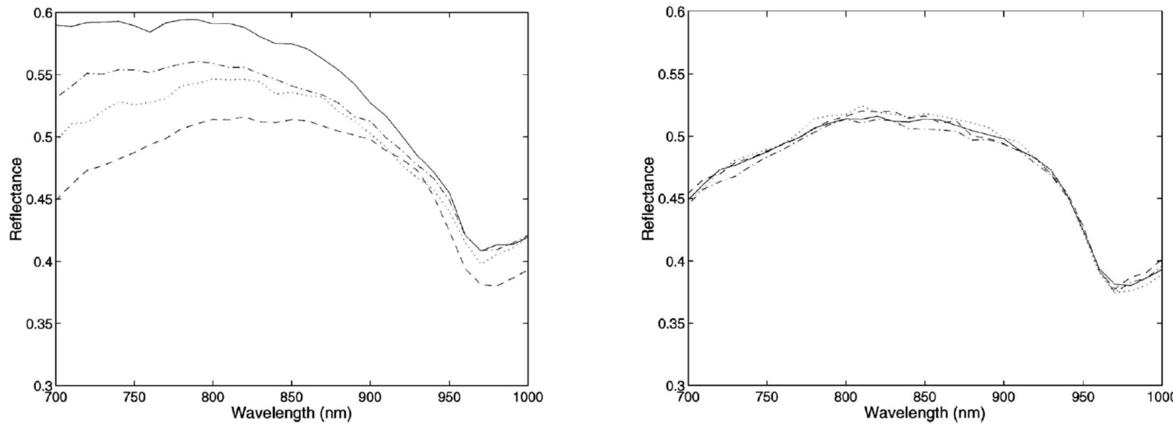


Figure 2.3: Reflectance measurements from four different subjects (left) and reflectance measurements from one subject (right). There are significant difference in both magnitude and shape for reflectance measurements for different subjects while the reflectance for one subject remains relatively similar. [39]

Di *et al.* [8] more recently expanded the use of HSI by using feature band selection. This study relied on that fact skin tissue has distinctive spectral reflectance feature in some bands that are insignificant in others. The authors chose to focus on hemoglobin as a feature because unlike melanin, hemoglobin is less likely to be influenced by environmental factors such as sunlight. The two bands chosen were 540nm and 580nm. [8]

Once the bands were selected three methods where chosen for processing the data. A method called $(2D)^2$ PCA was chosen because it simultaneously considers the rows and column directions to calculate the eigenvectors of the image covariance matrix-to-vector conversion. This technique helps to alleviate the small sample size problem and computational burden of PCA. The first method was $(2D)^2$ PCA analyzing over all 33 bands in the VIS light spectrum of (400 to 720nm). Next $(2D)^2$ PCA was accomplished only using single bands. Lastly, $(2D)^2$ PCA was used but with the feature bands of 540nm

and 580nm with image fusion. Pixel-level image fusion combines the important information from each spectral band and fuses it into one image. [8]

In order to classify the three methods, a minimum distance was used for the first method while the other two used decision level fusion, which applies a majority voting strategy. First, the set of minimum distances are calculated and then the cardinality of that set represents the total number of votes given by the feature band that classifies the test data. [8]

The results of this study indicated that using feature bands outperformed that of a single or whole band method. This result indicates the importance of understanding the spectral properties of skin when using HSI for characterization. In addition, the third method that used image fusion outperformed the other two methods. [8] Image fusion is advantageous because it reduces image noise while retaining important information [48]. Finally, the method outperformed conventional color imagery facial recognition which is consistent with the previous study. [8]

From the facial recognition studies it is important to note a few considerations. The first it that the two studies mentioned were conducted in highly controlled environments. All the images where taken in the labs with controlled variables such as illumination. A profitable dismount identification system should be able to operate under a wide variety of conditions to include varying illumination, orientation of the individual, and distance from the subject. In addition, dismount characterization does not have the luxury of knowing the amount or location of the skin that will be used to identify that individual.

Pan *et al.* [40] addressed one of the constraints in his previous study by testing the effects of illumination variations in facial recognition using HSI. They used the same database of 200 subjects but modeled illumination variance by including 100 outdoor illumination spectra that were measured in Boulder, Colorado. This dataset was used to synthesize reflected radiance spectra as well as create a low-dimensional linear model for

each tissue region to model illumination variations. The recognition algorithm projected the reflected radiance spectra of the different tissue types onto the linear models of each subset. The study was able to obtain similar results with 90% of probes correctly identified in the top 3 matches. [40]

### 2.5 Summary

HSI has the potential to enhance a dismount characterization system by using the spectral properties of skin. A system using HSI would benefit from the abundant data collected across a large portion of the electromagnetic spectrum. Since skin has characteristic optical properties because of melanin, hemoglobin, bilirubin, and $\beta$-carotene concentration, certain bands in the spectrum can be used to focus on relevant data. This is important because HSD is high dimensional and highly correlated therefore dimension reduction and classification techniques are required to properly analyze the data. Similar techniques were used in studies where HSI enhanced the performance of facial recognition. These studies were able to identify individuals based on the spectral properties of their skin with higher accuracy than traditional facial recognition methods. In addition, it was shown that an individual could be matched with their spectra with up to a five week period between image sessions. These studies confirm the viability of using HSI to distinguish individuals based on their skin. Unlike dismount characterization these results were recorded in a controlled environment. Issues such as distance, illumination variation, and skin location will need to be addressed in order to establish a profitable dismount characterization system.

# III. Methodology

THE methodological process for this thesis will consist of two major tasks: feature selection and classification. The feature selection portion will involve processing skin reflectance measurements collected using a laboratory spectroradiometer with the fast based correlation filter (FCBF) method [51]. This feature selection method will select an optimal feature subset that will be used to classify the hyperspectral data (HSD). The data is classified using a multi-layer artificial neural network (ANN). The performance of the ANN will be determined by its ability to locate a dismount of interest (DOI) amongst a group of non-DOI's.

This chapter will explain the details of data collection, feature selection, and classification. Section 3.1 describes the data that is collected using the spectroradiometer and the necessary equipment calibration. Section 3.2 will discuss the how the data is normalized. Section 3.3 will explain the FCBF feature selection method. Section 3.4 is a description of the ANN that is trained to classify the data.

## 3.1 Data Description

The hyperspectral skin data for this thesis is collected using a ASD FeildSpec3 Hi-Res spectroradiometer [1] with a contact probe. The contact probe provides complete contact with the skin to reduce the effects of environmental noise. In addition, the contact probe has a calibrated illumination source to control illumination variance. Each skin sample is collected from 350nm to 2500nm with 1nm spectral resolution. Figure 3.1 is an example skin reflectance measurement collected with the spectroradiometer. Each skin sample collected is labeled with an identifier to annotate its association with a specific dismount.

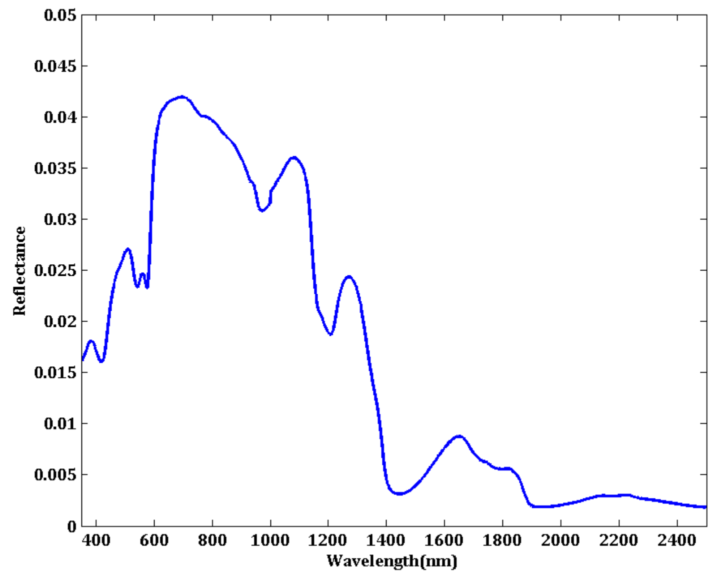


Figure 3.1: Example skin measurement from the ASD FeildSpec3 Hi-Res spectroradiometer.

In collecting the data, a variety of calibration techniques are required. These calibration steps are completed by using the data acquisition software supplied by ASD. The first calibration step is called optimization. This step ensures that the spectrometer is calibrated for the specific light source used in the experiments. The contact probe uses an incorporated halogen light source. The white reflectance step is achieved by collecting data from a white reflectance panel which represents a pure reflectance across 350nm to 2500nm. This step is completed between each collection to ensure the data is restricted between 0 and 1. [1]

### 3.2 Normalization

To preprocess the data each instance is normalized. The normalization step ensures that the data are standardized before analysis. This step is important to prevent any undue

biasing of the classifiers. The data is normalized by using the following equation [39]:

$$\overline{\boldsymbol{R}} = \frac{R}{||R||}, \tag{3.1}$$

where $R$ is the unnormalized spectral reflectance vector, and $||\cdot||$ is the $\ell^2$-norm.

### 3.3 Feature Selection

Hyperspectral data typically has redundant and irrelevant features that effect the classification accuracy [17, 51]. The goal is to determine only the wavelengths that are necessary for dismount identification. The method of feature selection chosen for this thesis is FCBF proposed by Yu *et al.* [51]. This method is specifically designed for high dimensional data because of its reasonable time complexity and its ability to identify redundant features. The symmetrical uncertainty (SU) described in Section 2.3.1.3 is used to determine the relevance of each feature. To select the features, a method called predominant correlation is proposed to identify the relevant and redundant features. To implement the method of predominant correlation, Yu *et al.* proposed three heuristics to identify the important features without analyzing the pairwise correlations between all the relevant features [51].

The FCBF method determines whether a feature is relevant to the class concept. A feature is deemed relevant if the SU value is greater than a user defined threshold. The SU value, that measures the correlation between class $C$ and feature $F_i$, is denoted as $SU_{i,c}$. Therefore, $S'$ is the subset of relevant features that is populated by features that have an SU value of $SU_{i,c} \geq \delta$, where $\delta$ is the threshold. [51]

The FCBF also determines the redundant features among the list of relevant features. Yu *et al.* uses a method called predominant correlation to remove the redundant features. The feature $F_i$ is determined to be predominant if and only if the $SU_{i,c} \geq \delta$ and no other feature ($F_j$) exists such that $SU_{j,i} \geq SU_{i,c}$. This method uses three heuristics that dictate when a feature is deemed redundant to another relevant feature. The heuristics are used to

prevent pairwise correlation calculations amongst all of the relevant features. The assumption is that there exists a feature ($F_j$) that is a redundant peer to $F_i$ and that $S_{R_i}$ is the set of all redundant peers to feature $i$. The list $S_{R_i}$ is divided into two parts, $S^+_{R_i}$ occurs when $SU_{j,c} > SU_{i,c}$ and $S^-_{R_i}$ occurs when $SU_{j,c} \leq SU_{i,c}$. [51] The heuristics are described as follows [51]:

- **Heuristic 1**: If $S^+_{R_i}$ list is empty, then treat $F_i$ as the predominant feature, remove all the features in $S^-_{R_i}$, and skip identifying the redundant peers for the features listed in $S^-_{R_i}$. [51]
- **Heuristic 2**: If $S^+_{R_i}$ is not empty, then process all features in $S^+_{R_i}$ before making a decision to remove $F_i$. If none are predominant, follow Heuristic 1; otherwise only remove $F_i$ and remove features in $S^-_{R_i}$ based on other features in $S'$. [51]
- **Heuristic 3**: The feature with the largest $SU_{i,c}$ value is always a predominant feature and can be a starting point to remove other features. [51]

### *3.3.1 Fast Correlation Based Filter Algorithm.*

The three heuristics are implemented in the FCBF algorithm described in the psuedocode labeled Algorithm 1 [51]. The input to the algorithm is a data set that contains $N$ features with labeled classes ($C$) and a predetermined threshold value $\delta$. The ouptut of the algorithm is $S_{best}$, which the list of ranked predominant features. There are two distinct parts in the algorithm. The first part is contained in lines 1-5. The SU value is calculated for every feature and deemed relevant if the value is greater than the threshold, $\delta$. The relevant features are stored in a list called $S'_{list}$ and sorted in descending order based on the SU value. In the second part, lines 6-14, the $S'_{list}$ is processed to remove the redundant features. Starting at Heuristic 3, the feature with the highest SU value is deemed the predominant feature $F_a$. The next feature on $S'_{list}$ is saved as $F_b$ and compared to $F_a$. If $F_b$ is found to be a redundant peer to $F_a$ it will be removed from $S'_{list}$. This

**Algorithm 1:** FCBF created by Yu *et al.* finds the optimal feature subset of a labeled training data set by evaluating the symmetrical uncertainty value [51].

**Input**: $S(F_1, F_2, ..., F_N, C)$: A labeled training data set

$\delta$: A predefined relevance threshold

**Output**: $S_{best}$: optimal subset of selected features

**for** $i = 1$ *to* $N$ **do**
- $SU_{temp} \leftarrow SU_{i,c}$ for $F_i$
- **if** $SU_{temp} \geq \delta$ **then**
  - append $F_i$ to $S'_{list}$

Sort $S'_{list}$ in descending $SU_{i,c}$value

$F_a \leftarrow$ first element of $S'_{list}$

**while** $F_a \neq NULL$ **do**
- $F_b \leftarrow$ next element of $S'_{list}$ after $F_a$
- **while** $F_b \neq NULL$ **do**
  - **if** $SU_{a,b} \geq SU_{b,c}$ **then**
    - remove $F_b$ from $S'_{list}$
  - $F_b \leftarrow$ next element of $S'_{list}$ after $F_b$
- $F_a \leftarrow$ next element of $S'_{list}$ after $F_a$

$S_{best} \leftarrow S'_{list}$

**return** $S_{best}$;

continues by comparing $F_a$ to all the other features in the list. Then the next feature on $S'_{list}$ becomes the new predominant feature $F_a$ and the comparison continues until no more features can be removed from the list. [51]

## 3.4 Classification

The final step of the data analysis methodology is classification. For this research, a multilayer neural network is used to classify the data. The back propagation algorithm as described in Section 2.3.2.2 is used to train the neural network. The network has $N$ inputs which is the number of features selected from the FCBF algorithm. The number of neurons in the hidden layers is determined by the following equation [13]:

$$h = \frac{N + O}{2} \tag{3.2}$$

where $h$ is the number of neurons in the hidden layers, $N$ is the number of features (inputs), and $O$ is the number of classes (outputs). The other predetermined parameters of the neural network include the learn rate, momentum, number of hidden layers, number of epochs, and $K$ for K-folds cross validation. These parameters are fixed throughout the training and testing of the classifier to ensure consistency of the results.

### *3.4.1 Dismount of Interest (DOI) Training and Testing Model.*

For this thesis, the performance of the feature selection and classification methods are determined by the ability to locate a dismount of interest (DOI). A DOI refers to a dismount that the system has been trained to find amongst a group of other dismounts. The neural network is trained using data samples from the DOI and samples from other dismounts using the one versus all method. This means that there are two classes, the first class is the DOI and the second class is the other dismounts which are treated as one class. Once the network is trained, the neural network model is saved and tested on another data set. This data set contains skin data from a larger group of dismounts that were not used during training. The one versus all model is used again for testing the DOI class versus the other class, consisting of samples from all of the other dismounts. Figure 3.2 is a depiction of the testing and training model. The red figure represent the DOI while the black figures represent the non-DOI's which are considered one class by the neural network.

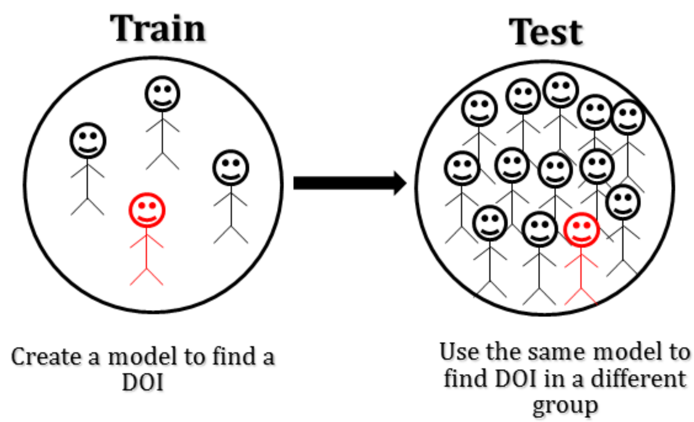


Figure 3.2: Depiction of the DOI training and testing model. The red figure represents the DOI while the black figures represent the non-DOI's. The model is created by training an artificial neural network to find a DOI amongst a small group of non-DOI's. The model is saved and tested to find the same DOI amongst a larger group of new non-DOI's.

### 3.5 Summary

The methodological process consists of feature selection and classification. The data is collected using a spectroradiometer, which collects skin reflectance measurements from 350nm to 2500nm with 1nm resolution. The data is then analyzed in three main steps: normalization, feature selection, and classification. The FCBF [51] was selected as the feature selection method because of its ability to efficiently process high dimensional data. This method extracts the relevant features by calculating the symmetrical uncertainty value for every feature. The redundant features are then eliminated by following a heuristic search approach. Finally, the reduced data set is classified using a ANN that is trained and tested to find a DOI.

# IV. Results and Analysis

The fast correlation based filter (FCBF) method is applied to a data set containing forearm skin reflectance measurements from 62 different dismounts (classes). The top four features selected by the FCBF are used to train and test a neural network for classification. The performance of the FCBF method was compared with three other feature selection methods. The standard deviation of the classes are evaluated to determine the average within and between class variability.

This chapter presents an overview of the data collected for this thesis in Section 4.1. Section 4.2 discusses the results and analysis of the FCFB feature selection method. Section 4.3 presents the neural network classifier's ability to locate a dismount of interest (DOI) amongst a group of 62 other dismounts. Section 4.3.2 compares the performance of the FCBF method to other feature selection methods. Finally, Section 4.4 discusses the results of the standard deviation tests to analyze within and between class variability.

## 4.1 Data

Hyperspectral skin data is collected using a ASD FeildSpec3 Hi-Res spectroradiometer [1] with a contact probe. Each measurement is collected from 350nm to 2500nm with 1nm spectral resolution which results in 2150 features per sample. Each collection from the spectroradiometer is an average of 10 separate measurements. The experimental set up consisted of subjectively recording the skin color of each dismount producing a range from fair to dark. The data only contains samples from dismounts that have fair to tan skin. To standardize the data set the dark skin samples were removed. A summary of the data sets and the corresponding color of each dismount are summarized in Appendix A.

Table 4.1: Description of the number of data samples within the training and testing data sets.

| Data Set | Number of Samples |
|---|---|
| Training | 90 DOI<br>300 non-DOI |
| Testing | 10 DOI<br>620 non-DOI |

There are two distinct data sets, the testing and training sets, which are described in Section 3.4.1. The training set is the collection of four dismounts of 100 forearm samples each, where one of the dismounts is the DOI. Ten samples of the DOI are randomly selected and held out for the testing group. In the training data set there are 90 samples of the DOI and 300 samples of the non-DOI's. The testing group is created by combining the 10 randomly selected samples of the DOI with a group of *different* non-DOI's. The non-DOI's in the testing set were not used for training in order to mimic a real world scenario. A model is trained to discriminate a specific dismount (DOI) amongst a small group of dismounts (non-DOI's) and then tested amongst a larger group. This group of non-DOI's consist of 62 dismounts with 10 forearm samples each. Therefore, the testing data set consists of 10 samples of the DOI and 620 samples of non-DOI's. Table 4.1 summarizes the number of samples of the DOI and non-DOI's in the testing and training data sets. Overall, the neural network is trained to find one DOI amoungst a group of three non-DOI's and tested to find the same DOI amongst a new group of 62 non-DOI's.

The average skin reflectance measurements for each dismount are plotted in Figure 4.1 and Figure 4.2. The skin reflectance measurements of each dismount are plotted separately in Appendix B. Evaluating the magnitude of the reflectance plots, it is evident

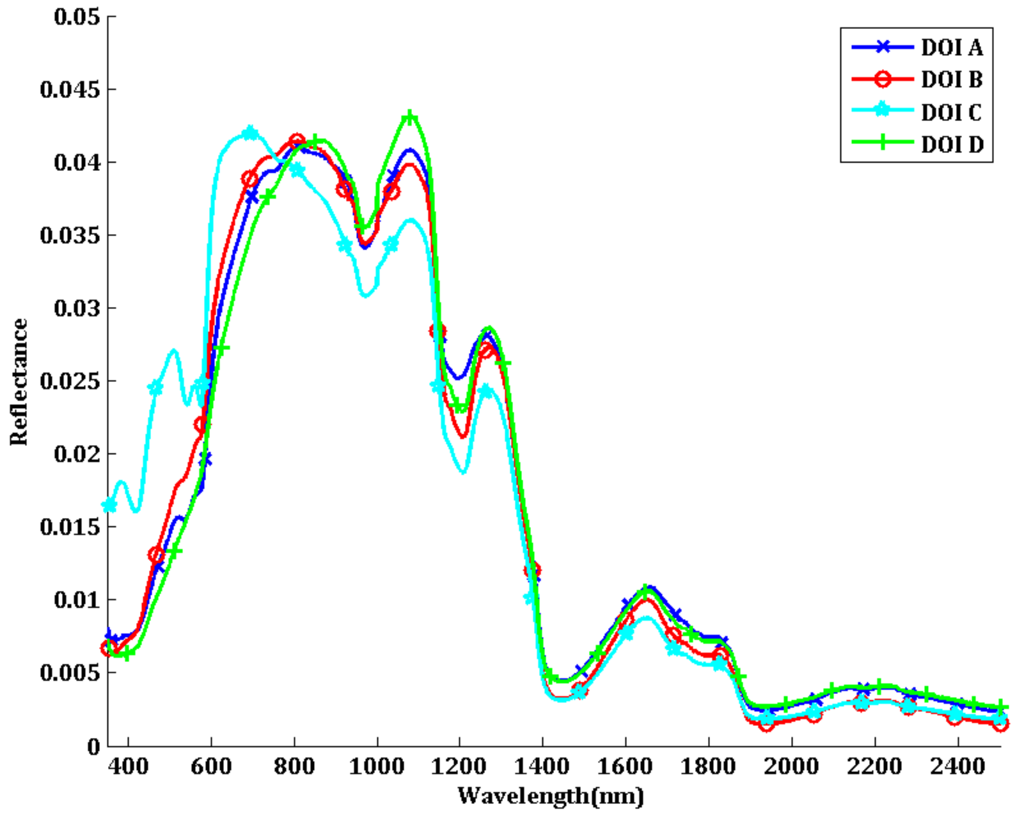


Figure 4.1: Average of 100 samples of forearm hyperspectral reflectance measurements from the 4 DOI's in the training data set.

that within the data set there is a wide range a melanin concentrations ( 350-1000nm). This is determined by the shape of the reflectance measurement as discussed in Section 2.2.1. For example, in Figure 4.1 DOI C has a noticeably different shape than the other DOI's. The different shape of DOI C is due to melanin concentration since DOI C was recorded to have fair skin whereas the other DOI's where recorded to have noticeably tan skin, see Appendix A. As discussed in Section 2.2.2, the hemoglobin feature around 560nm is dominated by melanin for individuals with high concentration of melanin. This

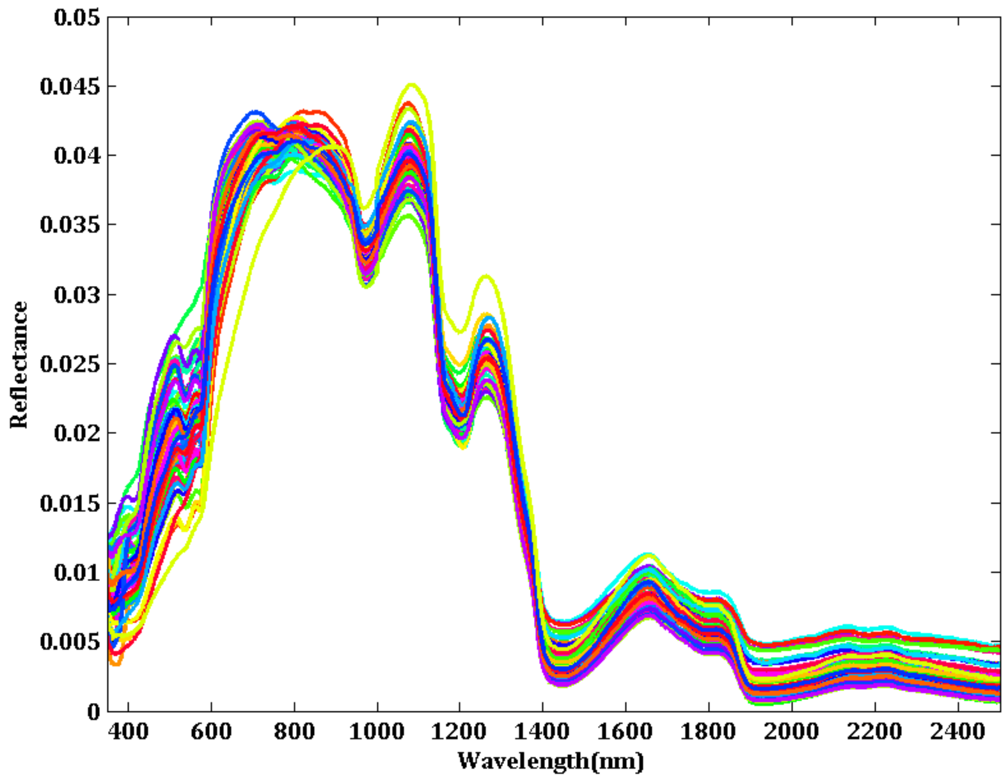


Figure 4.2: Average of 10 samples of forearm hyperspectral reflectance measurements from the 62 non-DOI's in the testing data set. Each colored line represents the reflectance measurements of a different dismount.

is evident on the reflectance measurement because the DOI's with high melanin concentration have a diminished *w*-shaped hemoglobin features.

### 4.2 Feature Selection

The fast correlation based filter (FCBF) is applied to the labeled data set that contains 62 dismounts, 10 samples each of forearm data. Feature selection was completed on this data set because it is the most diverse data set available for this thesis. The algorithm returns an optimal feature subset that contains the ranked features based on the calculated

symmetrical uncertainty (SU) value. For this data set the algorithm returned 100 ranked features. Figure 4.3 depicts the top 20 selected features (vertical blue lines) on the plot of the average skin reflectance measurements of the 62 dismounts. The majority of the selected features are concentrated around the 1000nm to 1200nm location. This region is dominated by the melanin chromophore. In addition, a feature at 500nm is selected which is the location of the hemoglobin feature.

To select the optimal number of features to use for classification, a neural network is trained and tested using DOI A as the selected DOI. The number of features are increased at each iteration and the amount of non-DOI instances that are misclassified as the DOI is recorded. Figure 4.4 depicts the effects of increasing the number of features on classification accuracy. Training the neural network with the top four features from the FCBF method results in the best classification accuracy. Using less than four features the DOI cannot be distinguished amongst the 62 non-DOI's. As the number of features increase past four, the misclassified instances remains steady. The top four features that were selected are 1024, 1014, 1033, and 1348nm. Figure 4.5 shows the top four features represented as blue vertical lines on the reflectance plot of the 62 dismounts. The feature selection is conducted only on the 62 dismounts from the testing data set. Using these four features the classifier was able to discriminate the four DOI's in the training set even though these dismounts were not used in the feature selection process. This indicates that the four selected features are candidates for a global feature set that provides a high degree of classification of dismounts. Creating a true global feature set is intractable because the selected features are dependent on the diversity of the data set. To create a semi-global feature set, feature selection must be applied to a large and diverse data set. Collecting skin reflectance from a diverse populous is both expensive and time consuming, therefore the data set containing the 62 dismounts is used to represent a diverse data set, even

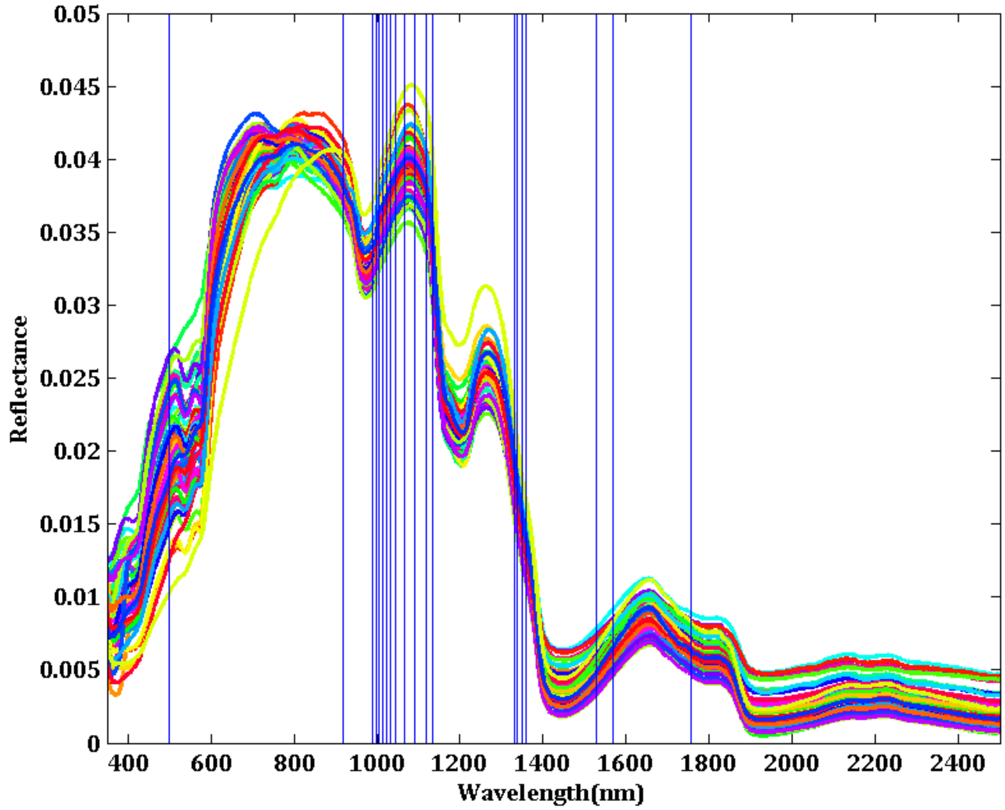


Figure 4.3: Top 20 selected features using the FCBF feature selection method. The blue vertical lines are a visual representation of the spectral location of the selected features. For example, the vertical line on the far left is the selected feature 499nm. The FCBF method iss applied to the forearm reflectance measurements of 62 dismounts. The colored lines are the average reflectance of each dismount.

though the same 62 dismounts where used during testing. Ideally, an entirely new testing data set would be used however this was not possible for the limited scope of this thesis.

## 4.3 Classification

The neural network is trained using the four selected features to discriminate one DOI from a group of four non-DOI's. The learned model is used to find the same DOI amongst

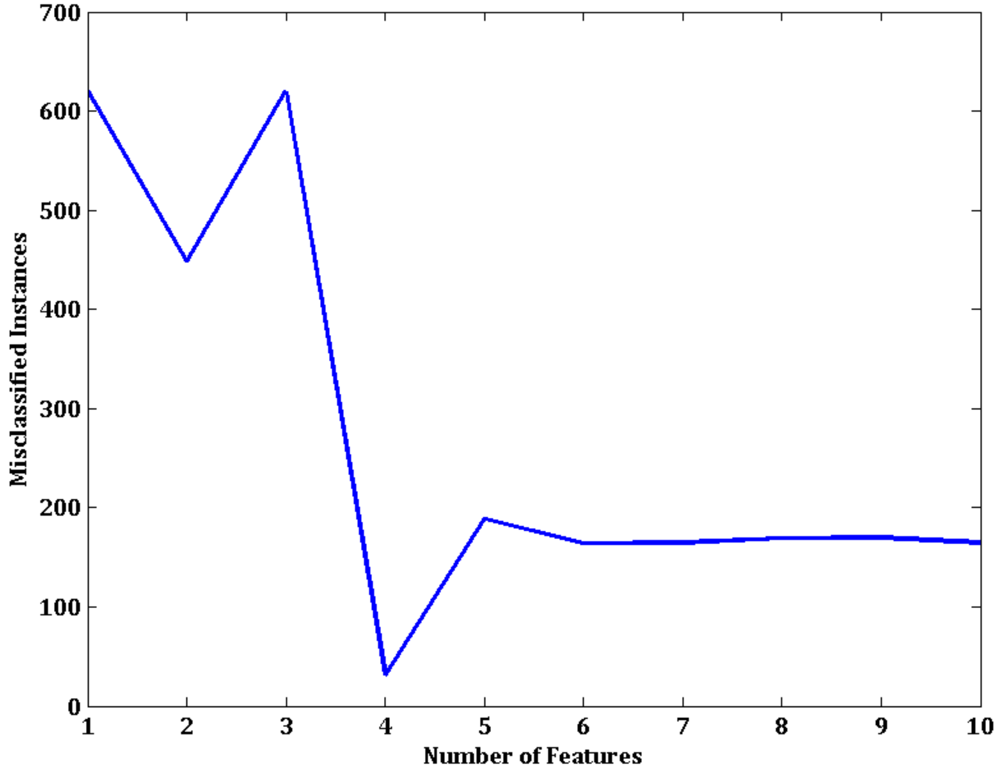


Figure 4.4: Effects of increasing the amount of selected features on testing classification accuracy. The amount of misclassified instances represent the number of instances of non-DOI instances that were incorrectly misclassified as DOI A during training. As the number of features increases the accuracy of the classifier increases until four features. At four features, only 31 instances are misclassified, resulting in the best classification performance. The accuracy of the classifier remains relatively steady after four features.

a group of 62 different non-DOI's. The parameters of the ANN are summarized in Table 4.2. The number of features (inputs) is four and the number of classes (outputs) is two, resulting in three neurons in the hidden layer. The learn rate and momentum are related to the amount of change that occurs to the weights between each iteration. The epoch parameter refers to the amount of times the entire data set is sent through the

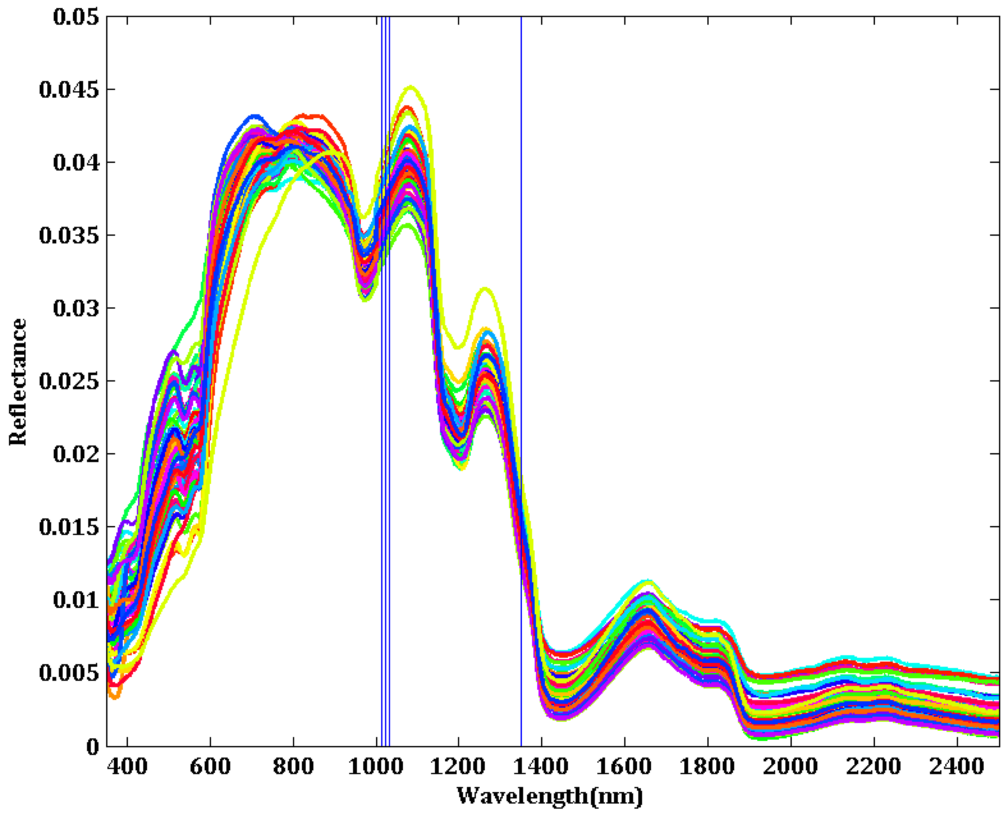


Figure 4.5: Location of top four selected features using the FCBF feature selection method. The blue vertical lines are a visual representation of the spectral location of the selected features. The selected features are 1024, 1014, 1033, and 1348nm.

network during each training fold. Finally, the cross validation parameter refers to K-folds cross validation where in this case $K = 5$.

The classification performance is evaluated for four different DOI's in four separate tests. These four separate tests are used to validate that the selected features will work for more than just one DOI. For each test, a different classification model is trained to discriminate a new DOI from the 3 other non-DOI's. Table 4.3 displays the contingency table for each DOI for the training and testing scenarios.

Table 4.2: Summary of neural network parameters implemented in WEKA® [13].

| **Parameter** | **Value** |
|---|---|
| Inputs | 4 ($N$, number of features) |
| Outputs | 2 ($O$, number of classes) |
| Neurons in hidden layer | $3 \left(h = \frac{N+O}{2}\right)$ |
| Hidden layers | 1 |
| Activation Function | Sigmoid: $f(x) = (1 + e^{-x})^{-1}$ |
| Learning rate | 0.3 |
| Momentum | 0.2 |
| Epochs | 500 |
| Cross Validation ($K$) | 5 |

In addition, Table 4.4 summarizes the equal-weighted accuracy (EWA) for each DOI tested. The EWA is calculated as:

$$EWA = \frac{1}{C} \sum_{c=1}^{C} \frac{A_c}{M_c} \tag{4.1}$$

where $C$ is the number of classes, $c$ is the class under evaluation, $A_c$ is the number of correctly classified instances for class $c$, and $M_c$ is the number of samples in class $c$. Table 4.4 lists the amount of non-DOI instances that are classified as the DOI during testing. For example in the DOI A test, 31 non-DOI's instances are classified as the DOI. In addition, the table lists the amount of "full" and "partial" misclassified dismounts. A "full" misclassified dismount means that every instance associated with a certain non-DOI is classified as the dismount. A "partial" misclassified dismount means that only a few instances of a particular non-DOI are misclassified. A partial misclassified dismount is assumed to not be the DOI, since the dismount is not completely misclassified as the DOI.

Table 4.3: Contingency tables for each DOI test for both training and testing of the ANN model.

| | **Training** | | | | **Testing** | | | |
|---|---|---|---|---|---|---|---|---|
| **DOI A** | | **Classified As** | | | | **Classified As** | | |
| | **Actual Class** | DOI A | Non-DOI | Total | **Actual Class** | DOI A | Non-DOI | Total |
| | DOI A | 90 | 0 | 90 | DOI A | 10 | 0 | 10 |
| | Non-DOI | 0 | 300 | 300 | Non-DOI | 31 | 589 | 620 |
| | Total | 90 | 300 | | Total | 41 | 589 | |
| **DOI B** | | **Classified As** | | | | **Classified As** | | |
| | **Actual Class** | DOI B | Non-DOI | Total | **Actual Class** | DOI B | Non-DOI | Total |
| | DOI B | 90 | 0 | 90 | DOI B | 10 | 0 | 10 |
| | Non-DOI | 0 | 300 | 300 | Non-DOI | 64 | 556 | 620 |
| | Total | 90 | 300 | | Total | 74 | 556 | |
| **DOI C** | | **Classified As** | | | | **Classified As** | | |
| | **Actual Class** | DOI C | Non-DOI | Total | **Actual Class** | DOI C | Non-DOI | Total |
| | DOI C | 90 | 0 | 90 | DOI C | 10 | 0 | 10 |
| | Non-DOI | 0 | 300 | 300 | Non-DOI | 262 | 358 | 620 |
| | Total | 90 | 300 | | Total | 272 | 358 | |
| **DOI D** | | **Classified As** | | | | **Classified As** | | |
| | **Actual Class** | DOI D | Non-DOI | Total | **Actual Class** | DOI D | Non-DOI | Total |
| | DOI D | 90 | 0 | 90 | DOI D | 10 | 0 | 10 |
| | Non-DOI | 0 | 300 | 300 | Non-DOI | 50 | 570 | 620 |
| | Total | 90 | 300 | | Total | 60 | 570 | |

Table 4.4: Training and testing classification performance for each DOI test. A "full" means that every instance of a non-DOI was classified as the DOI. A "partial" means that not all instances of the non-DOI was classified as the DOI.

| | **DOI A** | **DOI B** | **DOI C** | **DOI D** |
|---|---|---|---|---|
| Training | Equal-weighted Accuracy (%) | | | |
| | 100 | 100 | 100 | 100 |
| Testing | Equal-weighted Accuracy(%) | | | |
| | 97.5 | 94.8 | 78.8 | 95.9 |
| | Misclassified Instances | | | |
| | 31 | 64 | 262 | 50 |
| | "Full" Misclassified Dismounts | | | |
| | 3 | 6 | 24 | 5 |
| | "Partial " Misclassified Dismounts | | | |
| | 1 | 3 | 2 | 0 |

Using DOI A as an example, the results explain that a model can be trained to find the DOI amongst a group of 62 other individuals and narrow down the lists of possible DOI's to four suspects, which includes the actual DOI. This is a reasonable reduction of possible dismounts and when combined with other forms of identification such as facial recognition and clothing identification.

### *4.3.1 Importance of a Diverse Training Data Set.*

Table 4.4 indicates that for DOI C, there are 24 misclassified dismounts which is significantly higher then the other three dismounts. DOI C has fair skin relative to the other dismounts in the training set. Therefore, the model keyed in on the discrimination of fair versus dark skin rather than a specific DOI. To obtain a higher accuracy of identifying

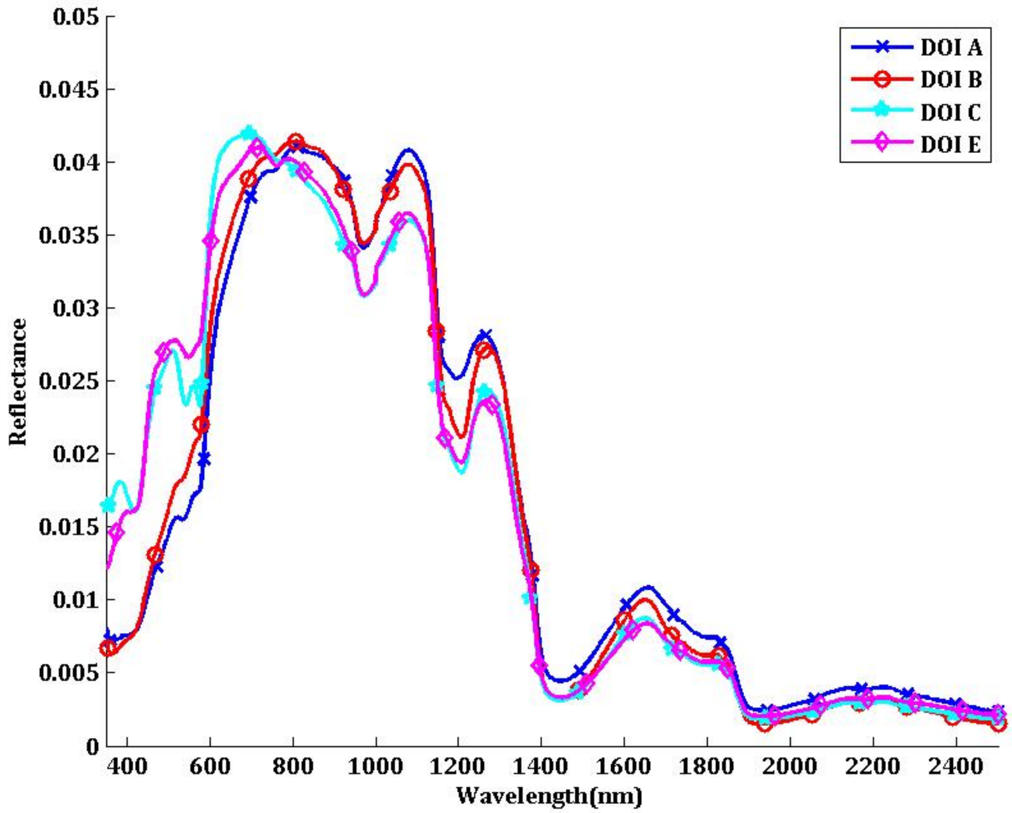


Figure 4.6: Average reflectance measurements for the updated training set that omit samples from DOI D and includes samples from DOI E.

DOI C amongst the 62 diverse dismounts, a better diverse dismount representation in the training data set is required. More specifically, instead of having three dark skin DOI's and one fair skin DOI, the updated training set contains two dark skin and two fair skin dismounts. This ensures that the model will distinguish a specific DOI amongst a diverse group of non-DOI's, for this research a diverse group is a mixture of fair and dark skin dismounts. Figure 4.6 displays the average reflectance measurements of the updated training set. This set omits the skin samples from DOI D and incorporates samples from DOI E which is recorded as having fair skin. Incorporating DOI E into the training set

Table 4.5: Contingency tables from DOI C with diverse training set that omits samples from DOI D and includes samples from DOI E.

| | Training | | | | | Testing | | | | |
|---|---|---|---|---|---|---|---|---|---|---|
| | | **Classified As** | | | | | **Classified As** | | | |
| | | DOI C | Non-DOI | Total | | | DOI C | Non-DOI | Total | |
| **DOI C** | **Actual Class** DOI C | 90 | 0 | 90 | **Actual Class** DOI C | 10 | 0 | 10 | | |
| | Non-DOI | 0 | 300 | 300 | Non-DOI | 0 | 620 | 620 | | |
| | Total | 90 | 300 | | Total | 10 | 620 | | | |

creates a more diverse training data set to create an effective model for discriminating DOI C from the other dismounts. Table 4.5 displays the resulting DOI C contingency table using the diverse training data set. This tests emphasizes the importance of a diverse training data set, the original test misclassified 24 dismounts, using the new model the classifier was able to identify DOI C with 100% accuracy.

### *4.3.2 Comparison of Feature Selection Methods.*

The performance of the FCBF method is compared with the features selected by ReliefF [25],ClassifierSubsetEval a wrapper method using genetic search [13], and ConsistencySubsetEval a consistency evaluator with greedy stepwise search [30]. The top four selected features for each method are recorded in Table 4.6. In addition, the selected features are plotted on a skin reflectance measurement in Figure 4.7. The consistency evaluator chose only three features as the optimal subset. As expected, the ReleifF method returned a group of consecutive features because it relies on nearest neighbor comparisons to select relevant features. As discussed in Section 2.3.1.2, ReleifF does not focus on removing redundant features [51]. The wrapper method combines the Naïve Bayes classifier with a genetic search [13]. This method trains a Naïve Bayes classifier using a randomly selected feature subset, also called a population.

Table 4.6: Top features selected from the 62 dismounts forearm data set using FCBF [51], ReliefF [25], wrapper method using genetic search [13], and a consistency evaluator [30] feature selection methods.

| **Feature Selection Method** | **Selected Features (nm)** |
|---|---|
| FCBF | 1024, 1014, 1033, and 1348 |
| ReleifF | 938, 937, 939, 940 |
| ClassifierSubsetEval | 541, 593, 673, 741 |
| ConsistencySubsetEval | 357, 487, 1528 |

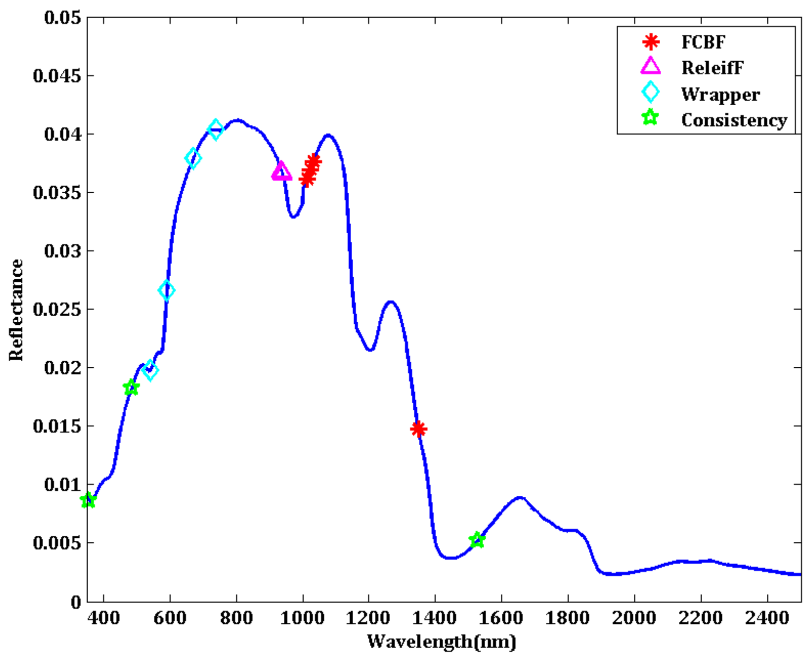


Figure 4.7: Comparison of features selected by FCBF [51], ReliefF [25], wrapper method using genetic search [13], and a consistency evaluator [30]. The different shapes represent the locations of the selected features from the different methods on a typical skin reflectance measurement.

Table 4.7: Contingency tables from DOI A using the feature subsets determined by ReleifF [25], wrapper, and the consistency evaluator methods [30].

| | Training | | | | Testing | | | |
|---|---|---|---|---|---|---|---|---|
| | | Classified As | | | | Classified As | | |
| | Actual Class | DOI A | Non-DOI | Total | Actual Class | DOI A | Non-DOI | Total |
| **FCBF** | DOI A | 90 | 0 | 90 | DOI A | 10 | 0 | 10 |
| | Non-DOI | 0 | 300 | 300 | Non-DOI | 31 | 589 | 620 |
| | Total | 90 | 300 | | Total | 41 | 589 | |
| **ReliefF** | DOI A | 0 | 90 | 90 | DOI A | 10 | 0 | 10 |
| | Non-DOI | 0 | 300 | 300 | Non-DOI | 190 | 430 | 620 |
| | Total | 0 | 390 | | Total | 200 | 430 | |
| **Wrapper** | DOI A | 88 | 2 | 90 | DOI A | 10 | 0 | 10 |
| | Non-DOI | 0 | 300 | 300 | Non-DOI | 149 | 471 | 620 |
| | Total | 88 | 302 | | Total | 159 | 471 | |
| **Consistency** | DOI A | 90 | 0 | 90 | DOI A | 10 | 0 | 10 |
| | Non-DOI | 0 | 300 | 300 | Non-DOI | 135 | 485 | 620 |
| | Total | 90 | 300 | | Total | 145 | 458 | |

The fitness value of the population (i.e. the performance) is evaluated and the population evolves and mutates until an acceptable classifier performance is achieved [33]. This method is efficient, however, the relevance of every feature is not evaluated and its performance is dependent on the selection of the initial population. The consistency evaluator determines the worth of a subset of features by the level of consistency in the class values when each training instance is projected onto the feature subsets [30].

To determine the performance of the other feature selection methods, a neural network is trained to find DOI A using the different feature subsets. Table 4.7 displays the training and testing contingency tables for each feature selection method. Based on these results, the FCBF method selected the best feature subset. On average the other feature selection methods had 15-20 misclassified dismounts as opposed to only 3 with the FCBF method. This test also illustrates the impact of selecting the correct feature subset on classification performance.

## 4.4 Standard Deviation Test

To study the feasibility of extending this method to a real world application of dismount identification, the standard deviation amongst different skin locations (e.g. forearm, hand, cheek, forehead) is evaluated. A robust identification system should function regardless of the location on a dismount. Understanding the variance of the skin measurements locations provides insight on this methods operability irrespective of the skin location imaged. The performance of a classifier is dependent on class separability, specifically, the variance *between* classes should be high while the variance *within* a class should be low to ensure accurate classification.

#### *4.4.0.1 Within Class Separability.*

The first variance test is completed for the original forearm data that contains the 62 dismounts with 10 samples each. These measurements were taken by placing the contact probe on a specific fixed location on the forearm. This test represents an analysis of the variance *within* a class, which should be relatively small. Figure 4.8 is the standard deviation plot for Dismount 1. The standard deviation plots for the other dismounts are located in Appendix C. The average reflectance is plotted with standard deviation bars at 50nm intervals on the plot. The bars represent the standard deviation between the 10 samples at that particular wavelength. Analyzing the plot, it is evident that there is a

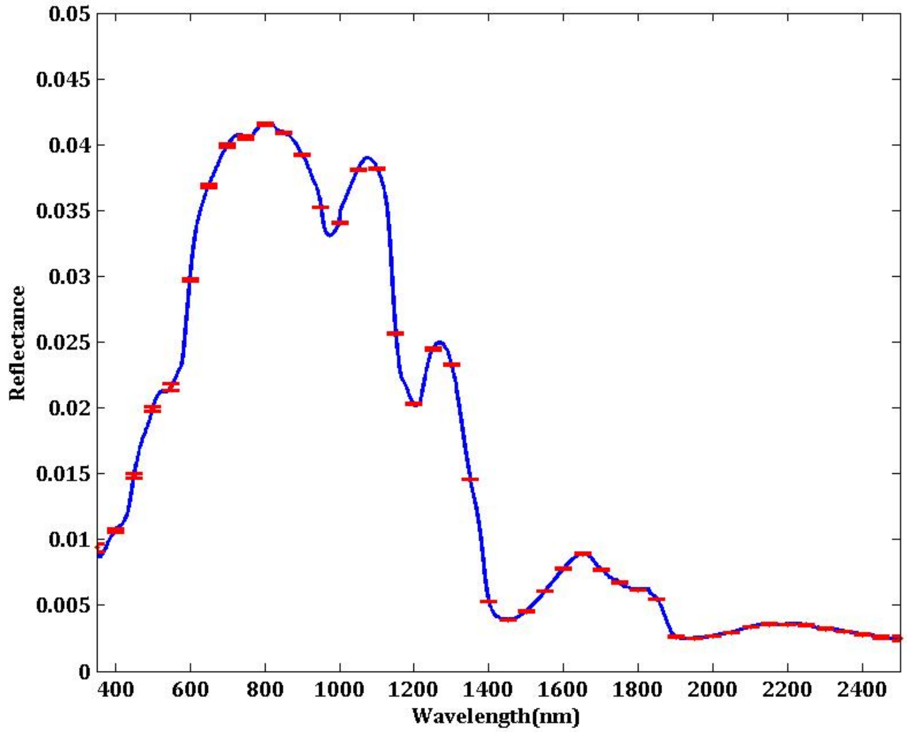


Figure 4.8: Standard deviation plot of one location on the forearm for Dismount 1. The average reflectance is plotted with standard deviation bars at 50nm intervals on the plot. The bars represent the standard deviation between the 10 samples at that particular wavelength.

negligible amount of variance between each measurement. The negligible variance for this test is expected because the contact probe is not moved during the collections.

The within class separability is extended by determining standard deviation for a particular region on each dismount. This is completed by taking skin reflectance measurements of 10 different locations on the forearm for four dismounts. The forearm location is gridded using lines that are projected from a video projector as shown in Figure 4.9. These lines ensure that the reflectance measurements are taken from

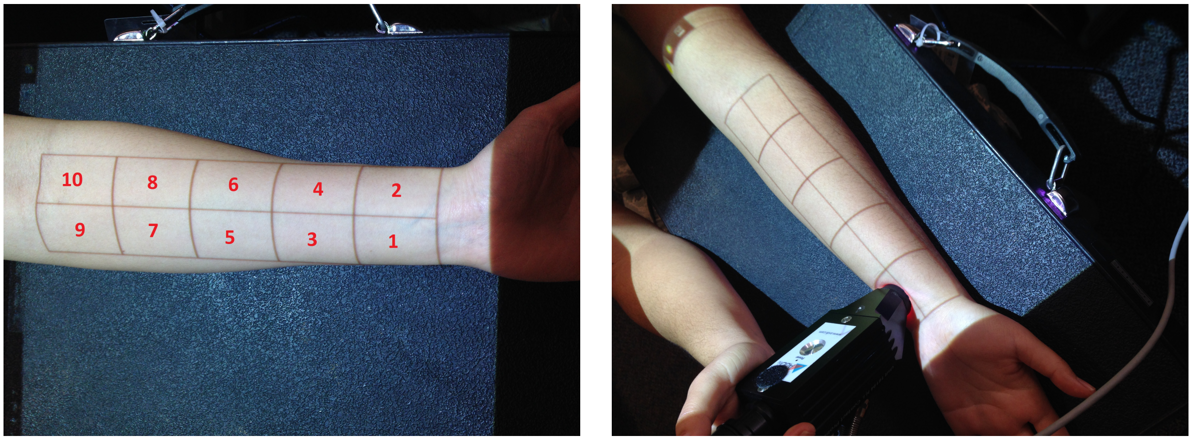


Figure 4.9: Test setup to evaluate variance of forearm skin reflectance measurements. A grid was projected onto the dismounts forearm to indicate the location the contact probe was to be placed for collection. The size of the grid was adjusted to accommodate varying sizes of forearms. The red numbers indicate the order in which the data was collected.

respectively the same location on every dismount. The edge of the gridlines are projected onto the wrist and extended to the crease of the elbow. The size of the grid can be changed to accommodate for the varying sizes of forearm amongst the dismounts. At each grid location 10 samples were collected resulting in 100 samples for each dismount. Figure 4.10 is a plot of the standard deviation for Dismount 1 across the gridded locations of the forearm. The standard deviation plots for all four dismounts for this test are found in Appendix D. The average standard deviation amongst the four dismounts on the gridded forearm is 0.0007 which is 6 times higher than the average standard deviation of the 62 dismounts from one location on the forearm.

The final within class separability test evaluates the standard deviation for different skin regions i.e. back of the hand, palm, forearm, top of the arm, forehead, and cheek and is completed for 10 dismounts each with 10 samples. This test represents typical skin locations that might be passively imaged on a dismount. In order to create a dismount

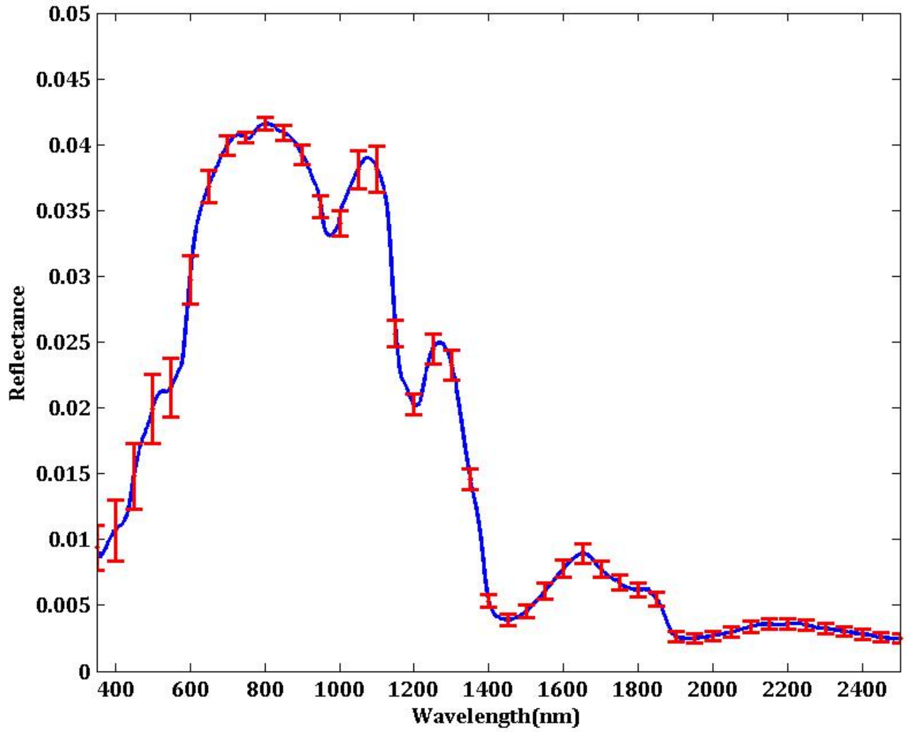


Figure 4.10: Standard deviation plot for the gridded forearm of Dismount 1. The average reflectance is plotted with standard deviation bars at interval positions on the plot. The bars represent the standard deviation between the samples from 10 different locations on the forearm.

identification system that could preform regardless of the skin location this within class variance should be relatively small. Figure 4.11 is a plot of the average reflectance for each location for Dismounts 1 and the standard deviation plot across the different skin locations. Appendix E contains the average reflectance and standard deviation plots for all 10 dismounts. On average for the 10 dismounts the standard deviation is 11 times higher than the variance for one location on the forearm. This within class variance may be an issue for creating a robust dismount classification system that can identify an individual based on any available imaged skin location.

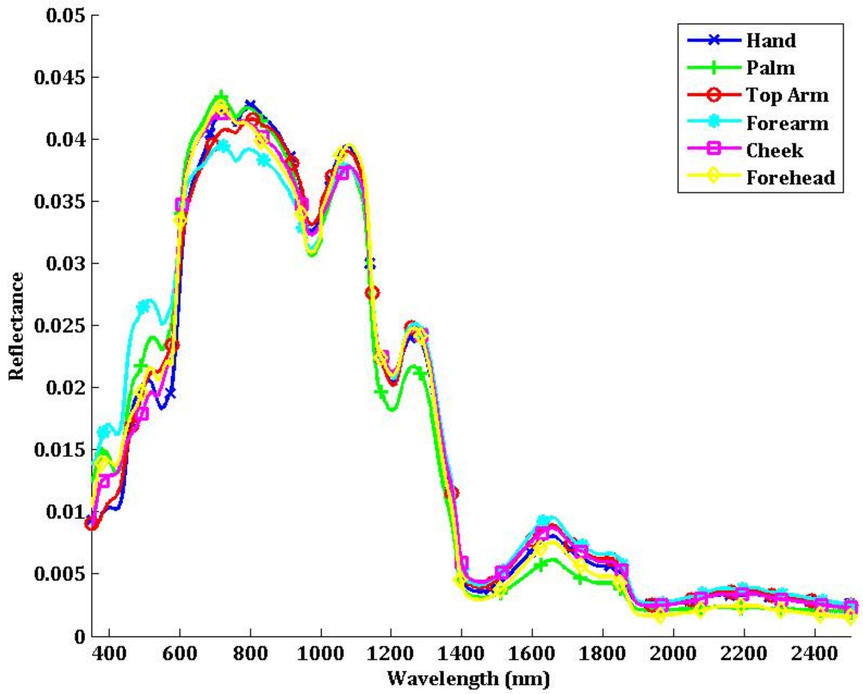


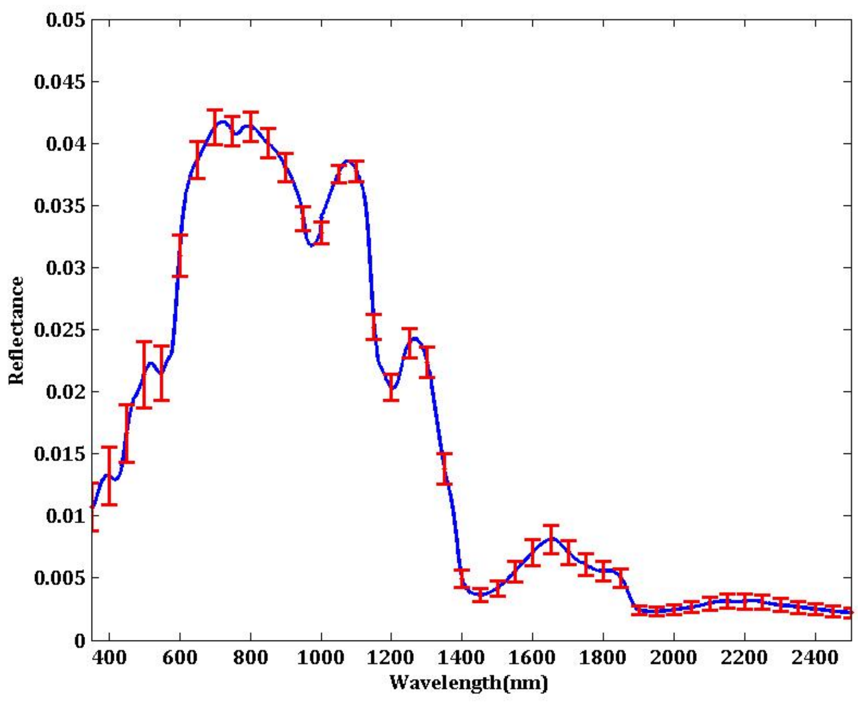


Figure 4.11: Average reflectance for Dismount 1 at each skin region (top). Standard deviation plot for Dismount 1 across the back of the hand, palm, forearm, top of the arm, forehead, and cheek (bottom).

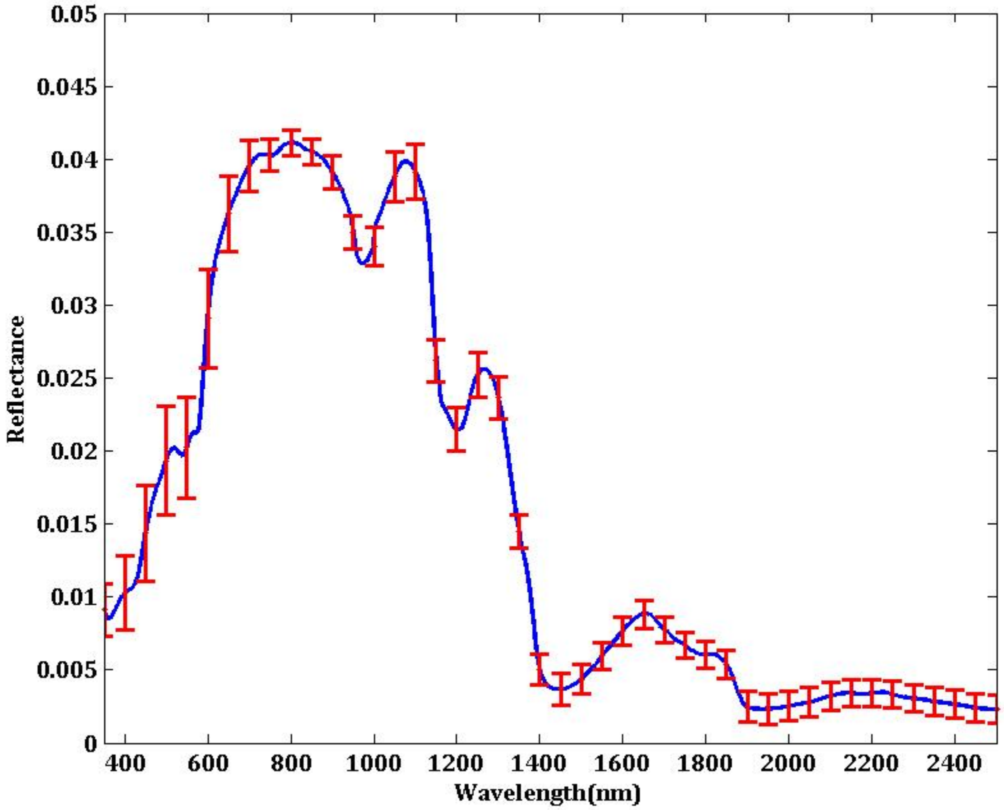


Figure 4.12: Standard deviation plot amongst all 62 dismounts for one location on the forearm

#### *4.4.0.2 Between Class Separability.*

The next test is to evaluate the variance that exists between all 62 dismounts for the forearm location. This test represents an analysis of the variance *between* classes, which should be relatively high. This variance test is important because it is a way to visualize the likelihood of a classifier to discriminate between dismounts. More specifically, a classifier's performance is dependent on the variability between classes. Figure 4.12 is a plot of the standard deviation across all 62 dismounts for the forearm location. The standard deviation for this test is 0.0014 which is 13 times higher than the within class

Table 4.8: Average standard deviation for within and between class scenarios.

| Test | Average Standard Deviation |
|---|---|
| Within Class | |
| Forearm | 0.0001 |
| Forearm (Gridded) | 0.0007 |
| All regions | 0.0012 |
| Between Class | |
| Forearm | 0.0014 |

forearm standard deviation which indicates considerable between class separability. However, when comparing to the all regions standard deviation which analyzes the variations for one dismount over multiple skin locations the standard deviations is only 0.16 times higher. This indicates that it may not be possible to discriminate between dismounts if multiple skin locations (i.e. skin on both the face and hands) are passively imaged to make a dismount identification. The results of the within and between class standard deviation test are summarized in Table 4.8. This table also lists the average standard deviation for each test.

### 4.5 Summary

This chapter demonstrates the results of using the FCBF method to select a subset of four features to locate a particular DOI amongst a group of 62 other dismounts. The neural network is trained to locate the DOI using a one versus all method. In most cases, the group of possible DOI's is narrowed down from 62 dismounts to 3-6 dismounts. This method could be combined with other forms of dismount identification techniques to create a robust multi-modal identification system. The FCBF is compared with three other

feature selection methods to confirm the importance of selecting the correct feature subset. Finally, a variety of standard deviation test were completed to determine the feasibility of using this method for reflectance measurements for imaging multiple skin location among the various dismounts.

# V. Conclusion

Current security and surveillance technologies will benefit from the ability to identify a dismount in an environment. As an example, facial recognition systems seek to identify people based on spatial discriminants such as the structural features of the face [39]. Hyperspectral imaging could enhance facial recognition by providing spectral discriminates, specifically the personal identification patterns determined by the variability of pigment distribution in skin.

However, hyperspectral data is notorious for creating highly redundant and irrelevant data sets. Therefore, it is necessary to reduce the data space to contain only the highly discriminating features. This is accomplished by employing a feature selection method. There are multitude of feature selection methods however, it is necessary to select a method that will not only remove the irrelevant features but also the redundant features.

The problem statement for this thesis was to determine a global feature set that would provide a high degree of classification of dismounts based on the spectral properties of their skin. To select a feature set that was highly discriminant, the fast correlation based filter (FCBF) [51] was applied to a hyperspectral data set collected from the forearms of 62 subjects. This feature selection method outperformed three other methods. An artificial neural network (ANN) was trained to classify the data to identify a dismount of interest (DOI) amongst a group of other dismounts. The trained model was then tested by finding the same DOI amongst a new group of dismounts.

## 5.1 Summary of Results

The FCBF [51] was applied to a data set containing forearm skin samples from 62 subjects. Based on an analysis of increasing the amount of features versus classification performance, the top four features were selected as the optimal feature subset (Figure 4.4).

Using the four features (1014, 1024, 1033, and 1348nm), the classifier was able to reduce the amount of possible DOI suspects from 62 dismounts to 3-6 dismounts (Table 4.4). To validate the performance of the feature selection four separate DOI tests where completed to analyze the performance of identifying four different DOIs. The classifier preformed to an equal-weighted average of 96.9% and combining with other modalities, such as clothing identification, will create a system to uniquely identify a DOI.

The FCBF method was compared to the performance of three feature selection methods: ReliefF [25], wrapper method using genetic search [13], and a consistency evaluator [30] (Table 4.6). The FCBF outperformed the other methods on average with 4 times less misclassified instances. The ability of the FCBF method to locate the redundant features within a set of irrelevant features makes it ideal for the hyperspectral data.

The within and between class separability were evaluated to determine the feasibility of using multiple skin locations i.e. back of the hand, palm, forearm, top of the arm, forehead, and cheek for dismount identification. The *within* class standard deviation across multiple skin location is 0.0012 while the *between* class standard deviation for a separable data set is 0.0014 (Table 4.8). This close margin of standard deviation indicates that it may require different techniques to accurately discriminate a dismount when multiple skin locations are imaged. This is based on the analysis of the average standard deviation for 10 subjects across the skin locations. Further analysis of the within and between class separability will need to be completed in order to establish a conclusion on the feasibility of using multiple skin location for HSI dismount identification.

Overall, the FCBF [51] selected a feature set that provided a high degree of classification of dismounts based on the spectral properties of their skin. Using the four features selected, the amount of possible DOIs was reduced to a manageable subset that can be further analyzed in order to make a unique identification using other forms of identification methods.

## 5.2 Recommendations for Future Work

There are multiple avenues in which this work can be expanded. The first would be a field data collect using a hyperspectral imager rather than a spectroradiometer. Collecting data from a hyperspectral imager will expand this study by determining the effect of environmental factors such as illumination variance on performance. The FCBF method is shown to be effective for multiple kind of hyperspectral data [51]. Applying the FCBF to skin reflectance data collected by a hyperspectral image could select the highly discriminating features to extend this study.

A robust identification system is accurate regardless of the time elapse between identifications. Studies of the spectral difference between collection for dismounts can be studied to determine if hyperspectral dismount identification is time invariant. It has been shown that factors as simple as stress can change the pigmentation of skin [5]. Additionally, a sunburn or tan will create visible changes to the skin and will likely affect the performance of a hyperspectral identification system. The amount of allowable time elapse between identification and significant events (tanning, stress, etc.) should quantified.

This study focused on selecting the correct features for dismount identification. A continuing study could investigate the optimal classification method. For example, the parameters of the ANN could be adjusted in order to achieve maximum classification performance. Like feature selection methods, there are a variety of classification methods that may be better suited for hyperspectral dismount identification.

## Appendix A: Table of Dismount Descriptions

A table that summarizes all the data collected by the ASD FeildSpec3 Hi-Res spectroradiometer with the contact probe. The table includes information about the dismount's skin tone, date of collection, and the skin location of collection.

**KEY:**

| | | | | | |
|---|---|---|---|---|---|
| **F**: | Fair | **DF**: | Dark Fair | **D**: | Dark |
| **BH**: | Back of hand | **P**: | Palm | **TA**: | Top of Arm |
| **FA**: | Forearm | **FH**: | Forehead | **C**: | Cheek |

| Dismount | Skin Tone | Date of Collection | # Samples per Location [Location] |
|---|---|---|---|
| 1 | DF | 4/26/13 | 10 [BH,P,TA,FA,FH,C] |
| 2 | DF | 4/26/13 | 10 [BH,P,TA,FA,FH,C] |
| 3 | F | 4/26/13 | 10 [BH,P,TA,FA,FH,C] |
| 4 | F | 4/28/13 | 10 [BH,P,TA,FA,FH,C] |
| 5 | F | 4/28/13 | 10 [BH,P,TA,FA,FH,C] |
| 6 | DF | 4/28/13 | 10 [BH,P,TA,FA,FH,C] |
| 7 | F | 4/28/13 | 10 [BH,P,TA,FA,FH,C] |
| 8 | F | 4/28/13 | 10 [BH,P,TA,FA,FH,C] |
| 9 | F | 4/28/13 | 10 [BH,P,TA,FA,FH,C] |
| 10 | F | 4/28/13 | 10 [BH,P,TA,FA,FH,C] |
| 11 | F | 6/4/13 | 10 [FA] |
| 12 | DF | 6/4/13 | 10 [FA] |
| 13 | F | 6/4/13 | 10 [FA] |
| 14 | F | 6/4/13 | 10 [FA] |

| Dismount | Skin Tone | Date of Collection | # Samples per Location [Location] |
|---|---|---|---|
| 15 | DF | 6/4/13 | 10 [FA] |
| 16 | F | 6/4/13 | 10 [FA] |
| 17 | F | 6/4/13 | 10 [FA] |
| 18 | F | 6/4/13 | 10 [FA] |
| 19 | F | 6/4/13 | 10 [FA] |
| 20 | F | 6/4/13 | 10 [FA] |
| 21 | F | 6/4/13 | 10 [FA] |
| 22 | F | 6/4/13 | 10 [FA] |
| 23 | F | 6/4/13 | 10 [FA] |
| 24 | F | 6/4/13 | 10 [FA] |
| 25 | D | 6/4/13 | 10 [FA] |
| 26 | F | 6/4/13 | 10 [FA] |
| 27 | F | 6/4/13 | 10 [FA] |
| 28 | F | 6/4/13 | 10 [FA] |
| 29 | F | 6/4/13 | 10 [FA] |
| 30 | F | 6/4/13 | 10 [FA] |
| 31 | F | 6/4/13 | 10 [FA] |
| 32 | F | 6/4/13 | 10 [FA] |
| 33 | F | 6/4/13 | 10 [FA] |
| 34 | F | 6/4/13 | 10 [FA] |
| 35 | F | 6/4/13 | 10 [FA] |
| 36 | F | 6/27/13 | 10 [FA] |
| 37 | F | 6/27/13 | 10 [FA] |
| 38 | F | 6/27/13 | 10 [FA] |
| 39 | F | 6/27/13 | 10 [FA] |
| 40 | F | 6/27/13 | 10 [FA] |
| 41 | F | 6/27/13 | 10 [FA] |
| 42 | DF | 6/27/13 | 10 [FA] |
| 43 | DF | 6/27/13 | 10 [FA] |
| 44 | DF | 6/27/13 | 10 [FA] |
| 45 | F | 6/27/13 | 10 [FA] |

| Dismount | Skin Tone | Date of Collection | # Samples per Location [Location] |
|---|---|---|---|
| 46 | F | 6/27/13 | 10 [FA] |
| 47 | DF | 6/27/13 | 10 [FA] |
| 48 | F | 6/27/13 | 10 [FA] |
| 49 | F | 6/27/13 | 10 [FA] |
| 50 | F | 6/27/13 | 10 [FA] |
| 51 | F | 6/27/13 | 10 [FA] |
| 52 | F | 6/27/13 | 10 [FA] |
| 53 | F | 6/27/13 | 10 [FA] |
| 54 | F | 6/27/13 | 10 [FA] |
| 55 | F | 6/27/13 | 10 [FA] |
| 56 | DF | 6/27/13 | 10 [FA] |
| 57 | F | 6/27/13 | 10 [FA] |
| 58 | FT | 6/27/13 | 10 [FA] |
| 59 | F | 6/27/13 | 10 [FA] |
| 60 | F | 6/27/13 | 10 [FA] |
| 61 | DF | 6/27/13 | 10 [FA] |
| 62 | D | 6/27/13 | 10 [FA] |
| DOI A | DF | 9/12/13 | 100 [FA] |
| DOI B | D | 9/12/13 | 100 [FA] |
| DOI C | F | 9/12/13 | 100 [FA] |
| DOI D | D | 9/12/13 | 100 [FA] |
| DOI E | F | 10/2/13 | 100 [FA] |
| Gridded Forearm 1 | DF | 10/4/13 | 10 [10 location on FA] |
| Gridded Forearm 2 | D | 10/4/13 | 10 [10 location on FA] |
| Gridded Forearm 3 | D | 10/4/13 | 10 [10 location on FA] |
| Gridded Forearm 4 | F | 10/4/13 | 10 [10 location on FA] |

## Appendix B: Reflectance Plots of All Dismounts

Average reflectance plots for every dismount described in Appendix A. The title of the plots corresponds to the same dismounts described in Appendix A.

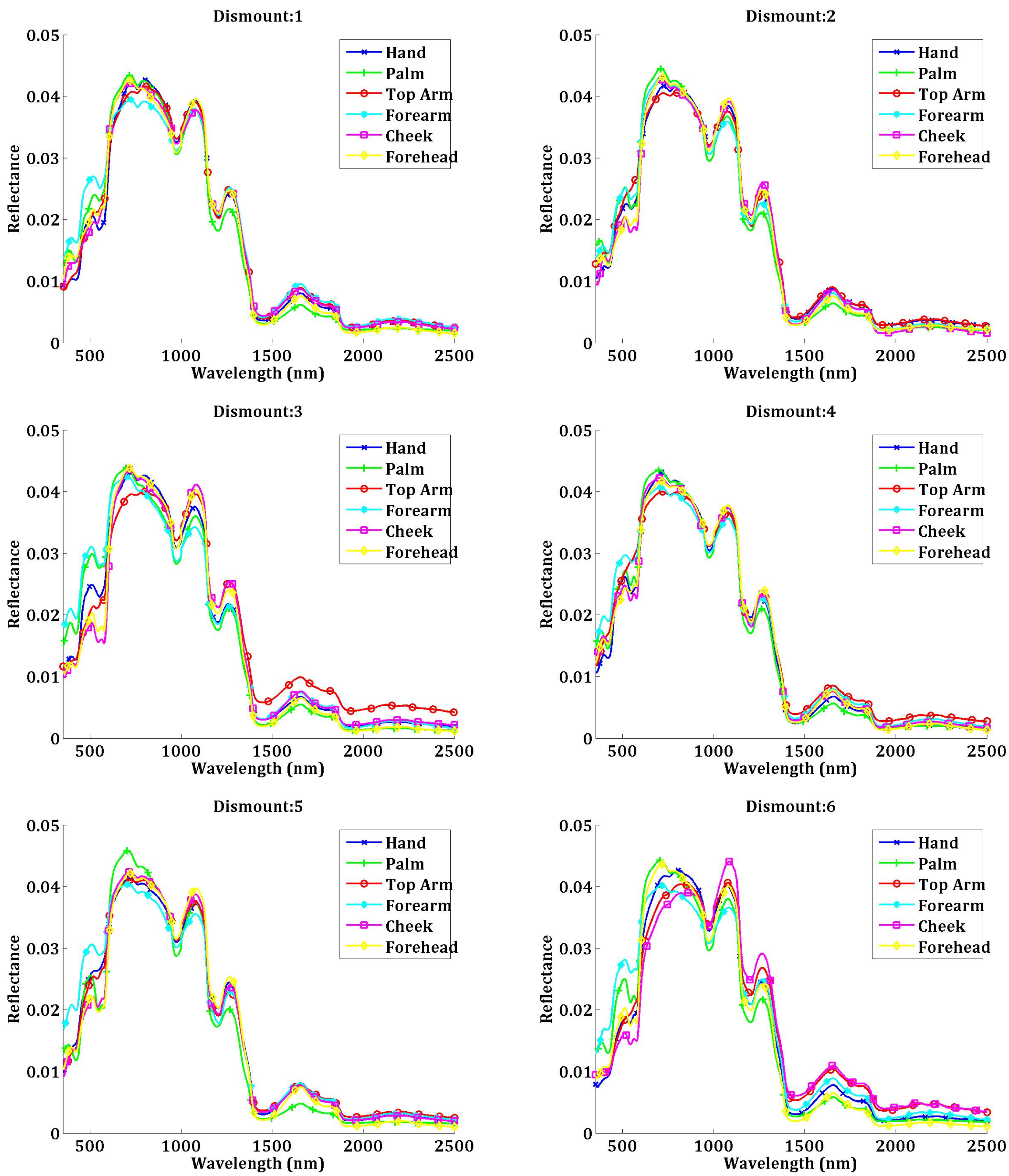

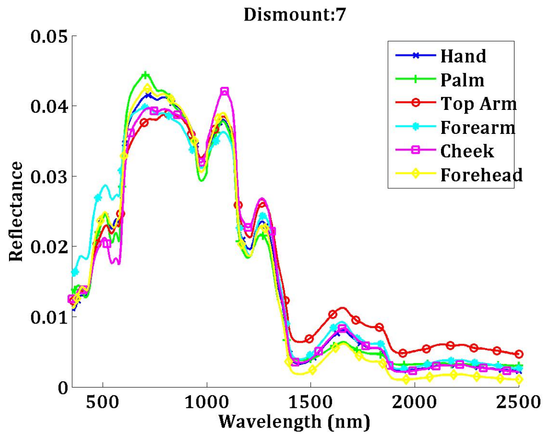
Dismount:7
Hand
Palm
Top Arm
Forearm
Cheek
Forehead
Reflectance
Wavelength (nm)
0
0.01
0.02
0.03
0.04
0.05
500
1000
1500
2000
2500

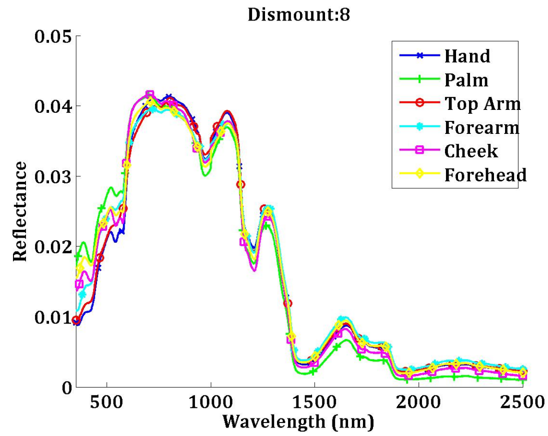
Dismount:8
Hand
Palm
Top Arm
Forearm
Cheek
Forehead
Reflectance
Wavelength (nm)
0
0.01
0.02
0.03
0.04
0.05
500
1000
1500
2000
2500

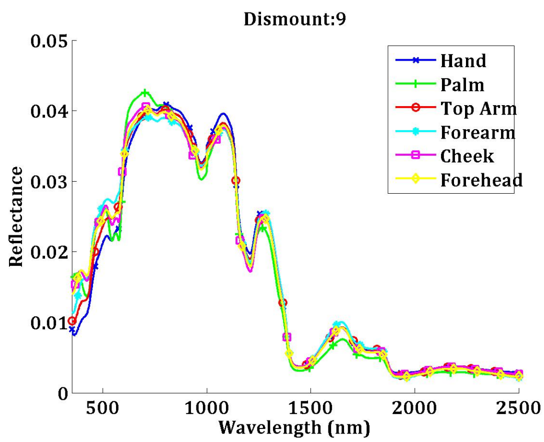
Dismount:9
Hand
Palm
Top Arm
Forearm
Cheek
Forehead
Reflectance
Wavelength (nm)
0
0.01
0.02
0.03
0.04
0.05
500
1000
1500
2000
2500

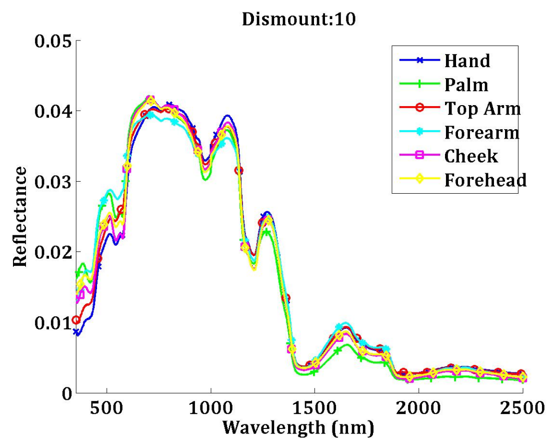
Dismount:10
Hand
Palm
Top Arm
Forearm
Cheek
Forehead
Reflectance
Wavelength (nm)
0
0.01
0.02
0.03
0.04
0.05
500
1000
1500
2000
2500

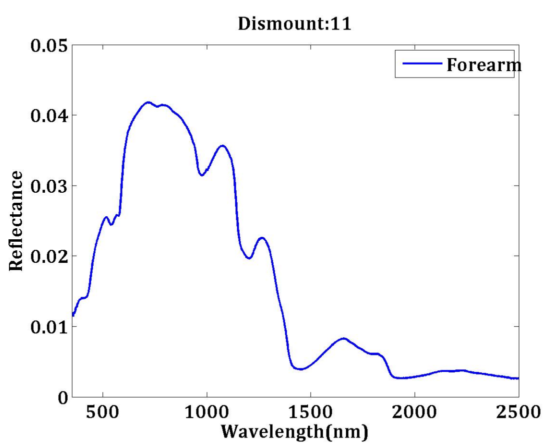
Dismount:11
Forearm
Reflectance
Wavelength(nm)
0
0.01
0.02
0.03
0.04
0.05
500
1000
1500
2000
2500

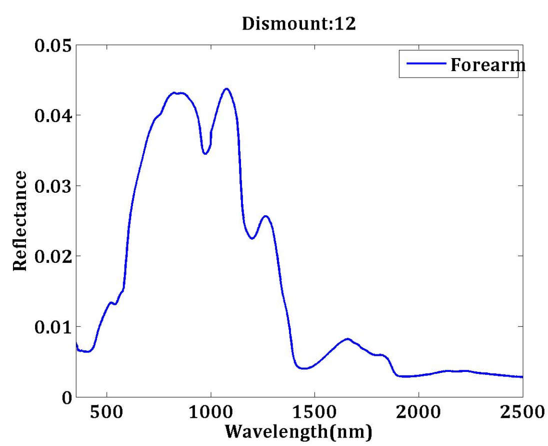
Dismount:12
Forearm
Reflectance
Wavelength(nm)
0
0.01
0.02
0.03
0.04
0.05
500
1000
1500
2000
2500

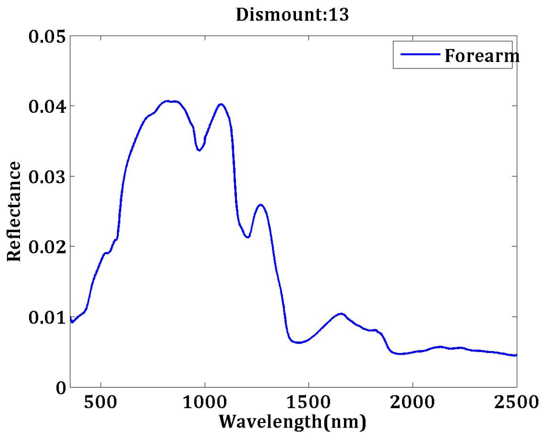
Dismount:13
Forearm
Reflectance
Wavelength(nm)
0 0.01 0.02 0.03 0.04 0.05
500 1000 1500 2000 2500

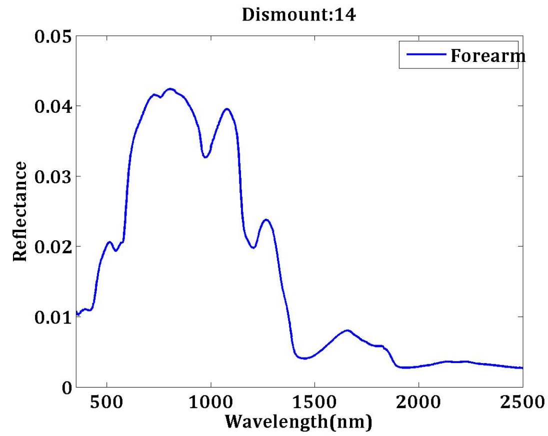
Dismount:14
Forearm
Reflectance
Wavelength(nm)
0 0.01 0.02 0.03 0.04 0.05
500 1000 1500 2000 2500

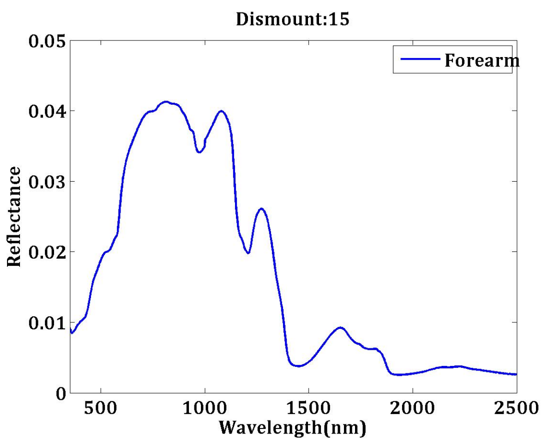
Dismount:15
Forearm
Reflectance
Wavelength(nm)
0 0.01 0.02 0.03 0.04 0.05
500 1000 1500 2000 2500

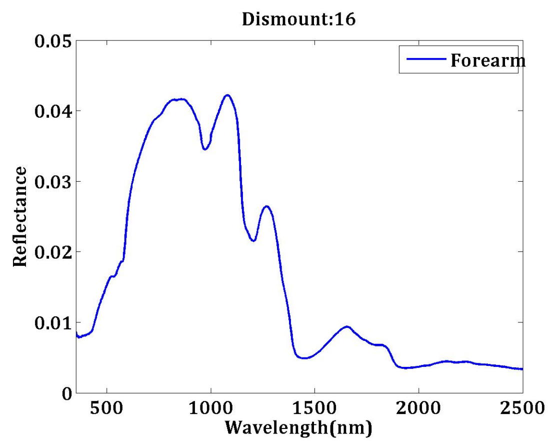
Dismount:16
Forearm
Reflectance
Wavelength(nm)
0 0.01 0.02 0.03 0.04 0.05
500 1000 1500 2000 2500

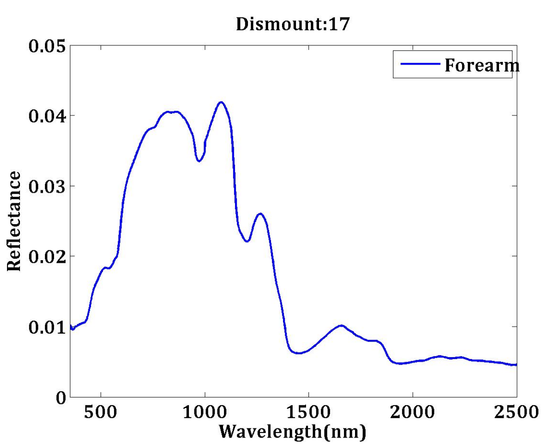
Dismount:17
Forearm
Reflectance
Wavelength(nm)
0 0.01 0.02 0.03 0.04 0.05
500 1000 1500 2000 2500

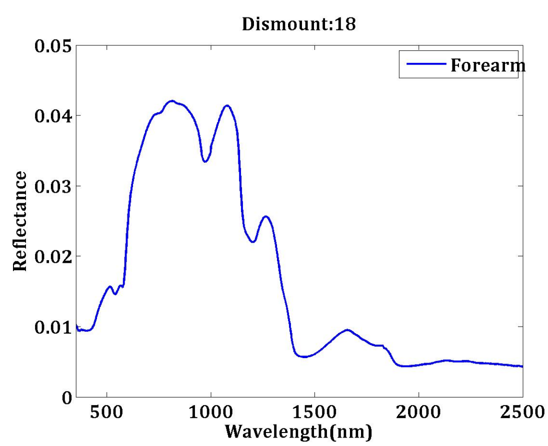
Dismount:18
Forearm
Reflectance
Wavelength(nm)
0 0.01 0.02 0.03 0.04 0.05
500 1000 1500 2000 2500

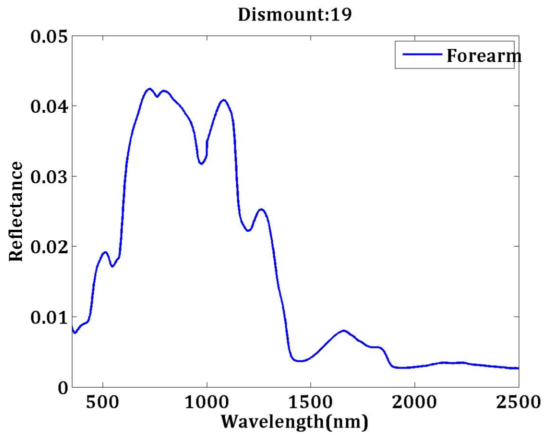
Dismount:19
Forearm
Reflectance
0.05
0.04
0.03
0.02
0.01
0
500
1000
1500
2000
2500
Wavelength(nm)

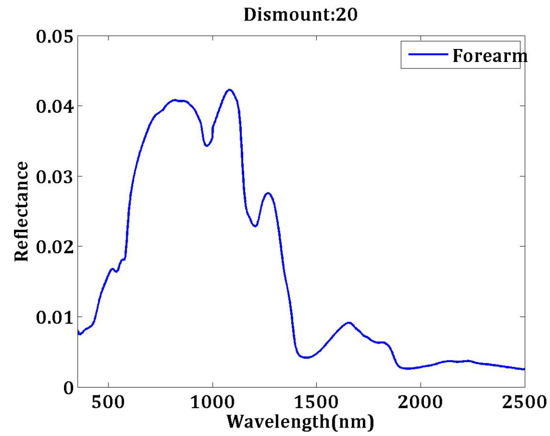
Dismount:20
Forearm
Reflectance
0.05
0.04
0.03
0.02
0.01
0
500
1000
1500
2000
2500
Wavelength(nm)

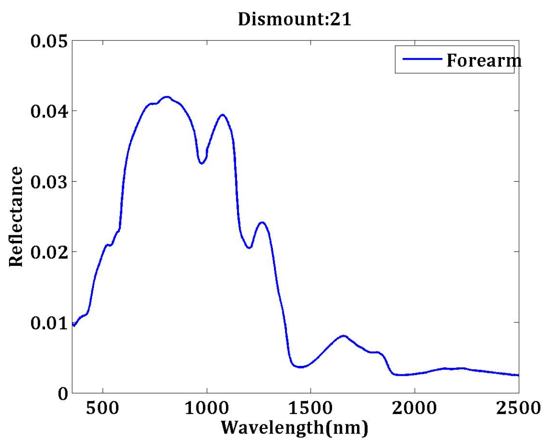
Dismount:21
Forearm
Reflectance
0.05
0.04
0.03
0.02
0.01
0
500
1000
1500
2000
2500
Wavelength(nm)

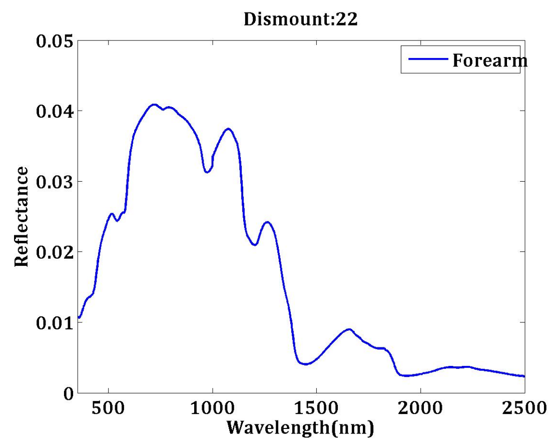
Dismount:22
Forearm
Reflectance
0.05
0.04
0.03
0.02
0.01
0
500
1000
1500
2000
2500
Wavelength(nm)

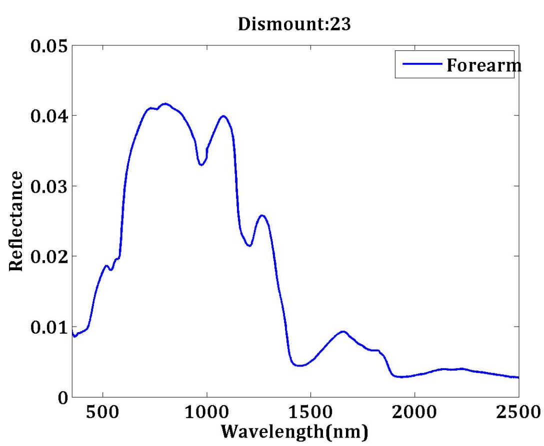
Dismount:23
Forearm
Reflectance
0.05
0.04
0.03
0.02
0.01
0
500
1000
1500
2000
2500
Wavelength(nm)

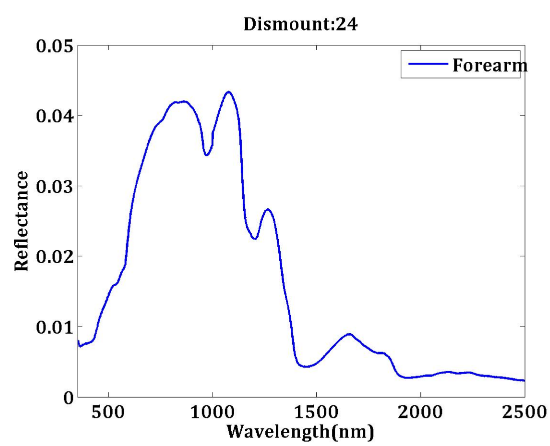
Dismount:24
Forearm
Reflectance
0.05
0.04
0.03
0.02
0.01
0
500
1000
1500
2000
2500
Wavelength(nm)

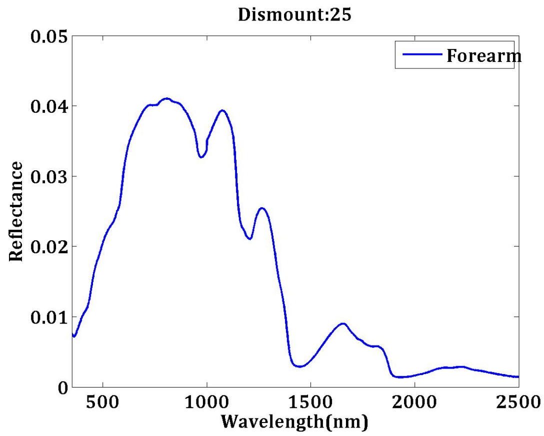
Dismount:25
Forearm
Reflectance
Wavelength(nm)
0.05
0.04
0.03
0.02
0.01
0
500
1000
1500
2000
2500

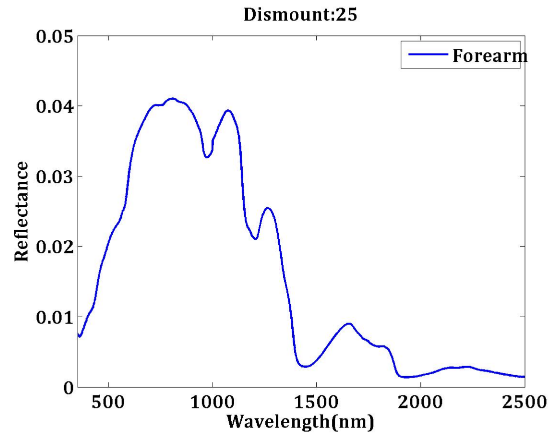
Dismount:25
Forearm
Reflectance
Wavelength(nm)
0.05
0.04
0.03
0.02
0.01
0
500
1000
1500
2000
2500

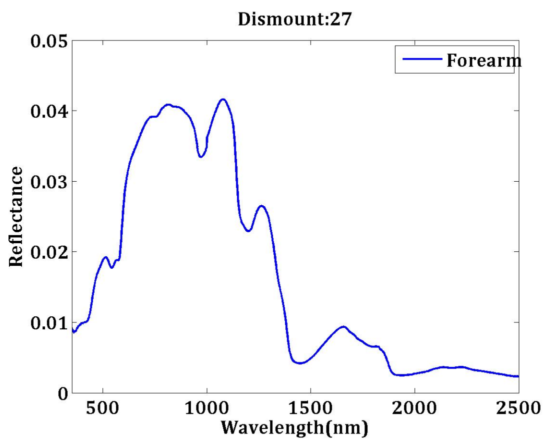
Dismount:27
Forearm
Reflectance
Wavelength(nm)
0.05
0.04
0.03
0.02
0.01
0
500
1000
1500
2000
2500

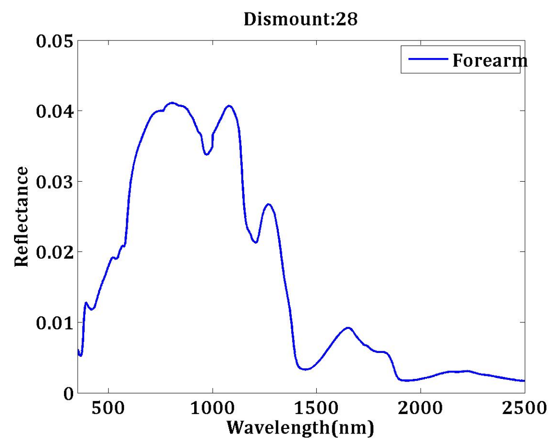
Dismount:28
Forearm
Reflectance
Wavelength(nm)
0.05
0.04
0.03
0.02
0.01
0
500
1000
1500
2000
2500

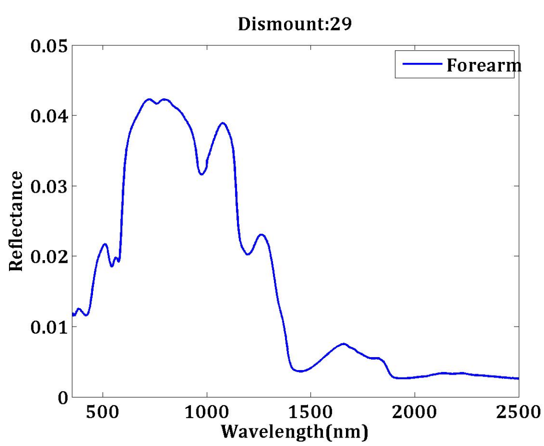
Dismount:29
Forearm
Reflectance
Wavelength(nm)
0.05
0.04
0.03
0.02
0.01
0
500
1000
1500
2000
2500

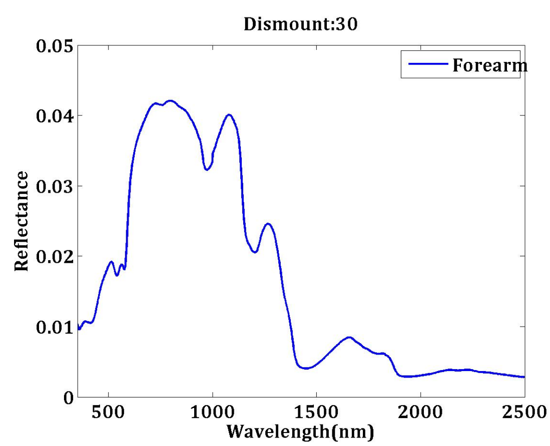
Dismount:30
Forearm
Reflectance
Wavelength(nm)
0.05
0.04
0.03
0.02
0.01
0
500
1000
1500
2000
2500

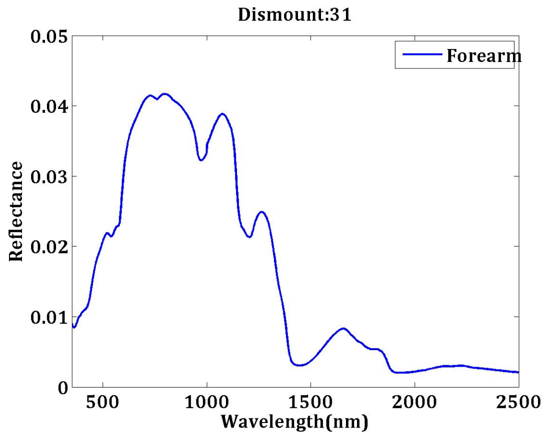
Dismount:31
Forearm
Reflectance
Wavelength(nm)

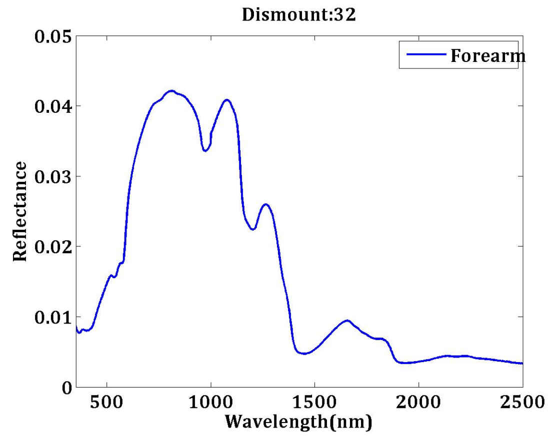
Dismount:32
Forearm
Reflectance
Wavelength(nm)

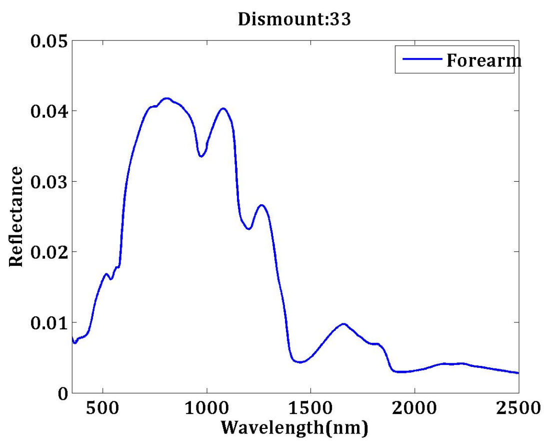
Dismount:33
Forearm
Reflectance
Wavelength(nm)

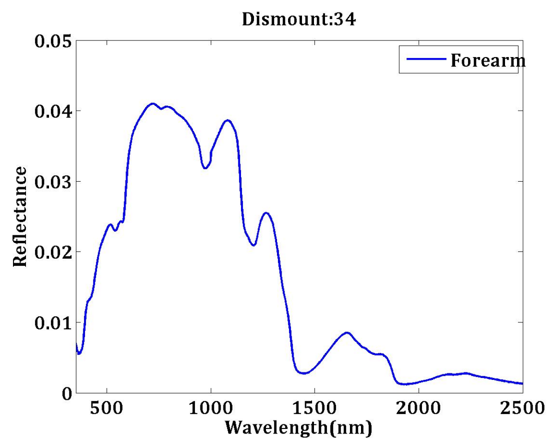
Dismount:34
Forearm
Reflectance
Wavelength(nm)

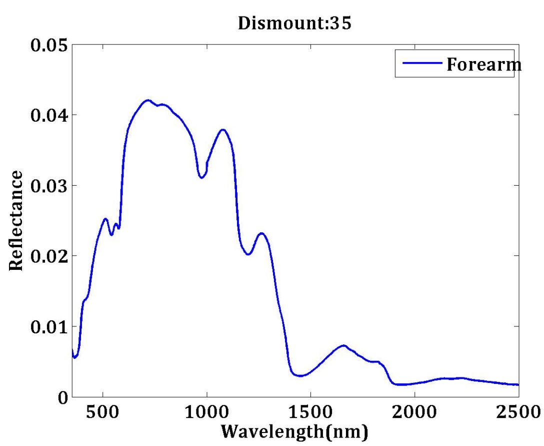
Dismount:35
Forearm
Reflectance
Wavelength(nm)

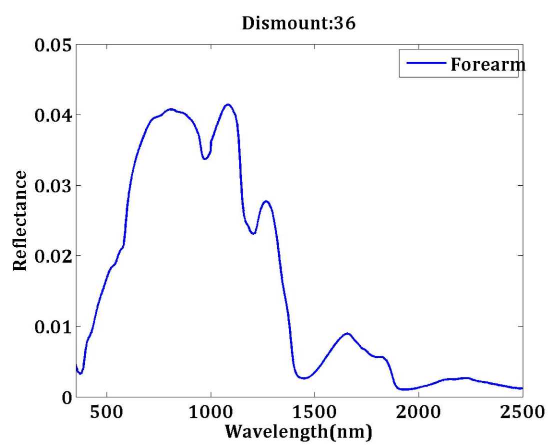
Dismount:36
Forearm
Reflectance
Wavelength(nm)

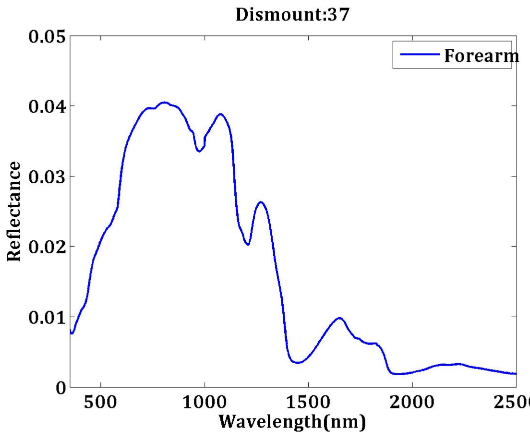
Dismount:37
Forearm
Reflectance
0.05
0.04
0.03
0.02
0.01
0
500
1000
1500
2000
2500
Wavelength(nm)

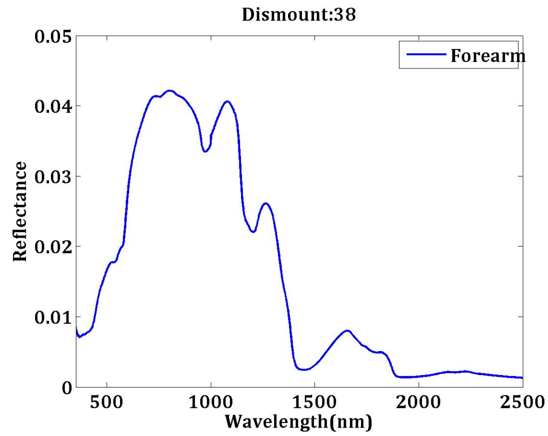
Dismount:38
Forearm
Reflectance
0.05
0.04
0.03
0.02
0.01
0
500
1000
1500
2000
2500
Wavelength(nm)

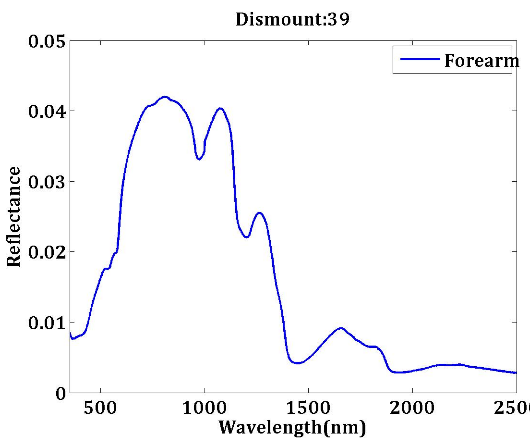
Dismount:39
Forearm
Reflectance
0.05
0.04
0.03
0.02
0.01
0
500
1000
1500
2000
2500
Wavelength(nm)

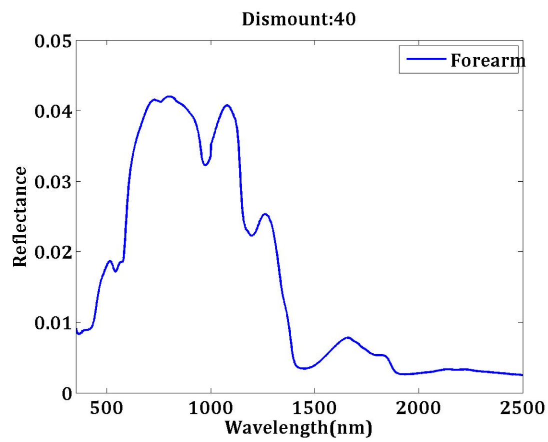
Dismount:40
Forearm
Reflectance
0.05
0.04
0.03
0.02
0.01
0
500
1000
1500
2000
2500
Wavelength(nm)

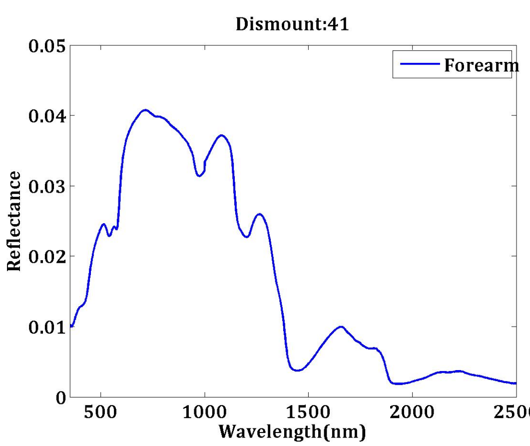
Dismount:41
Forearm
Reflectance
0.05
0.04
0.03
0.02
0.01
0
500
1000
1500
2000
2500
Wavelength(nm)

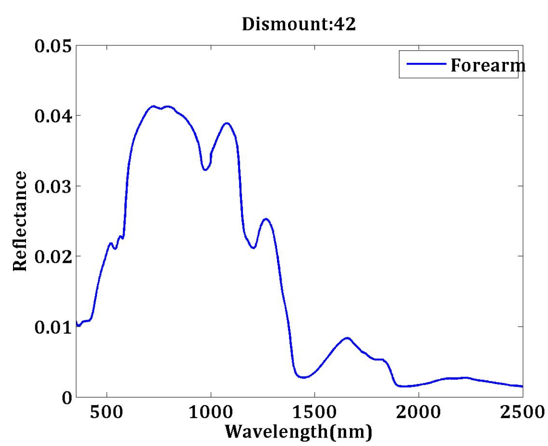
Dismount:42
Forearm
Reflectance
0.05
0.04
0.03
0.02
0.01
0
500
1000
1500
2000
2500
Wavelength(nm)

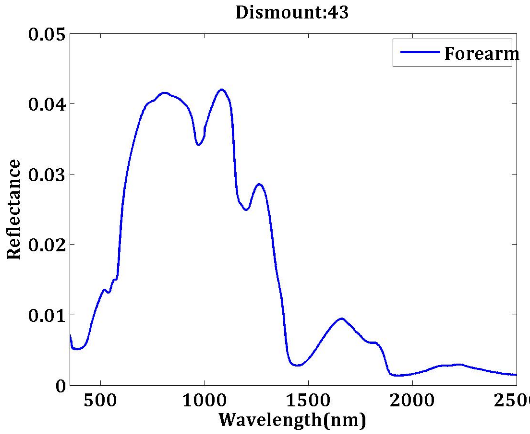
Dismount:43
Forearm
Reflectance
Wavelength(nm)
0.05
0.04
0.03
0.02
0.01
0
500
1000
1500
2000
2500

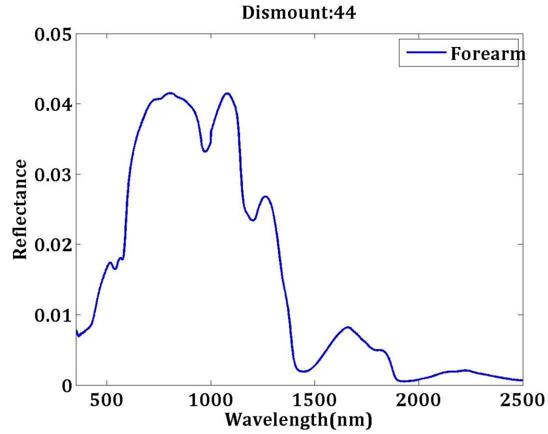
Dismount:44
Forearm
Reflectance
Wavelength(nm)
0.05
0.04
0.03
0.02
0.01
0
500
1000
1500
2000
2500

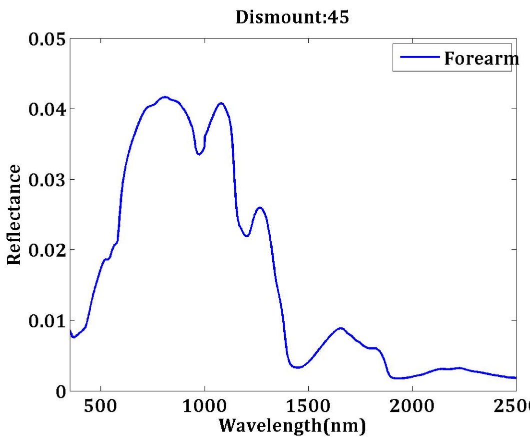
Dismount:45
Forearm
Reflectance
Wavelength(nm)
0.05
0.04
0.03
0.02
0.01
0
500
1000
1500
2000
2500

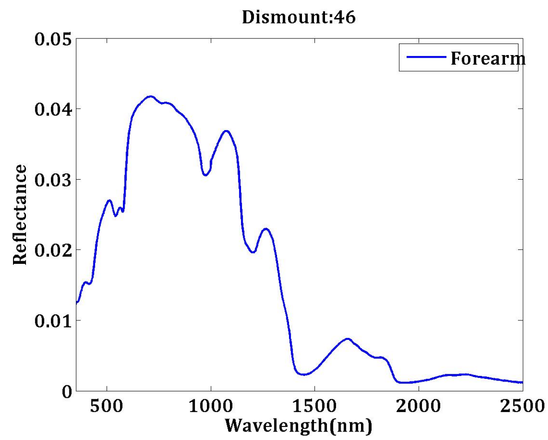
Dismount:46
Forearm
Reflectance
Wavelength(nm)
0.05
0.04
0.03
0.02
0.01
0
500
1000
1500
2000
2500

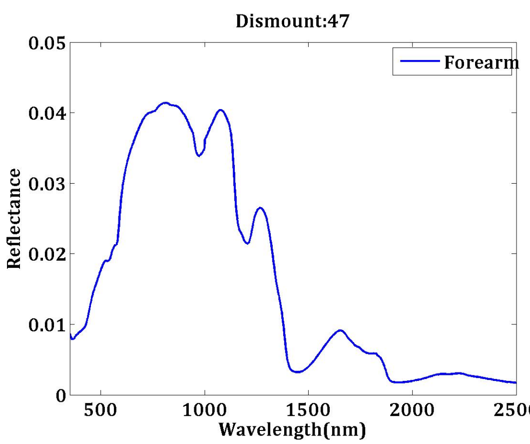
Dismount:47
Forearm
Reflectance
Wavelength(nm)
0.05
0.04
0.03
0.02
0.01
0
500
1000
1500
2000
2500

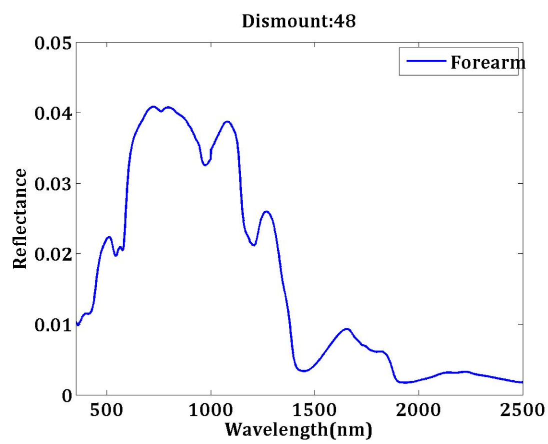
Dismount:48
Forearm
Reflectance
Wavelength(nm)
0.05
0.04
0.03
0.02
0.01
0
500
1000
1500
2000
2500

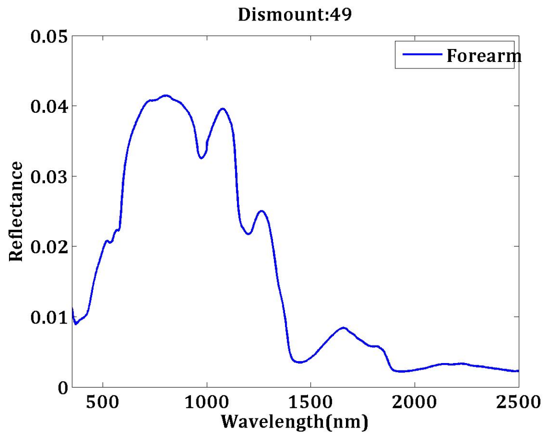
Dismount:49
Forearm
Reflectance
Wavelength(nm)

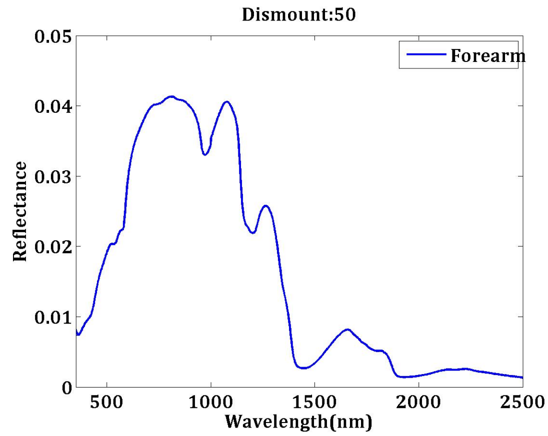
Dismount:50
Forearm
Reflectance
Wavelength(nm)

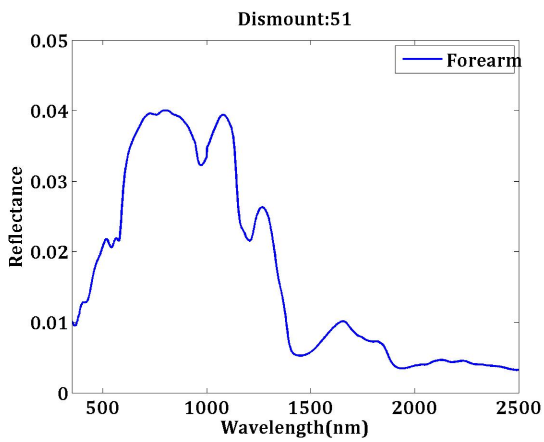
Dismount:51
Forearm
Reflectance
Wavelength(nm)

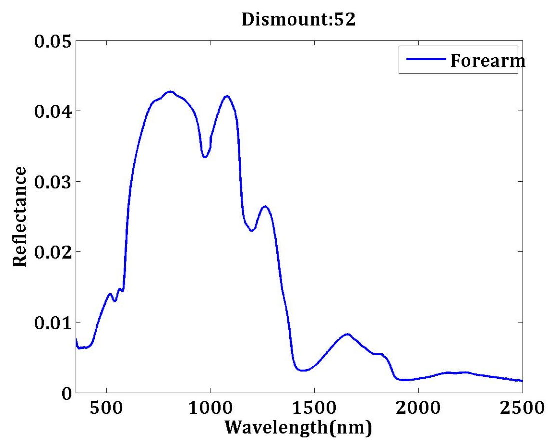
Dismount:52
Forearm
Reflectance
Wavelength(nm)

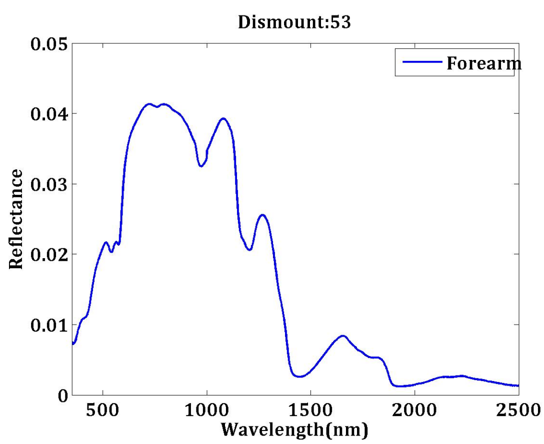
Dismount:53
Forearm
Reflectance
Wavelength(nm)

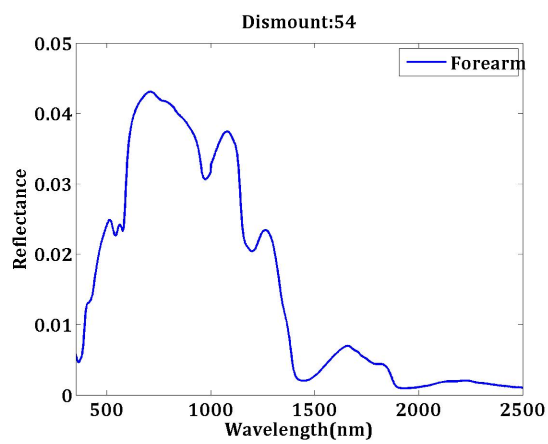
Dismount:54
Forearm
Reflectance
Wavelength(nm)

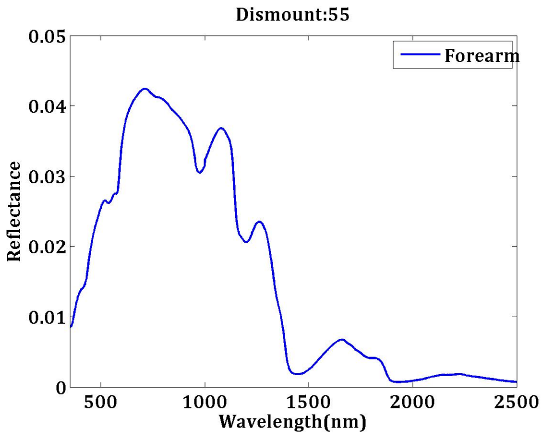
Dismount:55
Forearm
0.05
0.04
0.03
0.02
0.01
0
Reflectance
500
1000
1500
2000
2500
Wavelength(nm)

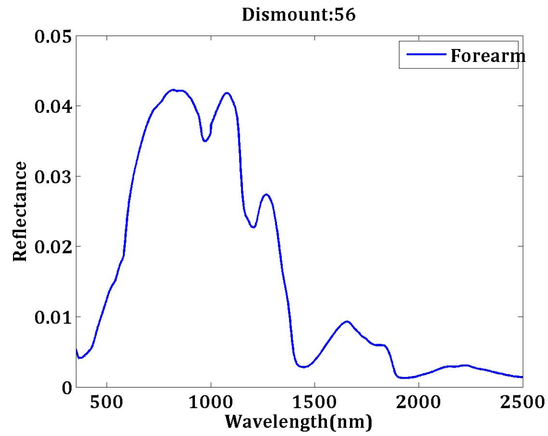
Dismount:56
Forearm
0.05
0.04
0.03
0.02
0.01
0
Reflectance
500
1000
1500
2000
2500
Wavelength(nm)

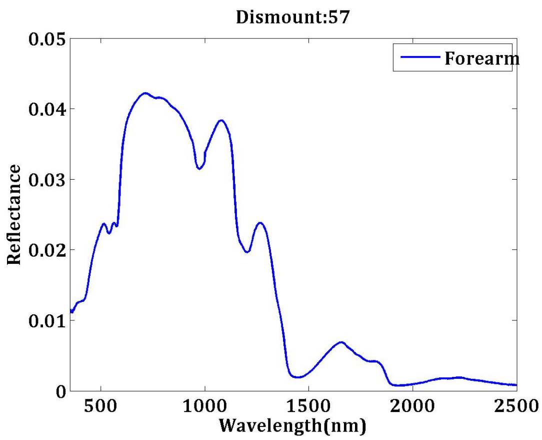
Dismount:57
Forearm
0.05
0.04
0.03
0.02
0.01
0
Reflectance
500
1000
1500
2000
2500
Wavelength(nm)

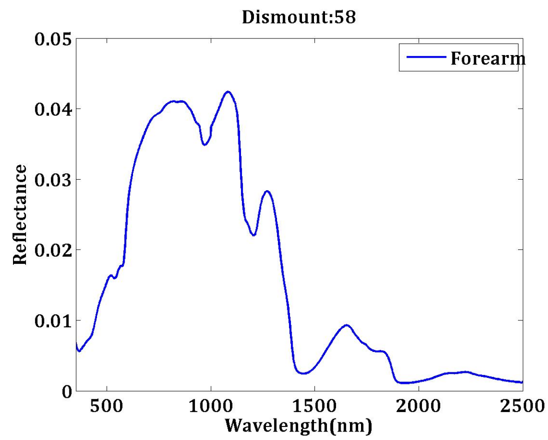
Dismount:58
Forearm
0.05
0.04
0.03
0.02
0.01
0
Reflectance
500
1000
1500
2000
2500
Wavelength(nm)

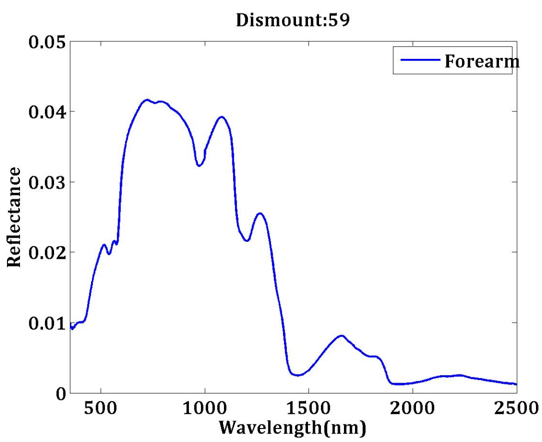
Dismount:59
Forearm
0.05
0.04
0.03
0.02
0.01
0
Reflectance
500
1000
1500
2000
2500
Wavelength(nm)

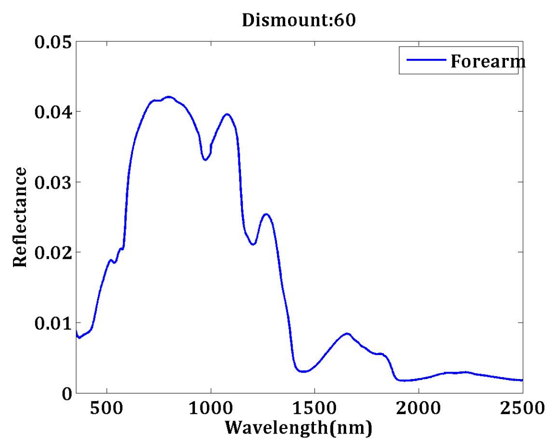
Dismount:60
Forearm
0.05
0.04
0.03
0.02
0.01
0
Reflectance
500
1000
1500
2000
2500
Wavelength(nm)

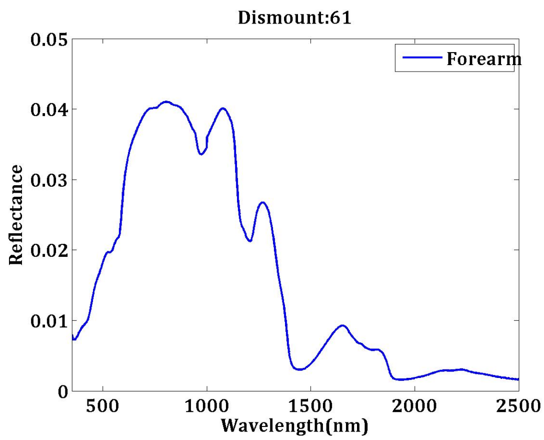
Dismount:61
Forearm
Reflectance
0.05
0.04
0.03
0.02
0.01
0
500
1000
1500
2000
2500
Wavelength(nm)

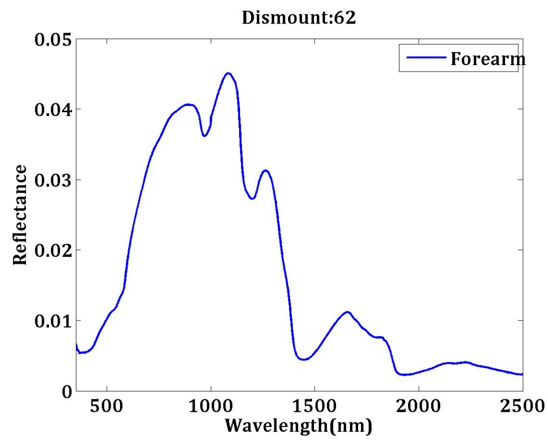
Dismount:62
Forearm
Reflectance
0.05
0.04
0.03
0.02
0.01
0
500
1000
1500
2000
2500
Wavelength(nm)

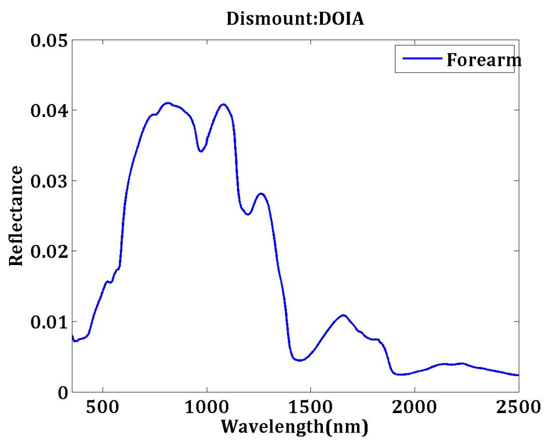
Dismount:DOIA
Forearm
Reflectance
0.05
0.04
0.03
0.02
0.01
0
500
1000
1500
2000
2500
Wavelength(nm)

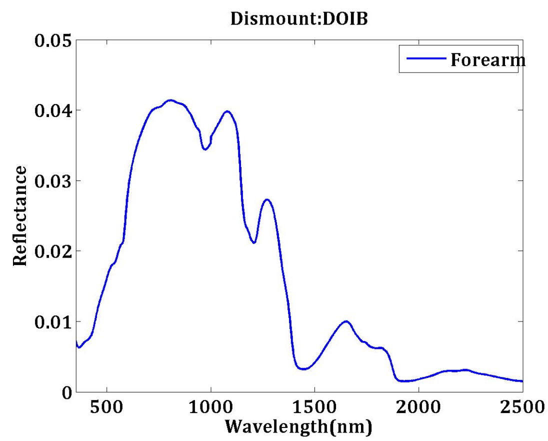
Dismount:DOIB
Forearm
Reflectance
0.05
0.04
0.03
0.02
0.01
0
500
1000
1500
2000
2500
Wavelength(nm)

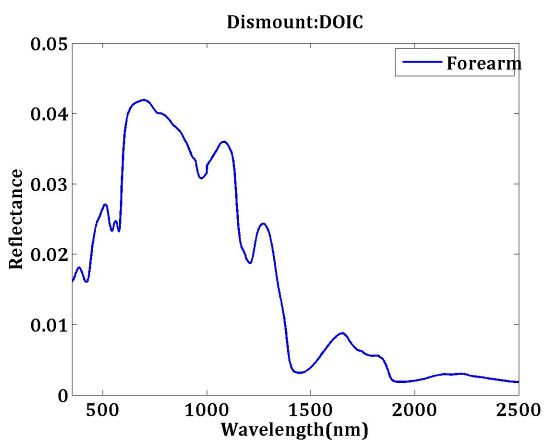
Dismount:DOIC
Forearm
Reflectance
0.05
0.04
0.03
0.02
0.01
0
500
1000
1500
2000
2500
Wavelength(nm)

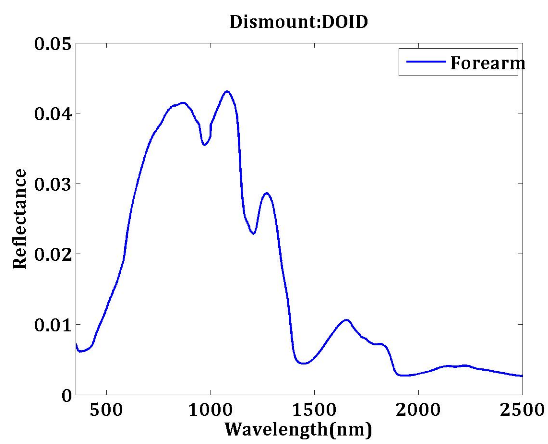
Dismount:DOID
Forearm
Reflectance
0.05
0.04
0.03
0.02
0.01
0
500
1000
1500
2000
2500
Wavelength(nm)

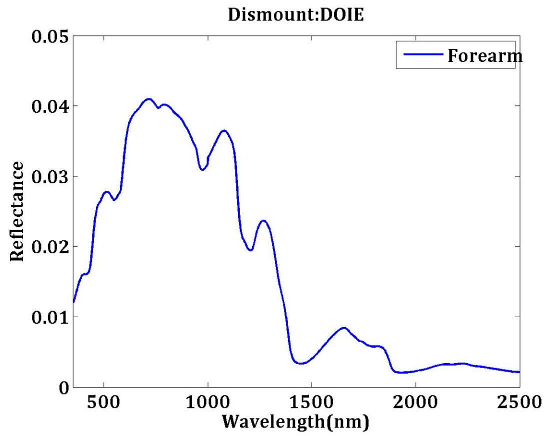


The location values on the plots below refer to the location numbers of the grid as indicated in Figure 4.9.

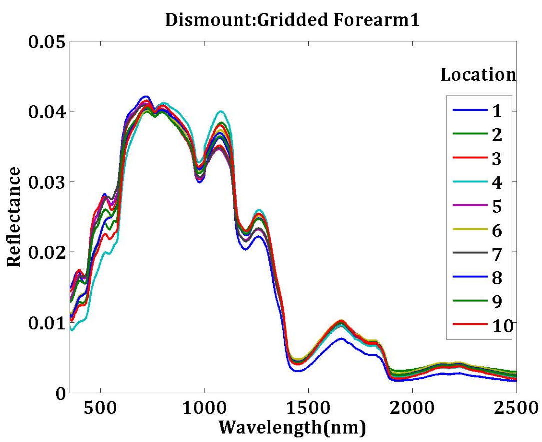


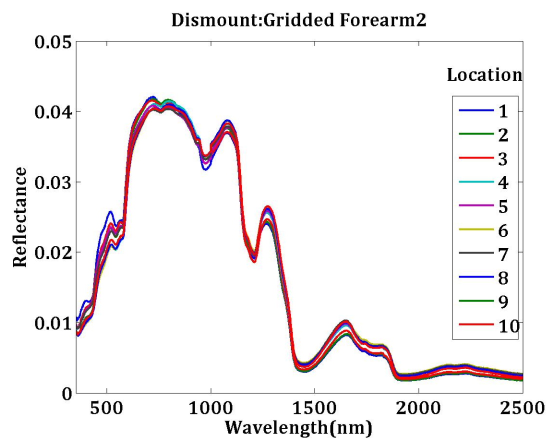


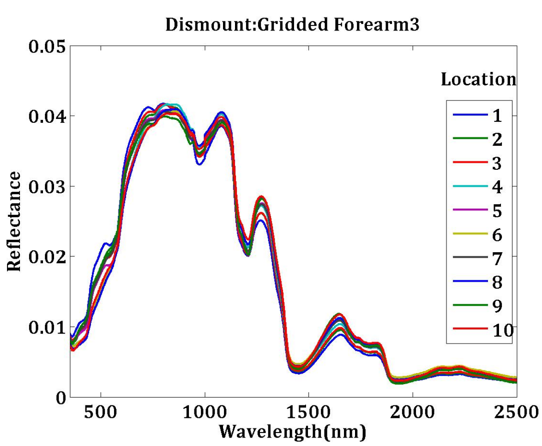


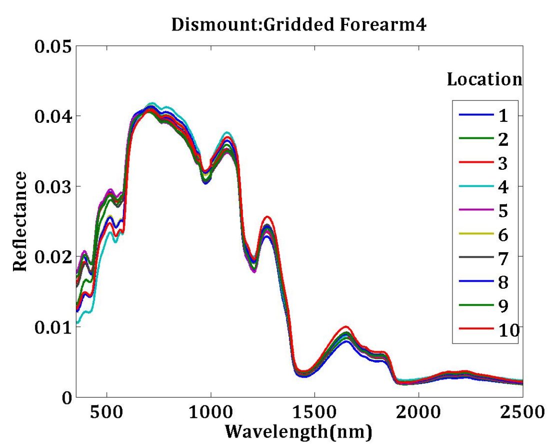

## Appendix C: Standard Deviation Plots - One Location on Forearm

Standard deviation plots for subjects 1-62. The average reflectance is plotted with standard deviation bars at 50nm intervals. The bars represent the standard deviation between 10 samples from one collection on the forearm.

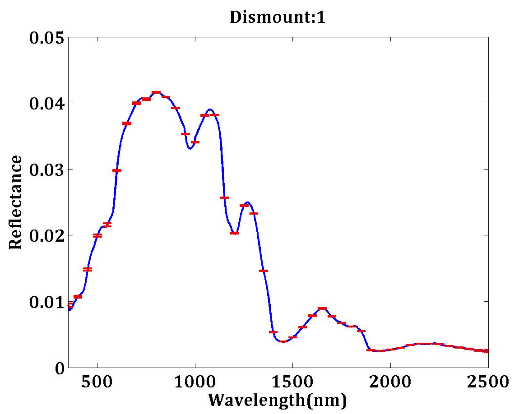


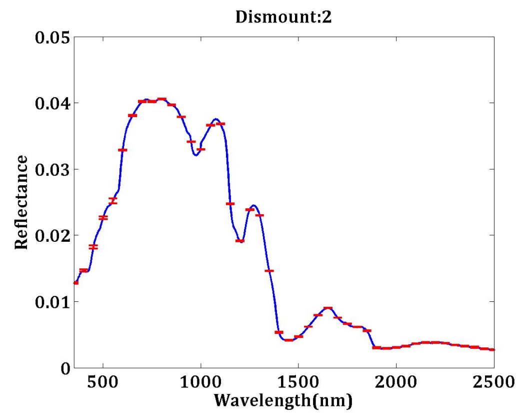


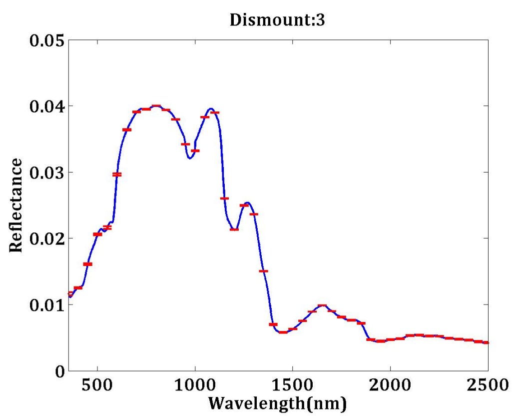


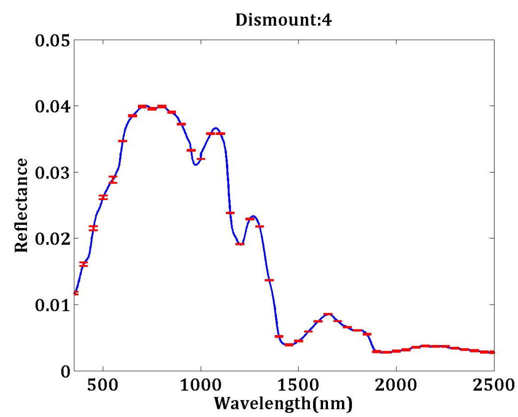


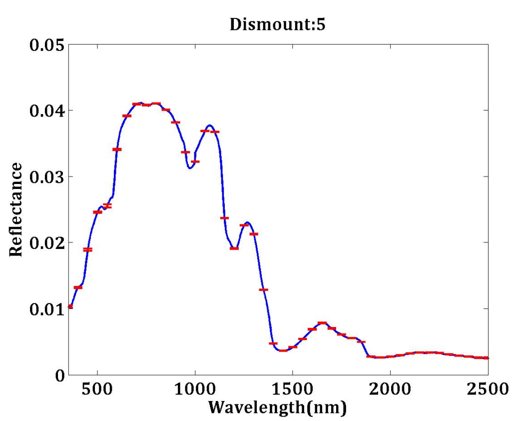


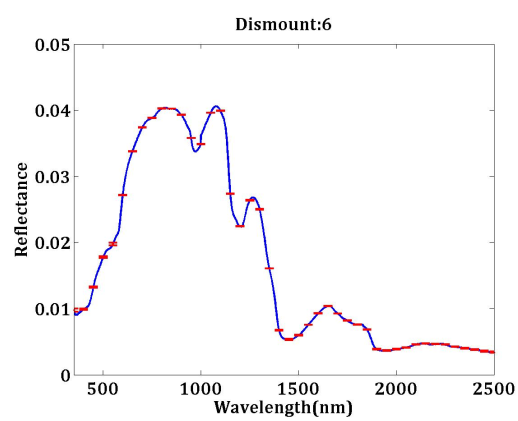

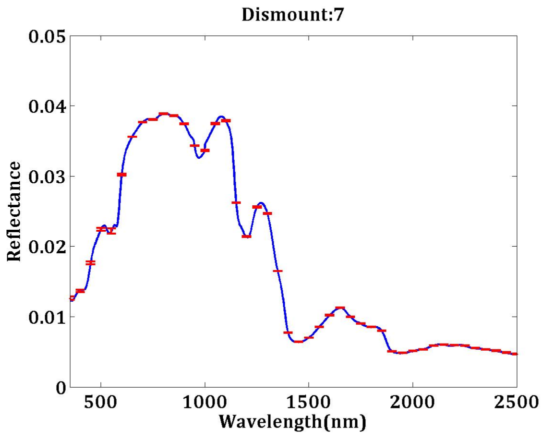
Dismount:7
Reflectance
0.05
0.04
0.03
0.02
0.01
0
500
1000
1500
2000
2500
Wavelength(nm)

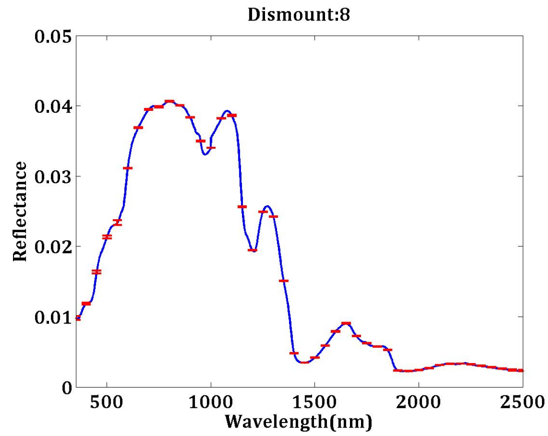
Dismount:8
Reflectance
0.05
0.04
0.03
0.02
0.01
0
500
1000
1500
2000
2500
Wavelength(nm)

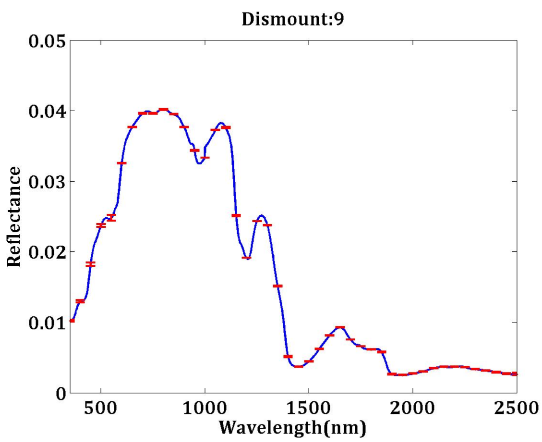
Dismount:9
Reflectance
0.05
0.04
0.03
0.02
0.01
0
500
1000
1500
2000
2500
Wavelength(nm)

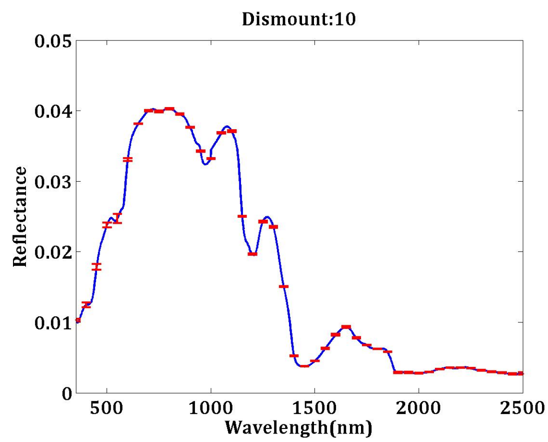
Dismount:10
Reflectance
0.05
0.04
0.03
0.02
0.01
0
500
1000
1500
2000
2500
Wavelength(nm)

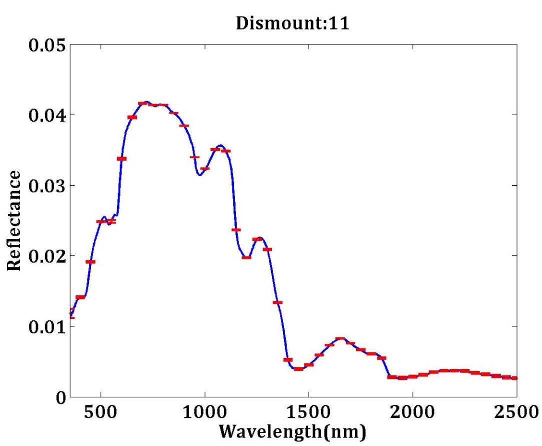
Dismount:11
Reflectance
0.05
0.04
0.03
0.02
0.01
0
500
1000
1500
2000
2500
Wavelength(nm)

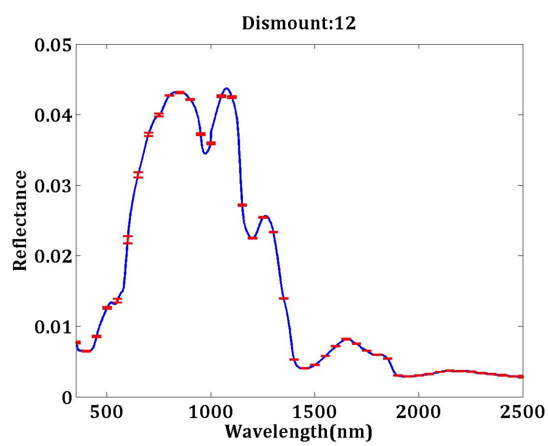
Dismount:12
Reflectance
0.05
0.04
0.03
0.02
0.01
0
500
1000
1500
2000
2500
Wavelength(nm)

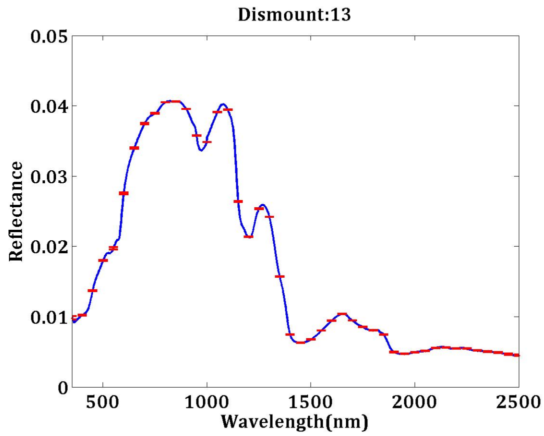
Dismount:13
Reflectance
Wavelength(nm)
0.05
0.04
0.03
0.02
0.01
0
500
1000
1500
2000
2500

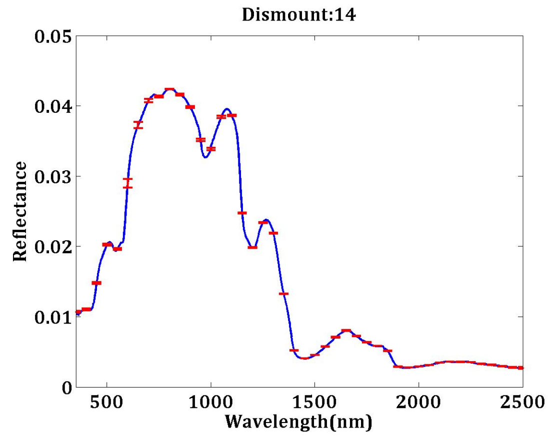
Dismount:14
Reflectance
Wavelength(nm)
0.05
0.04
0.03
0.02
0.01
0
500
1000
1500
2000
2500

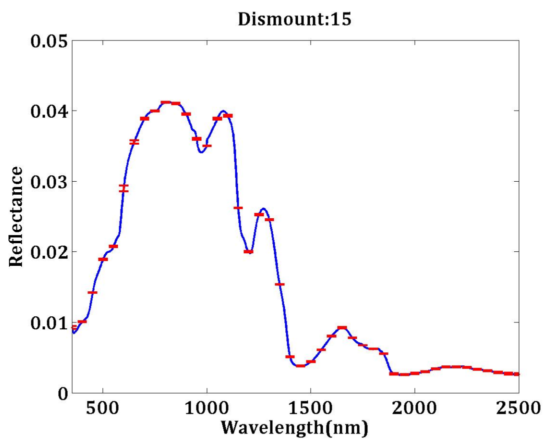
Dismount:15
Reflectance
Wavelength(nm)
0.05
0.04
0.03
0.02
0.01
0
500
1000
1500
2000
2500

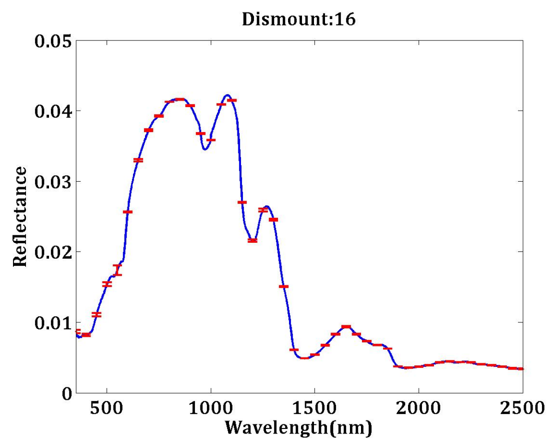
Dismount:16
Reflectance
Wavelength(nm)
0.05
0.04
0.03
0.02
0.01
0
500
1000
1500
2000
2500

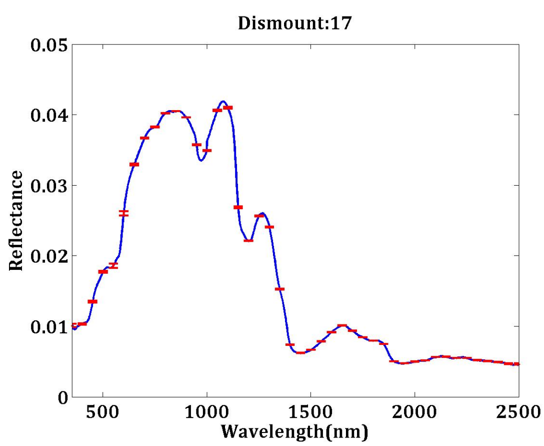
Dismount:17
Reflectance
Wavelength(nm)
0.05
0.04
0.03
0.02
0.01
0
500
1000
1500
2000
2500

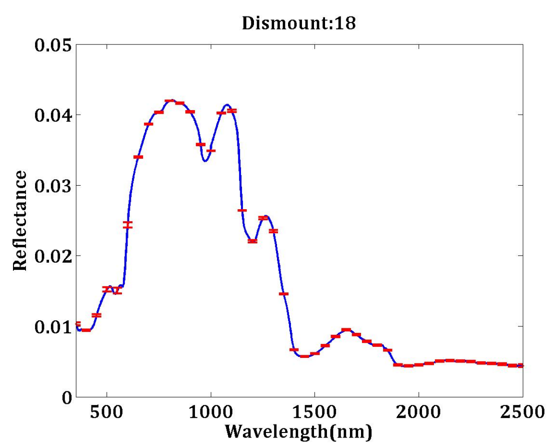
Dismount:18
Reflectance
Wavelength(nm)
0.05
0.04
0.03
0.02
0.01
0
500
1000
1500
2000
2500

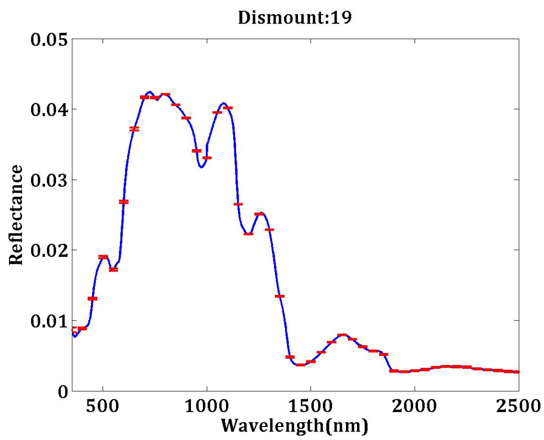
Dismount:19
Reflectance
0.05
0.04
0.03
0.02
0.01
0
500
1000
1500
2000
2500
Wavelength(nm)

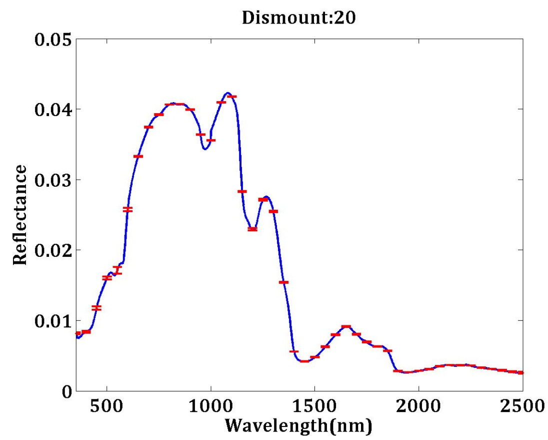
Dismount:20
Reflectance
0.05
0.04
0.03
0.02
0.01
0
500
1000
1500
2000
2500
Wavelength(nm)

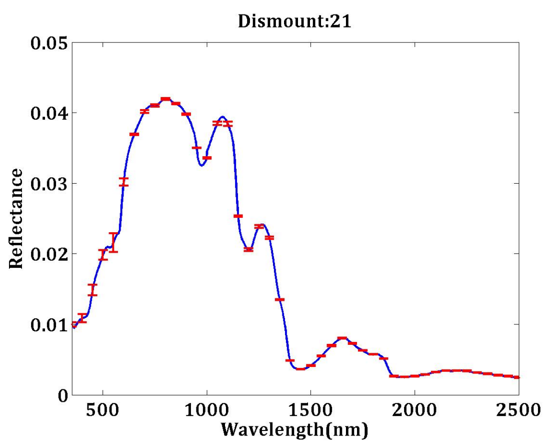
Dismount:21
Reflectance
0.05
0.04
0.03
0.02
0.01
0
500
1000
1500
2000
2500
Wavelength(nm)

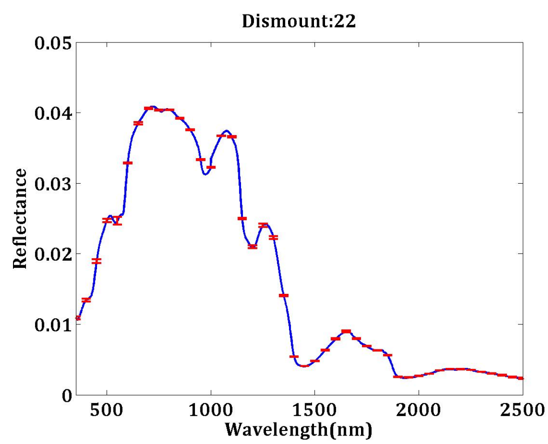
Dismount:22
Reflectance
0.05
0.04
0.03
0.02
0.01
0
500
1000
1500
2000
2500
Wavelength(nm)

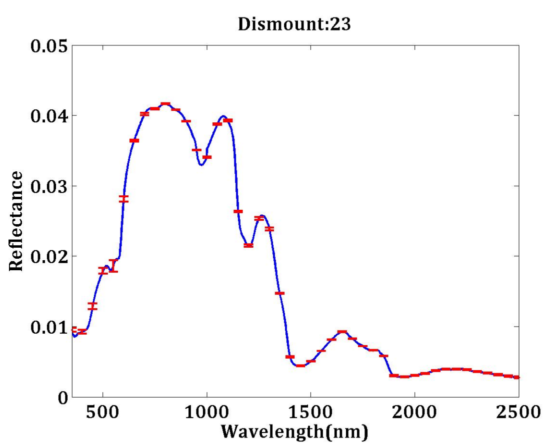
Dismount:23
Reflectance
0.05
0.04
0.03
0.02
0.01
0
500
1000
1500
2000
2500
Wavelength(nm)

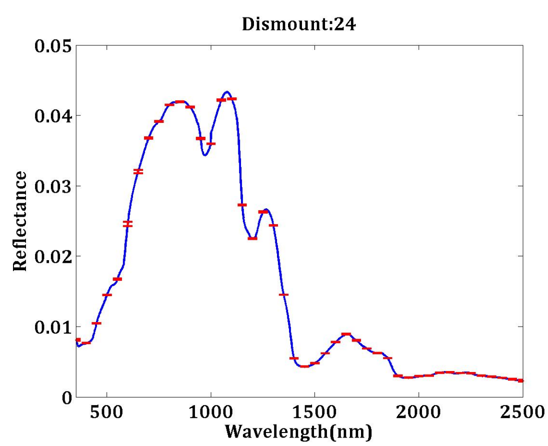
Dismount:24
Reflectance
0.05
0.04
0.03
0.02
0.01
0
500
1000
1500
2000
2500
Wavelength(nm)

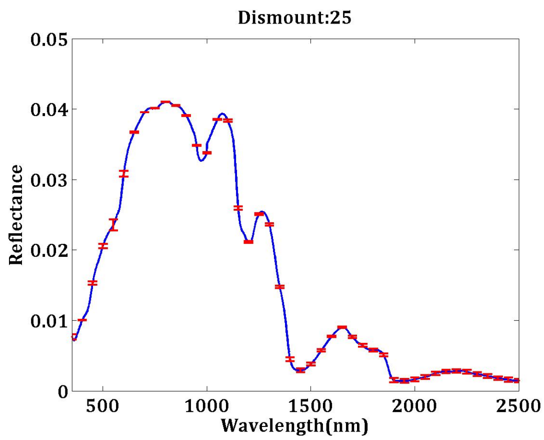
Dismount:25
Reflectance
0.05
0.04
0.03
0.02
0.01
0
500
1000
1500
2000
2500
Wavelength(nm)

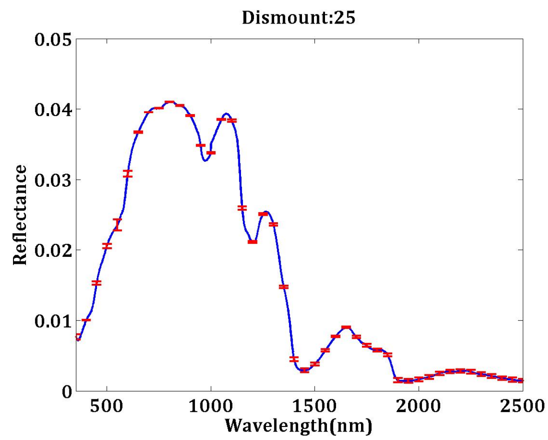
Dismount:25
Reflectance
0.05
0.04
0.03
0.02
0.01
0
500
1000
1500
2000
2500
Wavelength(nm)

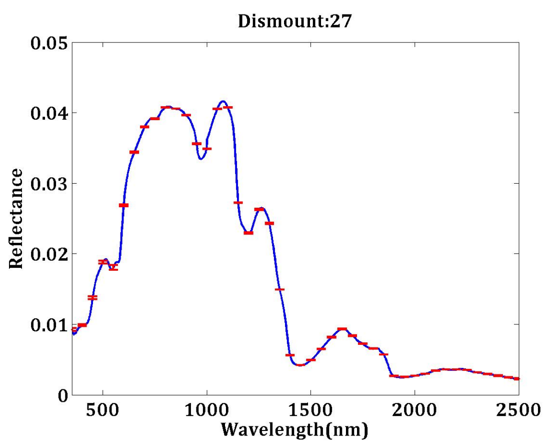
Dismount:27
Reflectance
0.05
0.04
0.03
0.02
0.01
0
500
1000
1500
2000
2500
Wavelength(nm)

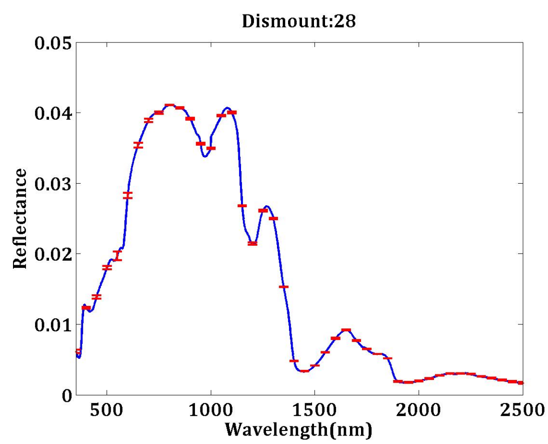
Dismount:28
Reflectance
0.05
0.04
0.03
0.02
0.01
0
500
1000
1500
2000
2500
Wavelength(nm)

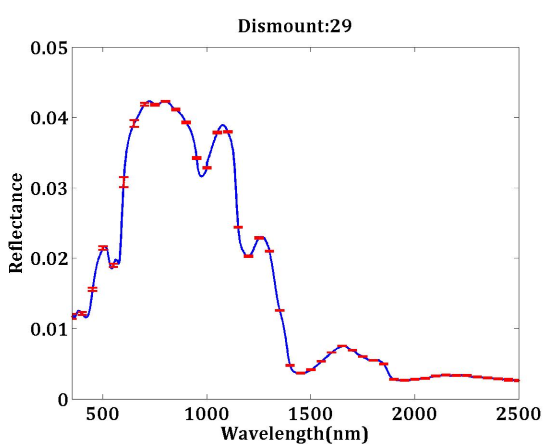
Dismount:29
Reflectance
0.05
0.04
0.03
0.02
0.01
0
500
1000
1500
2000
2500
Wavelength(nm)

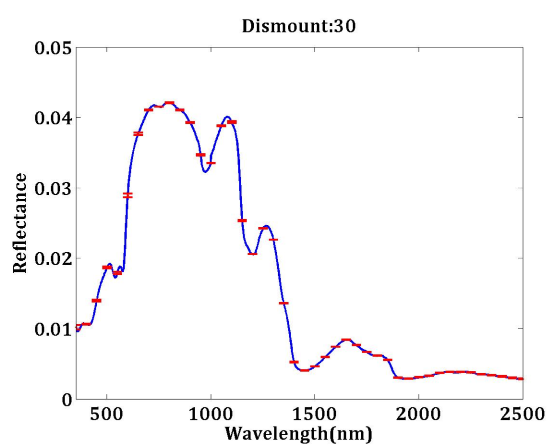
Dismount:30
Reflectance
0.05
0.04
0.03
0.02
0.01
0
500
1000
1500
2000
2500
Wavelength(nm)

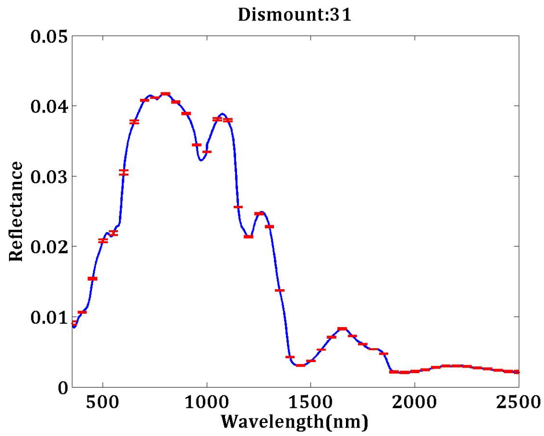
Dismount:31
0.05
0.04
0.03
0.02
0.01
0
Reflectance
500
1000
1500
2000
2500
Wavelength(nm)

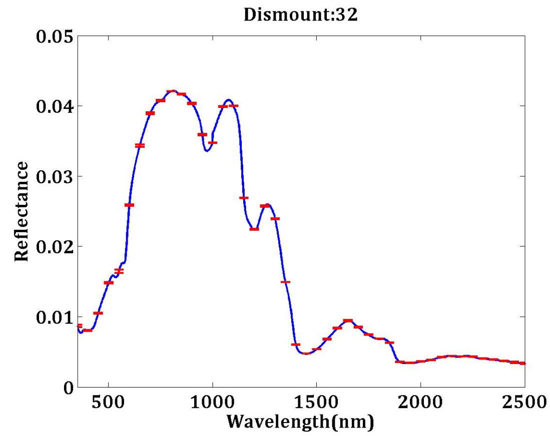
Dismount:32
0.05
0.04
0.03
0.02
0.01
0
Reflectance
500
1000
1500
2000
2500
Wavelength(nm)

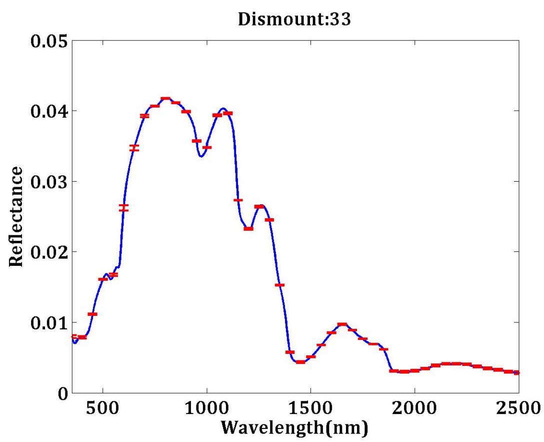
Dismount:33
0.05
0.04
0.03
0.02
0.01
0
Reflectance
500
1000
1500
2000
2500
Wavelength(nm)

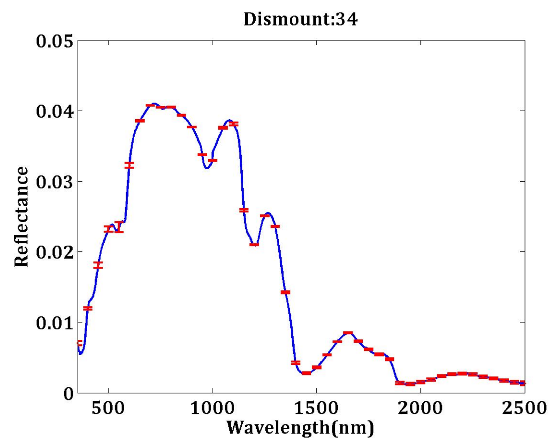
Dismount:34
0.05
0.04
0.03
0.02
0.01
0
Reflectance
500
1000
1500
2000
2500
Wavelength(nm)

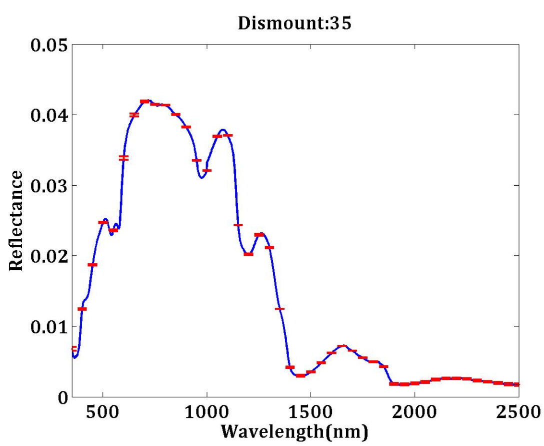
Dismount:35
0.05
0.04
0.03
0.02
0.01
0
Reflectance
500
1000
1500
2000
2500
Wavelength(nm)

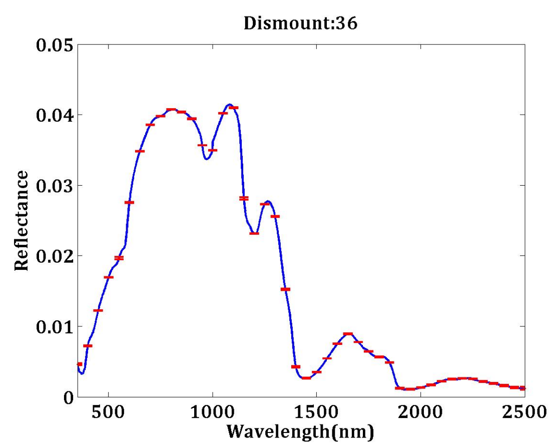
Dismount:36
0.05
0.04
0.03
0.02
0.01
0
Reflectance
500
1000
1500
2000
2500
Wavelength(nm)

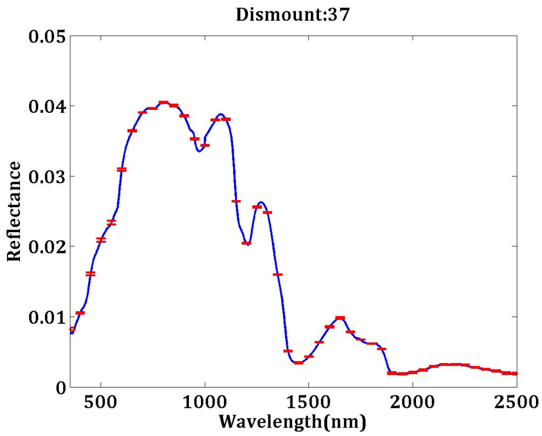
Dismount:37
Reflectance
0.05
0.04
0.03
0.02
0.01
0
500
1000
1500
2000
2500
Wavelength(nm)

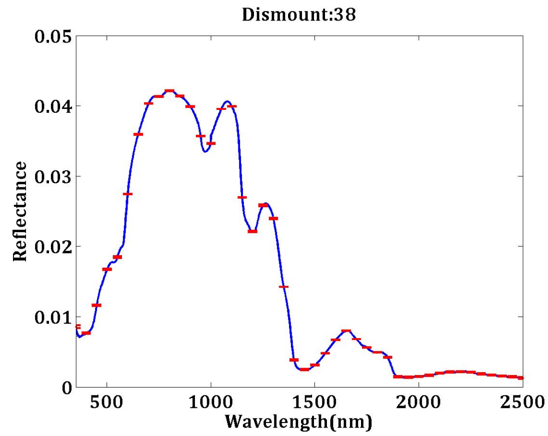
Dismount:38
Reflectance
0.05
0.04
0.03
0.02
0.01
0
500
1000
1500
2000
2500
Wavelength(nm)

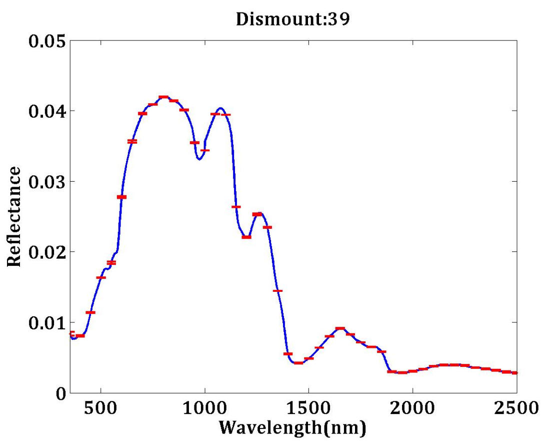
Dismount:39
Reflectance
0.05
0.04
0.03
0.02
0.01
0
500
1000
1500
2000
2500
Wavelength(nm)

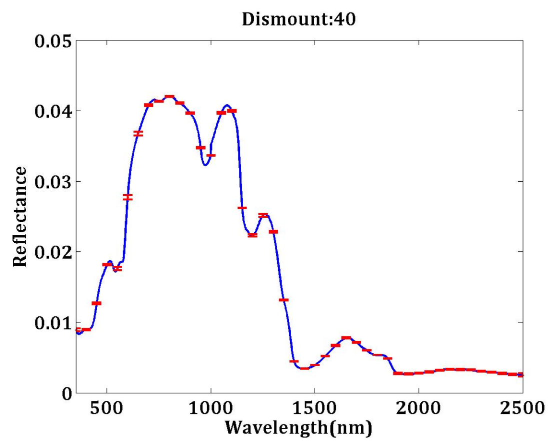
Dismount:40
Reflectance
0.05
0.04
0.03
0.02
0.01
0
500
1000
1500
2000
2500
Wavelength(nm)

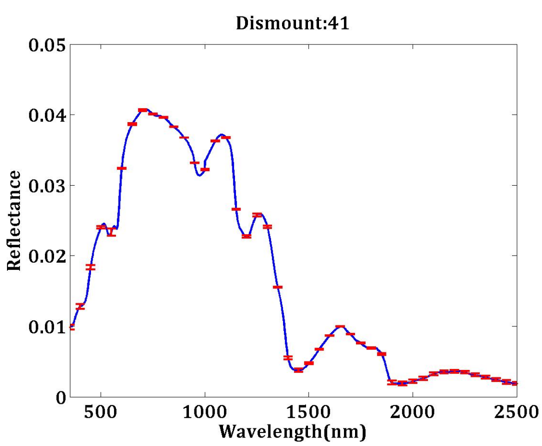
Dismount:41
Reflectance
0.05
0.04
0.03
0.02
0.01
0
500
1000
1500
2000
2500
Wavelength(nm)

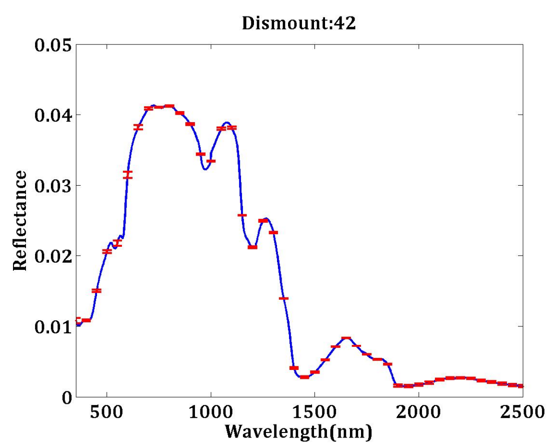
Dismount:42
Reflectance
0.05
0.04
0.03
0.02
0.01
0
500
1000
1500
2000
2500
Wavelength(nm)

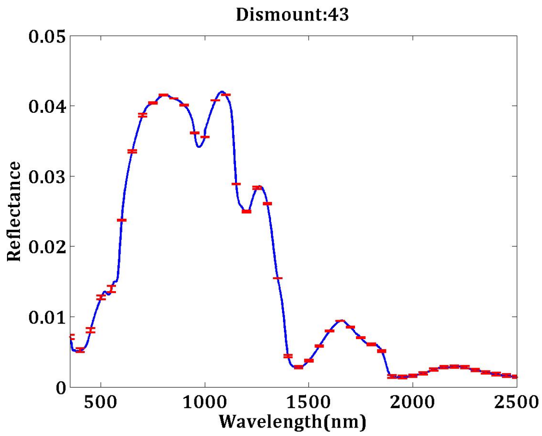
Dismount:43
Reflectance
0.05
0.04
0.03
0.02
0.01
0
500
1000
1500
2000
2500
Wavelength(nm)

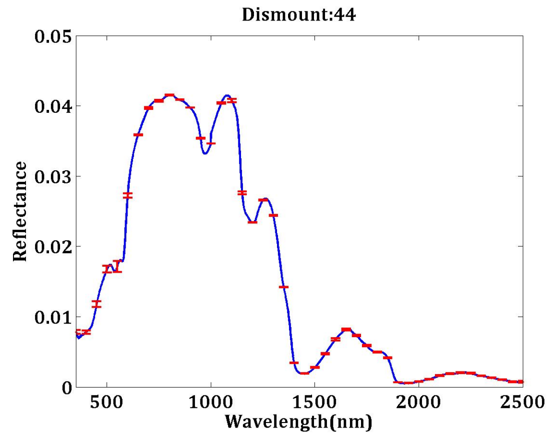
Dismount:44
Reflectance
0.05
0.04
0.03
0.02
0.01
0
500
1000
1500
2000
2500
Wavelength(nm)

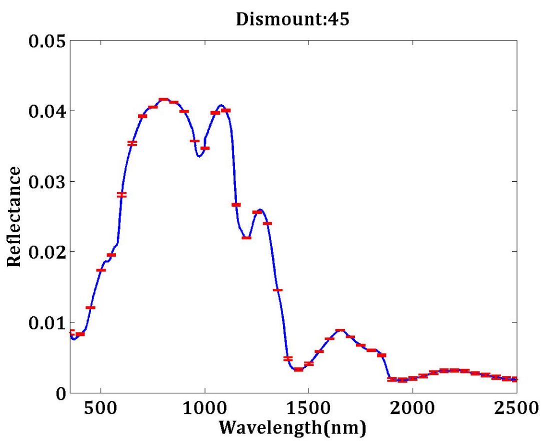
Dismount:45
Reflectance
0.05
0.04
0.03
0.02
0.01
0
500
1000
1500
2000
2500
Wavelength(nm)

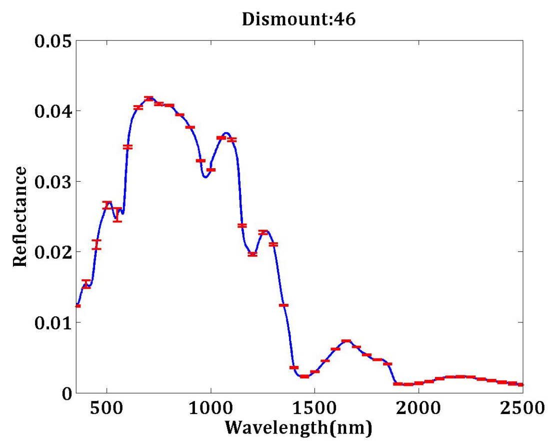
Dismount:46
Reflectance
0.05
0.04
0.03
0.02
0.01
0
500
1000
1500
2000
2500
Wavelength(nm)

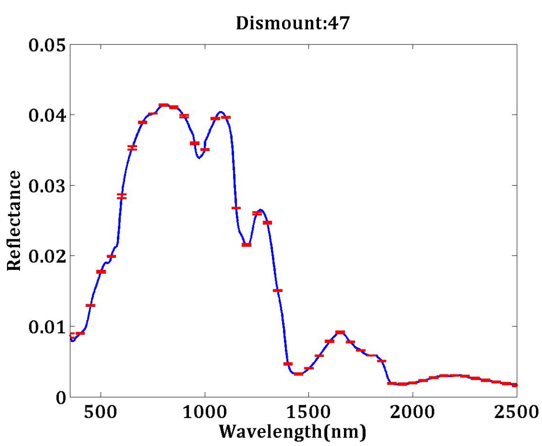
Dismount:47
Reflectance
0.05
0.04
0.03
0.02
0.01
0
500
1000
1500
2000
2500
Wavelength(nm)

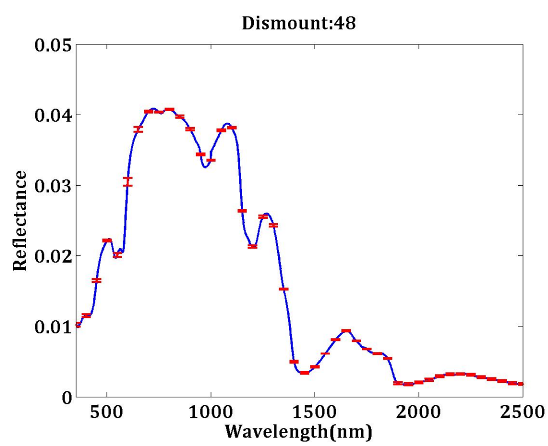
Dismount:48
Reflectance
0.05
0.04
0.03
0.02
0.01
0
500
1000
1500
2000
2500
Wavelength(nm)

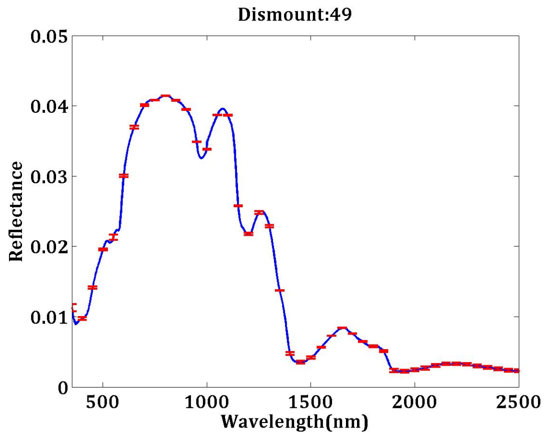
Dismount:49
Reflectance
Wavelength(nm)
0.05
0.04
0.03
0.02
0.01
0
500
1000
1500
2000
2500

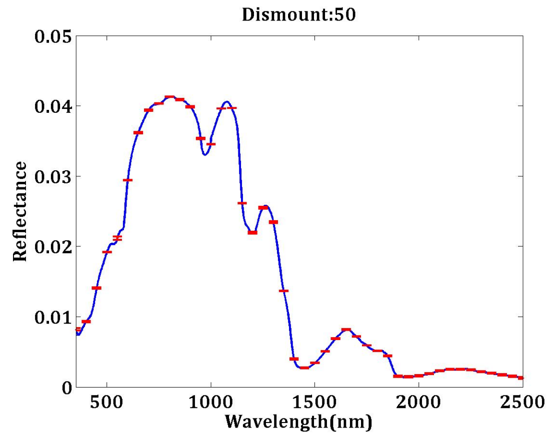
Dismount:50
Reflectance
Wavelength(nm)
0.05
0.04
0.03
0.02
0.01
0
500
1000
1500
2000
2500

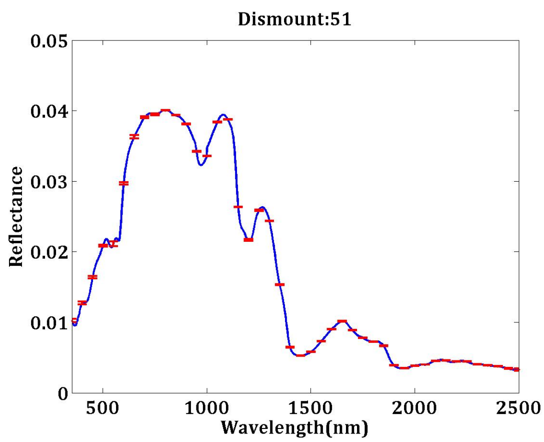
Dismount:51
Reflectance
Wavelength(nm)
0.05
0.04
0.03
0.02
0.01
0
500
1000
1500
2000
2500

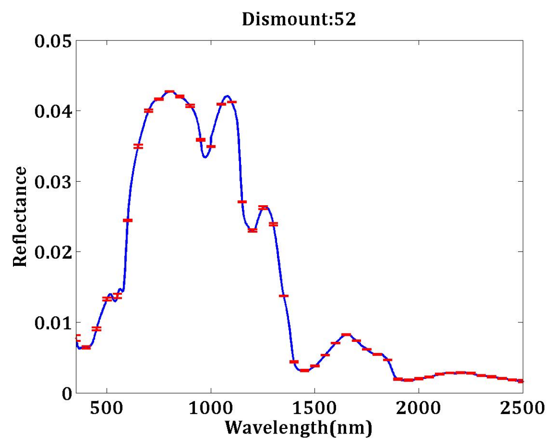
Dismount:52
Reflectance
Wavelength(nm)
0.05
0.04
0.03
0.02
0.01
0
500
1000
1500
2000
2500

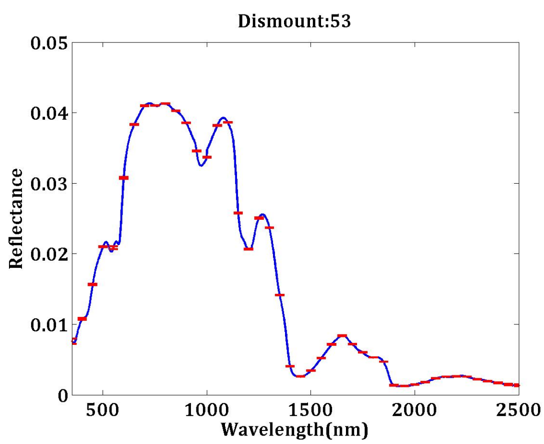
Dismount:53
Reflectance
Wavelength(nm)
0.05
0.04
0.03
0.02
0.01
0
500
1000
1500
2000
2500

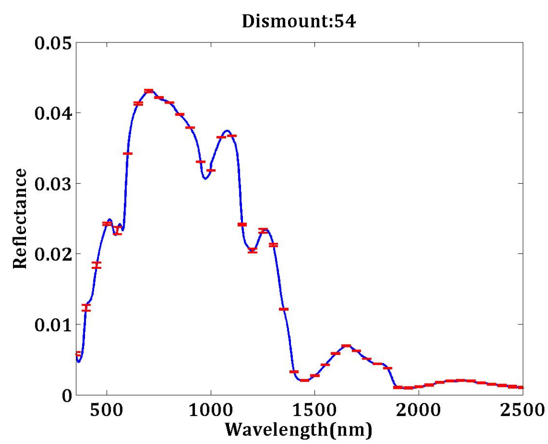
Dismount:54
Reflectance
Wavelength(nm)
0.05
0.04
0.03
0.02
0.01
0
500
1000
1500
2000
2500

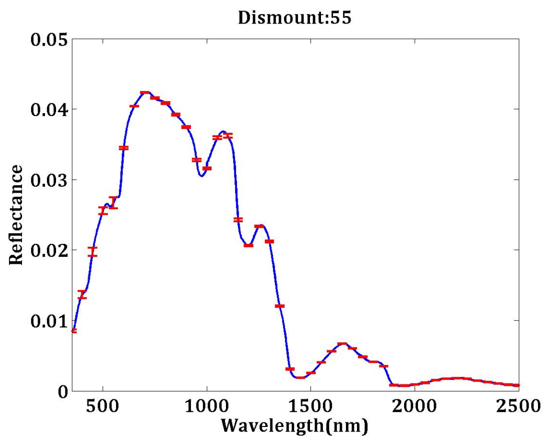
Dismount:55
Reflectance
Wavelength(nm)
0
0.01
0.02
0.03
0.04
0.05
500
1000
1500
2000
2500

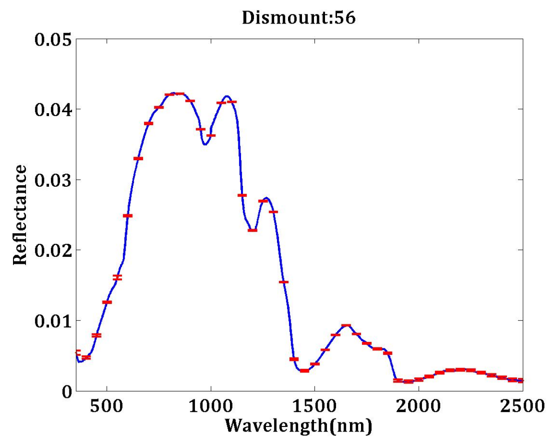
Dismount:56
Reflectance
Wavelength(nm)
0
0.01
0.02
0.03
0.04
0.05
500
1000
1500
2000
2500

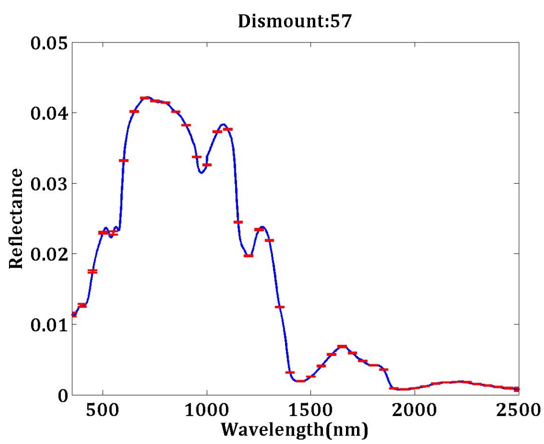
Dismount:57
Reflectance
Wavelength(nm)
0
0.01
0.02
0.03
0.04
0.05
500
1000
1500
2000
2500

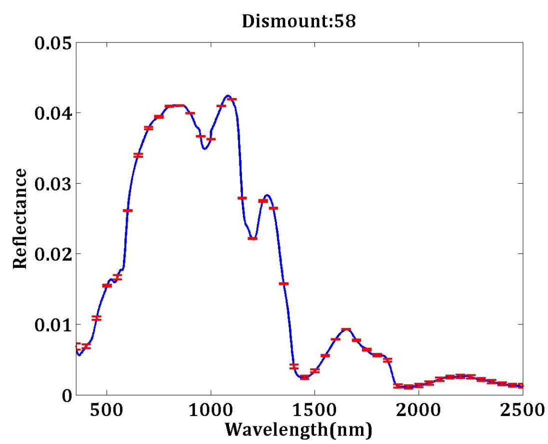
Dismount:58
Reflectance
Wavelength(nm)
0
0.01
0.02
0.03
0.04
0.05
500
1000
1500
2000
2500

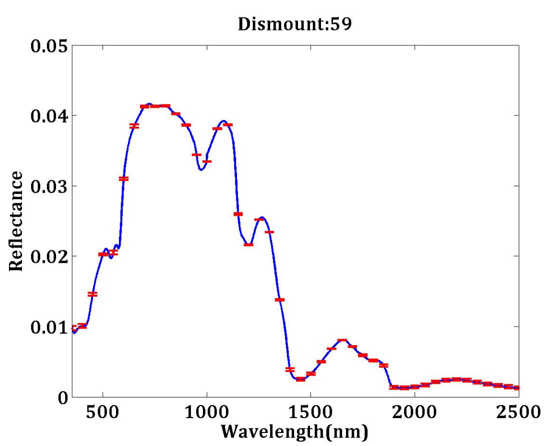
Dismount:59
Reflectance
Wavelength(nm)
0
0.01
0.02
0.03
0.04
0.05
500
1000
1500
2000
2500

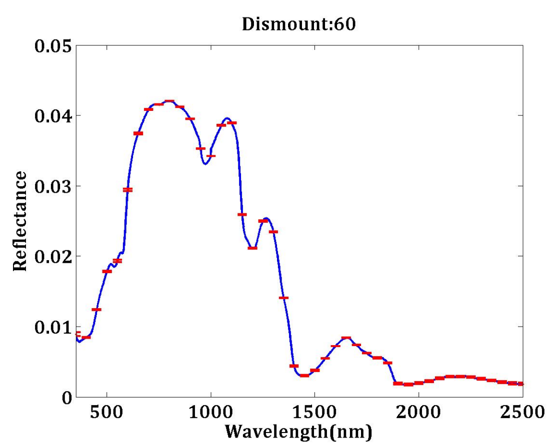
Dismount:60
Reflectance
Wavelength(nm)
0
0.01
0.02
0.03
0.04
0.05
500
1000
1500
2000
2500

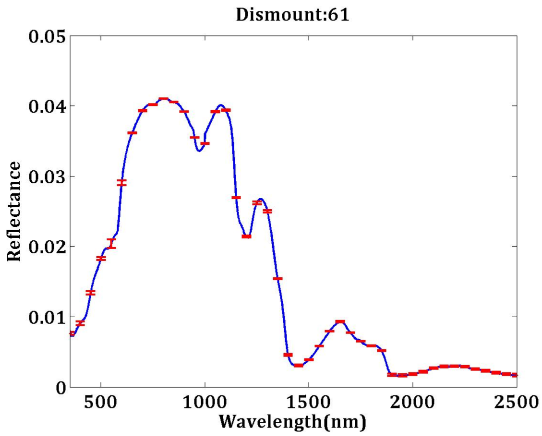
Dismount:61
0.05
0.04
0.03
0.02
0.01
0
Reflectance
500
1000
1500
2000
2500
Wavelength(nm)

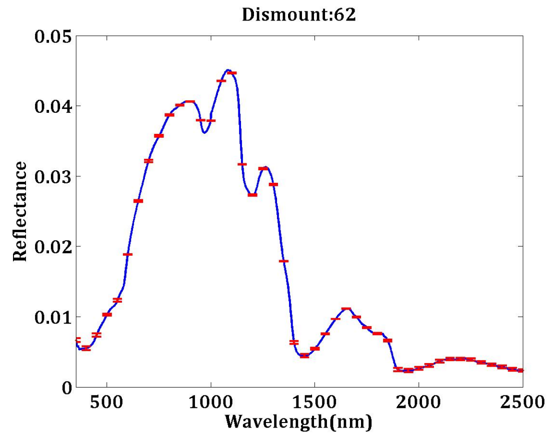
Dismount:62
0.05
0.04
0.03
0.02
0.01
0
Reflectance
500
1000
1500
2000
2500
Wavelength(nm)

## Appendix D: Standard Deviation Plots - Gridded Locations on Forearm

Standard deviation plots for dismounts gridded forearm 1 through 4. The average reflectance is plotted with standard deviation bars at 50nm interval on the plot. The bars represent the standard deviation across 100 samples from the gridded locations on the forearm.

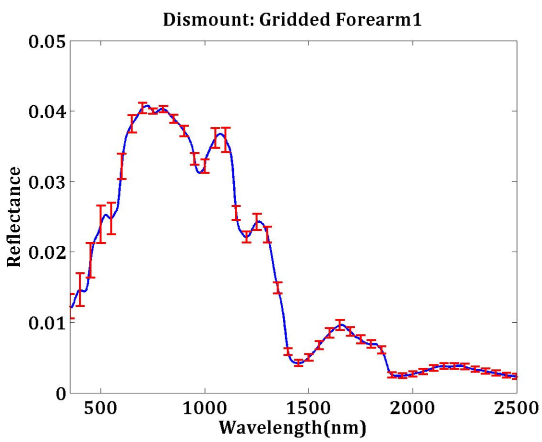


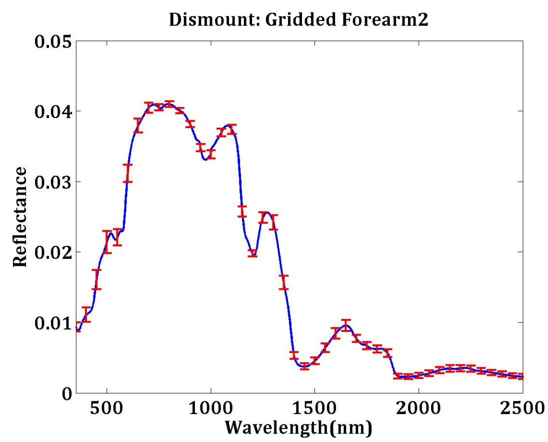


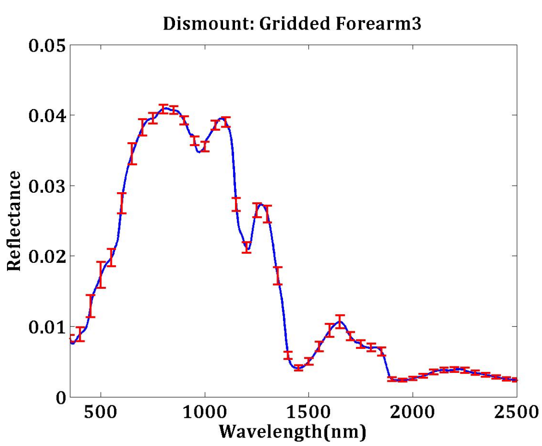


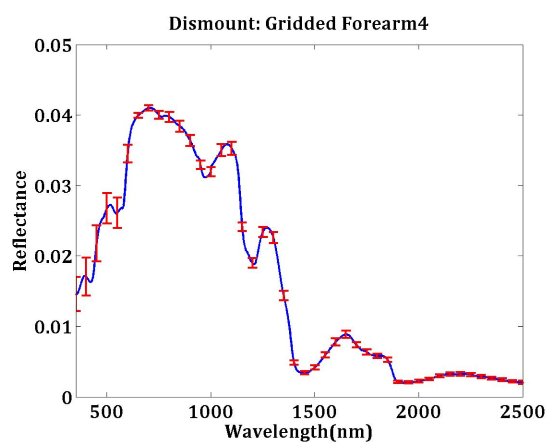

## Appendix E: Standard Deviation Plots - Multiple Locations

Standard deviation plots for dismounts 1 through 10 described in Appendix A. The average reflectance is plotted with standard deviation bars at 50nm intervals on the plot. The bars represent the standard deviation across the back of the hand, palm, forearm, top of the arm, forehead, and cheek.

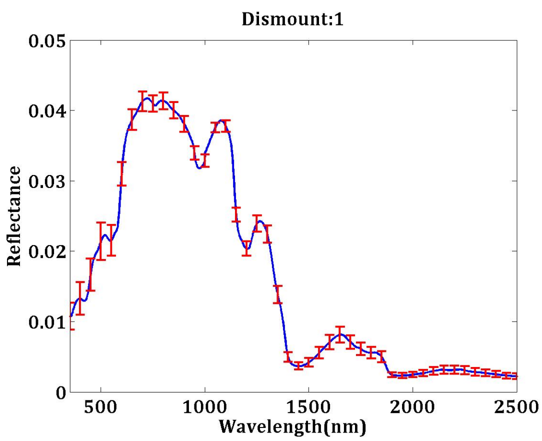


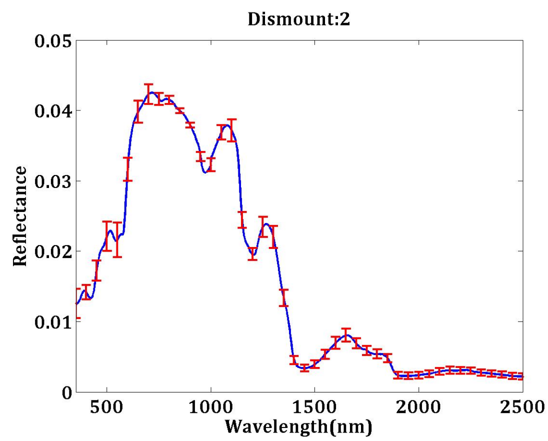


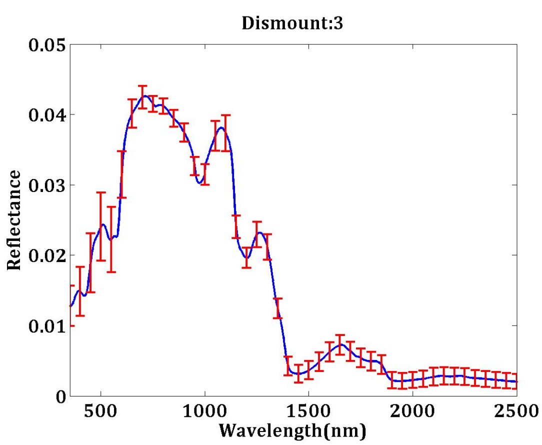


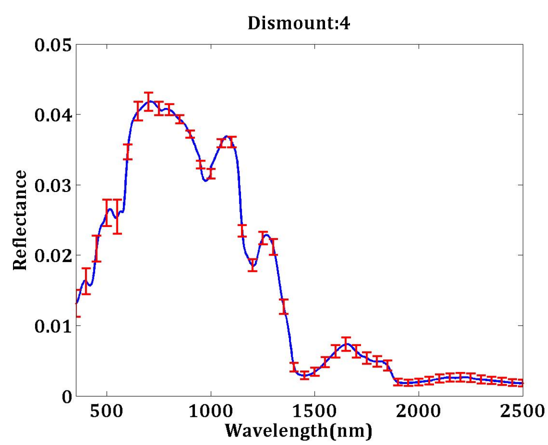

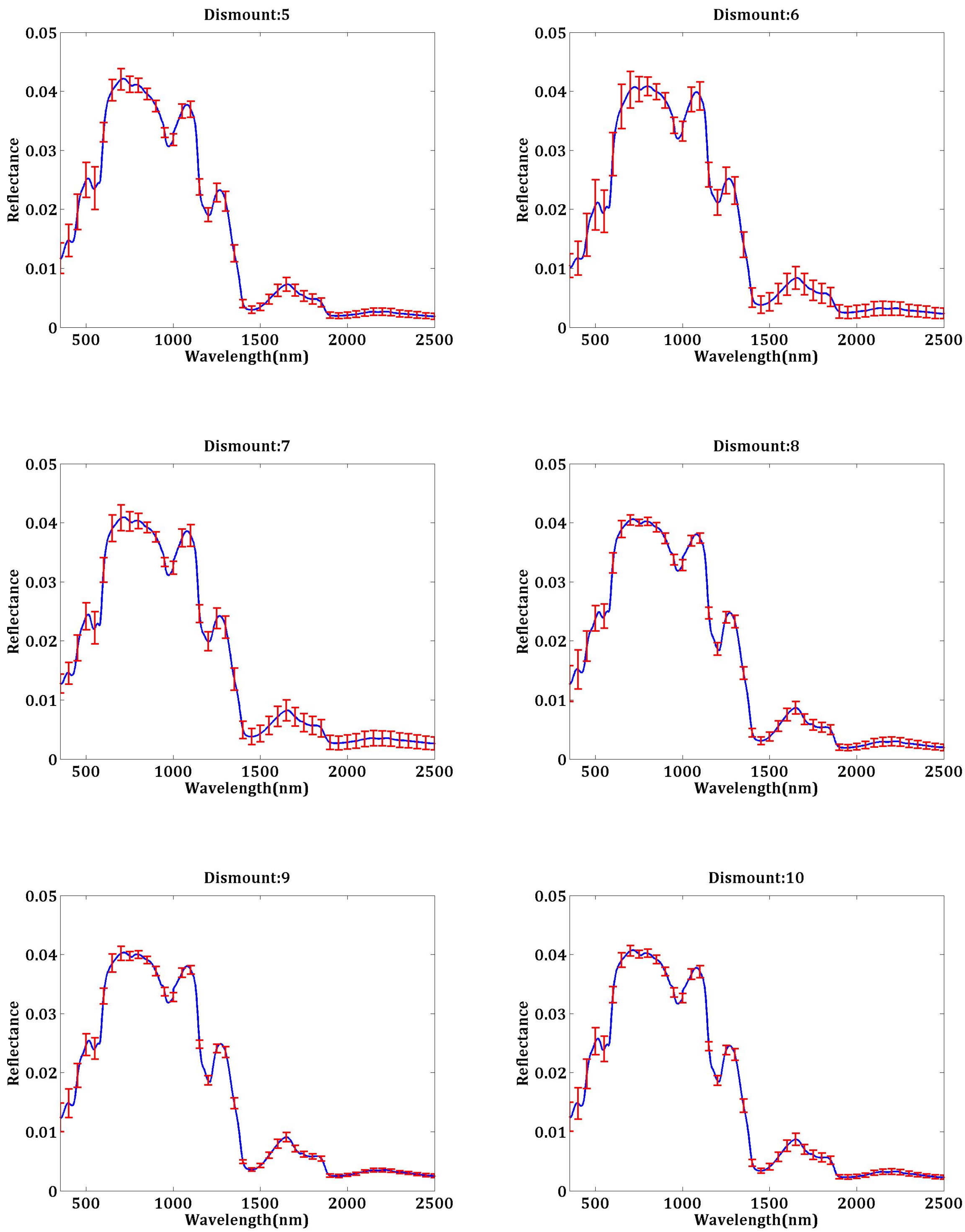
Dismount:5
Dismount:6
Dismount:7
Dismount:8
Dismount:9
Dismount:10
Reflectance
Wavelength(nm)
0
0.01
0.02
0.03
0.04
0.05
500
1000
1500
2000
2500

## Bibliography


[1] ASD Inc. *FieldSpec 3 User Manual*, 1st edition.

[2] Bashkatov, A., E. Genia, and V. Tuchin. "Optical properties of skin, subcutaneous, and muscle tissues: a review". *Journal of Innovative Optical Health Sciences*, 04(01):9–38, 2011. URL http://www.worldscientific.com/doi/abs/10.1142/S1793545811001319.

[3] Beisley, A. *Spectral detection of human skin in VIS-SWIR hyperspectral imagery without radiometric calibration*. Master's thesis, Air Force Institute of Technology, 2012.

[4] Clark, J. *Distributed spacing stochastic feature selection and its application to textile classification*. Ph.D. thesis, Wright Patterson AFB, OH, USA, 2011. AAI3474103.

[5] Costin, G. and V. Hearing. "Human skin pigmentation: melanocytes modulate skin color in response to stress". *Faseb Journal*, 21:976–994, 2007.

[6] Dash, M., H. Liu, and H. Motoda. "Consistency based feature selection". *Knowledge Discovery and Data Mining. Current Issues and New Applications*, 98–109. Springer, 2000.

[7] Davis, L. "Globalization's Security Implications". 2003.

[8] Di, W., L. Zhang, D. Zhang, and Q. Pan. "Studies on Hyperspectral Face Recognition in Visible Spectrum With Feature Band Selection". *Systems, Man and Cybernetics, Part A: Systems and Humans, IEEE Transactions on*, 40(6):1354 –1361, nov. 2010. ISSN 1083-4427.

[9] Dicker, D., J. Lerner, P. Van Belle, D. Guerry, M. Meenhard, D. Elder, W. El-Deiry, et al. "Differentiation of normal skin and melanoma using high resolution hyperspectral imaging". *Cancer biology & therapy*, 5(8):1033–1038, 2006.

[10] Gomez-Chova, L., J. Calpe, G. Camps-Valls, J. Martin, E. Soria, J. Vila, L. Alonso-Chorda, and J. Moreno. "Feature selection of hyperspectral data through local correlation and SFFS for crop classification". *Geoscience and Remote Sensing Symposium, 2003. IGARSS '03. Proceedings. 2003 IEEE International*, volume 1, 555–557 vol.1. July.

[11] Grieve, D. "Scientific Working Group on Friction Ridge Analysis, Study and Technology". *Journal of Forensic Identification*, 51(3):222–299, 2001.

[12] Hall, M. "Feature selection for discrete and numeric class machine learning". 1999.

[13] Hall, M., E. Frank, G. Holmes, B. Pfahringer, P. Reutemann, and I. Witten. "The WEKA data mining software: an update". *ACM SIGKDD Explorations Newsletter*, 11(1):10–18, 2009.

[14] Harsanyi, J. and C. Chang. "Hyperspectral image classification and dimensionality reduction: an orthogonal subspace projection approach". *Geoscience and Remote Sensing, IEEE Transactions on*, 32(4):779–785, Jul. ISSN 0196-2892.

[15] Haykin, S. *Neural networks and learning machines*, volume 3. Prentice Hall New York, 2009.

[16] Hersey, R.K, L Melvin W, and E. Culpepper. "Dismount modeling and detection from small aperture moving radar platforms". *Radar Conference, 2008. RADAR '08. IEEE*, 1–6. 2008. ISSN 1097-5659.

[17] Hughes, G. "On the mean accuracy of statistical pattern recognizers". *Information Theory, IEEE Transactions on*, 14(1):55–63, Jan. ISSN 0018-9448.

[18] Igarashi, T., K. Nishino, and S.K. Nayar. *The Appearance of Human Skin*. Technical report, Jun 2005.

[19] Jacques, S. "Origins of tissue optical properties in the UVA, visible and NIR regions". *Advances in Optical Imaging and Photon Migration*, 2:364–371, 1996.

[20] Kaewpijit, S., J. Le Moigne, and T. El-Ghazawi. "Automatic reduction of hyperspectral imagery using wavelet spectral analysis". *Geoscience and Remote Sensing, IEEE Transactions on*, 41(4):863–871, 2003.

[21] Kenji, K. and L. Rendell. "The feature selection problem: traditional methods and a new algorithm". *Proceedings of the tenth national conference on Artificial intelligence*, AAAI'92, 129–134. AAAI Press, 1992. ISBN 0-262-51063-4. URL http://dl.acm.org/citation.cfm?id=1867135.1867155.

[22] Keshava, N. "Distance metrics and band selection in hyperspectral processing with applications to material identification and spectral libraries". *Geoscience and Remote Sensing, IEEE Transactions on*, 42(7):1552–1565, 2004. ISSN 0196-2892.

[23] Kira, K. and L. Rendell. "The feature selection problem: Traditional methods and a new algorithm". *AAAI*, 129–134. 1992.

[24] Kohavi, R. and G. John. "Wrappers for feature subset selection". *Artificial intelligence*, 97(1):273–324, 1997.

[25] Kononenko, I. "Estimating attributes: analysis and extensions of RELIEF". *Machine Learning: ECML-94*, 171–182. Springer, 1994.

[26] Kotsiantis, S., A. Zaharakis, and P. Pintelas. "Supervised machine learning: A review of classification techniques", 2007.

[27] Krishnaswamy, A. and G. Baranoski. *A Study on Skin Optics*. Technical report, University of Waterloo, 2004.

[28] Landgrebe, D. "Hyperspectral image data analysis". *Signal Processing Magazine, IEEE*, 19(1):17–28, 2002.

[29] Langley, P. *Selection of relevant features in machine learning*. Defense Technical Information Center, 1994.

[30] Liu, H. and R. Setiono. "A probabilistic approach to feature selection-a filter solution". *ICML*, volume 96, 319–327. Citeseer, 1996.

[31] Manolakis, D. and G. Shaw. "Detection algorithms for hyperspectral imaging applications". *Signal Processing Magazine, IEEE*, 19(1):29 –43, jan 2002. ISSN 1053-5888.

[32] MATLAB and Statistics Toolbox. *Release R2011b*. The MathWorks Inc., Natick, Massachusetts, 2011.

[33] Mitchell, M. "An introduction to genetic algorithms". *Cambridge, Massachusetts London, England, Fifth printing*, 3, 1999.

[34] Nagaoka, T., A. Nakamura, Y. Kiyohara, and T. Sota. "Melanoma screening system using hyperspectral imager attached to imaging fiberscope". *Engineering in Medicine and Biology Society (EMBC), 2012 Annual International Conference of the IEEE*, 3728 –3731. 28 2012-sept. 1 2012. ISSN 1557-170X.

[35] Nguyen, H., A. Banerjee, and R. Chellappa. "Tracking via object reflectance using a hyperspectral video camera". *Computer Vision and Pattern Recognition Workshops (CVPRW), 2010 IEEE Computer Society Conference on*, 44 –51. june 2010. ISSN 2160-7508.

[36] Nunez, A. *A physical model of human skin and its application for search and rescue*. Ph.D. thesis, Wright Patterson AFB, OH, USA, 2010. ADA511354.

[37] Nunez, A. and M. Mendenhall. "Detection of Human Skin in Near Infrared Hyperspectral Imagery". *Geoscience and Remote Sensing Symposium, 2008. IGARSS 2008. IEEE International*, volume 2, II–621 –II–624. july 2008.

[38] Nunez, A., M. Mendenhall, and K. Gross. "Melanosome level estimation in human skin from hyperspectral imagery". *Hyperspectral Image and Signal Processing: Evolution in Remote Sensing, 2009. WHISPERS '09. First Workshop on*, 1 –4. aug. 2009.

[39] Pan, Z., G. Healey, M. Prasad, and B. Tromberg. "Face recognition in hyperspectral images". *Pattern Analysis and Machine Intelligence, IEEE Transactions on*, 25(12):1552 – 1560, dec. 2003. ISSN 0162-8828.

[40] Pan, Z., G. Healey, M. Prasad, and B. Tromberg. "Illumination-invariant face recognition in hyperspectral images". 275–282, 2003. URL +http://dx.doi.org/10.1117/12.488561.

[41] Park, B., W. Windham, K. Lawrence, and D. Smith. "Contaminant Classification of Poultry Hyperspectral Imagery using a Spectral Angle Mapper Algorithm". *Biosystems Engineering*, 96(3):323 – 333, 2007. ISSN 1537-5110. URL http://www.sciencedirect.com/science/article/pii/S1537511006004065.

[42] Phillips, P. "Human identification technical challenges". *Image Processing. 2002. Proceedings. 2002 International Conference on*, volume 1, I–49–I–52 vol.1. ISSN 1522-4880.

[43] Plaza, A., P. Martinez, J. Plaza, and R. Perez. "Dimensionality reduction and classification of hyperspectral image data using sequences of extended morphological transformations". *Geoscience and Remote Sensing, IEEE Transactions on*, 43(3):466–479, March. ISSN 0196-2892.

[44] Proksch, E., J. Brandner, and J. Jensen. "The skin: an indispensable barrier". *Experimental Dermatology*, 17(12):1063–1072, 2008. ISSN 1600-0625. URL http://dx.doi.org/10.1111/j.1600-0625.2008.00786.x.

[45] Randeberg, L., I. Baarstad, T. Loke, P. Kaspersen, and L.Svaasand. "Hyperspectral imaging of bruised skin". *Proc. SPIE*, volume 6078, 60780O. 2006.

[46] Robila, S. "Quo vadis face recognition: Spectral considerations". *Systems, Applications and Technology Conference, 2009. LISAT '09. IEEE Long Island*, 1 –5. may 2009.

[47] Shaw, G. and D. Manolakis. "Signal processing for hyperspectral image exploitation". *Signal Processing Magazine, IEEE*, 19(1):12 –16, jan 2002. ISSN 1053-5888.

[48] Sims, R. and M. Phillips. "Target signature consistency of image data fusion alternatives". *Optical Engineering*, 36(3):743–754, 1997. URL +http://dx.doi.org/10.1117/1.601272.

[49] Stamatas, G., B. Zmudzka, N. Kollias, and J. Beer. "Non-Invasive Measurements of Skin Pigmentation In Situ". *Pigment Cell Research*, 17(6):618–626, 2004. ISSN 1600-0749. URL http://dx.doi.org/10.1111/j.1600-0749.2004.00204.x.

[50] Storring, M., H. Andersen, and E. Granum. "Physics-based modelling of human skin colour under mixed illuminants". *Robotics and Autonomous Systems*, 35:131–142, 2001.

[51] Yu, L. and H. Liu. "Feature selection for high-dimensional data: A fast correlation-based filter solution". *ICML*, volume 3, 856–863. 2003.

# REPORT DOCUMENTATION PAGE

*Form Approved*
*OMB No. 0704–0188*

The public reporting burden for this collection of information is estimated to average 1 hour per response, including the time for reviewing instructions, searching existing data sources, gathering and maintaining the data needed, and completing and reviewing the collection of information. Send comments regarding this burden estimate or any other aspect of this collection of information, including suggestions for reducing this burden to Department of Defense, Washington Headquarters Services, Directorate for Information Operations and Reports (0704–0188), 1215 Jefferson Davis Highway, Suite 1204, Arlington, VA 22202–4302. Respondents should be aware that notwithstanding any other provision of law, no person shall be subject to any penalty for failing to comply with a collection of information if it does not display a currently valid OMB control number. **PLEASE DO NOT RETURN YOUR FORM TO THE ABOVE ADDRESS.**

| 1. REPORT DATE *(DD–MM–YYYY)* | 2. REPORT TYPE | 3. DATES COVERED *(From — To)* |
|---|---|---|
| 27–03–2014 | Master's Thesis | Oct 2012 - Mar 2014 |

**4. TITLE AND SUBTITLE**
Feature Selection on Hyperspectral Data for
Dismount Skin Analysis

**5a. CONTRACT NUMBER**

**5b. GRANT NUMBER**

**5c. PROGRAM ELEMENT NUMBER**

**6. AUTHOR(S)**
Cain, Lindsay R., Second Lieutenant, USAF

**5d. PROJECT NUMBER**
JON 14G282

**5e. TASK NUMBER**

**5f. WORK UNIT NUMBER**

**7. PERFORMING ORGANIZATION NAME(S) AND ADDRESS(ES)**
Air Force Institute of Technology
Graduate School of Engineering and Management (AFIT/EN)
2950 Hobson Way
WPAFB, OH 45433-7765

**8. PERFORMING ORGANIZATION REPORT NUMBER**
AFIT-ENG-14-M-15

**9. SPONSORING / MONITORING AGENCY NAME(S) AND ADDRESS(ES)**
Air Force Research Laboratories
711th Human Performance Wing
2800 Q Street, Bldg 824
Wright Patterson AFB, OH 45433
Dr Darrell F. Lochtefeld, Lead Scientist
darrell.lochtefeld@us.af.mil

**10. SPONSOR/MONITOR'S ACRONYM(S)**
AFRL/RHXBA

**11. SPONSOR/MONITOR'S REPORT NUMBER(S)**

**12. DISTRIBUTION / AVAILABILITY STATEMENT**
Distrubution Statement A: Approved for Public Release; Distribution Unlimited

**13. SUPPLEMENTARY NOTES**
This work is declared a work of the U.S. Government and is not subject to copyright protection in the United States.

**14. ABSTRACT**
Many security applications require the ability to accurately identify dismounts based on their distinctive identification properties. A dismount can be identified by many personal characteristics to include clothing, height, and gait. In particular, a dismount's skin can be used as an identifying feature because of the vast variability of skin pigmentation amongst individuals. Hyperspectral data, which is comprised of hundreds of spectral channels sampled from a nearly contiguous electromagnetic spectrum, is used to detect skin spectral variability amongst dismounts. However, hyperspectral data is often highly correlated and computationally expensive to process. Feature selection methods can be employed to reduce the data to a manageable size. This thesis presents the results of applying the fast correlation based filter (FCFB) [51] to a data set that contains hyperspectral data from the forearms of 62 subjects. The reduced data is used to train an artificial neural network (ANN) to discriminate a dismount of interest (DOI) amongst a group of 4 non-DOI's. The trained model is then tested to find the same DOI amongst a group of 62 new non-DOI's. The FCBF selected four features (1014, 1024, 1033, and 1348nm) to discriminate amongst the dismounts. Using these four features, the ANN on average misclassified 4 dismounts amongst four separate DOI validation tests. More specifically, the amount of possible DOI suspects was reduced from 62 to 4 dismounts. The FCBF outperformed three other feature selection methods with 4 times less misclassified instances.

**15. SUBJECT TERMS**
dismount, Fast Correlation Based Filter, hyperspectral, identification

| 16. SECURITY CLASSIFICATION OF: | | | 17. LIMITATION OF ABSTRACT | 18. NUMBER OF PAGES | 19a. NAME OF RESPONSIBLE PERSON |
|---|---|---|---|---|---|
| a. REPORT | b. ABSTRACT | c. THIS PAGE | | | Lt Col Jeffrey D. Clark, PhD (ENG) |
| | | | | | 19b. TELEPHONE NUMBER *(include area code)* |
| U | U | U | UU | 110 | (937) 255-3636 x4614 Jeffrey.Clark@afit.edu |